Contract No:

This document was prepared in conjunction with work accomplished under Contract No. DE-AC09-08SR22470 with the U.S. Department of Energy (DOE) Office of Environmental Management (EM).

Disclaimer:

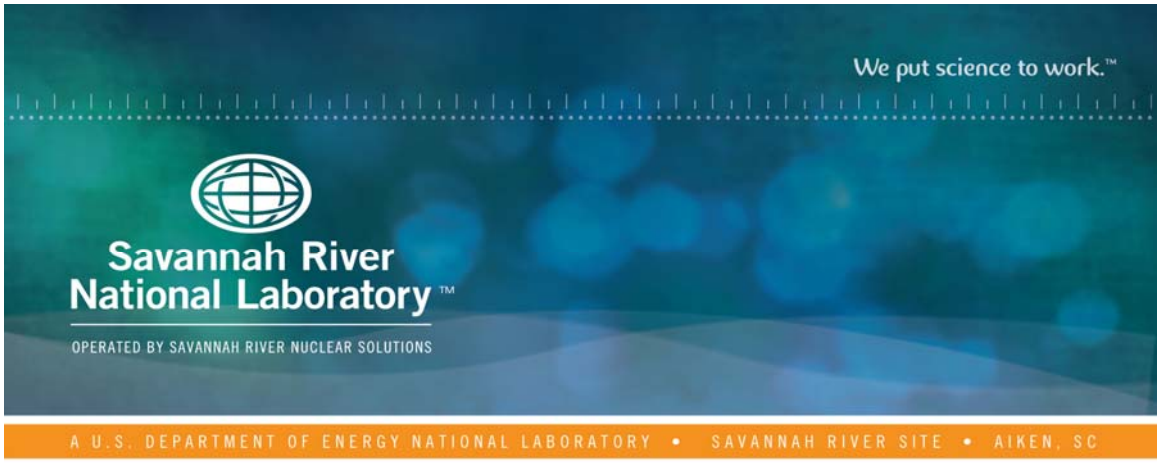

Flowsheet Evaluation for the Dissolving and Neutralization of Sodium Reactor Experiment Used Nuclear Fuel

W. E. Daniel
E. K. Hansen
T. C. Shehee

March 2015

SRNL-STI-2012-00279 Revision 2

DISCLAIMER

Printed in the United States of America

Prepared for
U.S. Department of Energy

SRNL-STI-2012-00279
Revision 2

Keywords: *Dissolution, Neutralization, HMI, DR3, SRE, UNF*

Retention: *Permanent*

Flowsheet Evaluation for the Dissolving and Neutralization of Sodium Reactor Experiment Used Nuclear Fuel

W. E. Daniel
E. K. Hansen
T. C. Shehee

March 2015

Prepared for the U.S. Department of Energy under contract number DE-AC09-08SR22470.

Savannah River National Laboratory™
OPERATED BY SAVANNAH RIVER NUCLEAR SOLUTIONS

REVIEWS AND APPROVALS

AUTHORS:

W. E. Daniel, Process Technology Programs Date

E. K. Hansen, Engineering and Process Development Date

T. C. Shehee, Separations & Actinide Science Programs Date

TECHNICAL REVIEW:

S. D. Fink, WTP Technical Support, Reviewed per E7, 2.60 Date

APPROVAL:

T. B. Brown, Manager Date
Separations & Actinide Science Programs

S. L. Marra, Manager Date
Environmental & Chemical Process Technology Research Programs

S. L. Garrison, Manager Date
H-Canyon Engineering

PREFACE OR ACKNOWLEDGEMENTS

Thanks to Bill Clifton and Ric Castles for providing data and drawings of the various used nuclear fuel assemblies.

EXECUTIVE SUMMARY

This report includes the literature review, hydrogen off-gas calculations, and hydrogen generation tests to determine that H-Canyon can safely dissolve the Sodium Reactor Experiment (SRE; thorium fuel), Ford Nuclear Reactor (FNR; aluminum alloy fuel), and Denmark Reactor (DR-3; silicide fuel, aluminum alloy fuel, and aluminum oxide fuel) assemblies in the L-Bundles with respect to the hydrogen levels in the projected peak off-gas rates. This is provided that the number of L-Bundles charged to the dissolver is controlled. Examination of SRE dissolution for potential issues has aided in predicting the optimal batching scenario.

As demonstrated in prior work on the dissolution of the University of Missouri Research Reactor (MURR) assemblies, this work relies on the literature composite lower flammability limits (LFL) for H_2 in an air/NO/N_2O mixture and pilot-scale studies on the dissolution of Savannah River Site (SRS) fuels. How the various used nuclear fuels are charged to the dissolver, the depth of the dissolver solution, and the concentrations of nitric acid and catalysts (mercury and fluoride) will control the dissolution rate during the initial stage of the dissolution cycle. The concentration of catalysts (mercury and fluoride), the nitric acid concentration, and the dissolved metals concentrations (aluminum, thorium) impact the off-gas generation rates and thus the hydrogen generated during dissolution. The calculations detailed in this report demonstrate that the FNR, SRE, and DR-3 used nuclear fuel (UNF) are bounded by MURR UNF and may be charged using the controls outlined for MURR dissolution in a prior report.

The physical property measurements and flow calculations on the dissolved SRE, FNR, and DR-3 UNF simulants indicate that the material should flow down the waste header in Building 221-H. For conservativeness, the analysis assumed the lines were partially full of fluid with no air bubble entrapment. The flow calculations show that the initial section of the waste lines leaving Building 221-H is limited to 27.2 gpm since the waste header has no vertical drop in the piping. The flow calculations showed that the secondary sections of waste lines provide a flow of at least 45.3 gpm. These calculated flow rates are for dirty piping. For clean piping, the calculated flow rates would be slightly larger. When the various sections of pipe are completely filled with fluid the calculated minimum flow rate increases to 58.4 gpm. This indicates that the hydrostatic head has increased relative to the pressure drop associated with the additional piping. The calculations show that the waste lines leaving Building 221-H could handle the 25 to 30 gpm flow that the steam jets provide. In reality, the waste lines are most likely not at full pipe flow.

It is recommended that Waste Header #1, 4, or 3 (transfer lines WF1100 , WF1101, or WF1102 respectively) be used if there is a potential for the fluid to have a Bingham Plastic yield stress of larger than 1 Pa such as those of the 12,000L dissolver batch fluids. If Waste Header #2 (WF1103) is used for such fluids, the fluid will backup in to the header in Building 221-H. The 10-inch header associated with WH #2 may backup and provide the necessary head for 25 gpm, but this was not analyzed.

The deposition velocity was calculated between 3.5 to 4.1 ft/s. Given a discharge rate of 25 gpm, only the steepest transfer lines have a potential to mitigate settling of solids. Intermittent flushing with inhibited water is recommended in minimizing undissolved solids buildup at the maximum achievable flow rate with a minimum of at least 3 waste line volumes or an acceptable drop rate in the waste header liquid level is observed.
.

TABLE OF CONTENTS

LIST OF TABLES

LIST OF FIGURES

LIST OF ABBREVIATIONS

DABT	Disassembly L-Area Bundling Tube or L-Bundle
DI	Distilled and deionized
DR-3	Denmark Reactor
DU	Depleted Uranium
FNR	Ford Nuclear Reactor
HA/LU	High Aluminum / Low Uranium
HMI	Hahn-Meitner-Institute
HPP	H-Area Pump Pit
LFL	Lower Flammability Limit
MURR	University of Missouri Research Reactor
PSD	particle size distribution
scfm	standard cubic feet per minute
SG	Specific gravity
SRE	Sodium Reactor Experiment
SRNL	Savannah River National Laboratory
STDEV	Standard Deviation
UDS	undissolved solids
UNF	used nuclear fuel
WH	Waste Header

1.0 Introduction

The H-Canyon processing of Sodium Reactor Experiment (SRE)[1] Used Nuclear Fuel (UNF) is to begin in 2012. The SRE fuel is currently being stored in L-Basin. SRE is a thorium/uranium alloy that is sealed in aluminum cans in a Disassembly L-Area Bundling Tube (DABT) also known as an L-Bundle. This fuel is identified as "vulnerable" and needs a timely disposition. The SRE fuel will be dissolved in H-Canyon along with a High Aluminum/Low Uranium-235 (HA/LU) UNF. Once dissolved, depleted uranium will be added to the dissolver solution to reduce the ^{235}U enrichment in the material if required to meet liquid waste requirements.

The candidate HA/LU fuels are the FNR and DR-3 fuels. The DR-3 UNF originated from the Risø National Laboratory in Roskilde, Denmark. The majority of this fuel is an aluminum clad silicide type fuel where the fuel "meat" is U_3Si_2-Al alloy. Dissolution of silicide fuel should be such that the [Si] remains well below the threshold concentration of 0.1 M silicon. This concentration avoids formation of gelatinous silicic acid.[2] Another DR-3 UNF, recently identified for processing, is either U-Al_x or U_3O_8-Al (cermet). Hahn-Meitner-Institute (HMI) UNF was an early candidate HA/LU fuels. This fuel was included in the surface area calculations, but will not be dissolved at this time.

SRNL was tasked with determining through literature search and laboratory experimentation the flowsheet parameters necessary to safely and effectively dissolve, process, and neutralize the SRE and HA/LU UNF in H-Canyon. The flowsheet evaluation defined the number of SRE and HA/LU bundles that can safely be charged to the dissolver batch without exceeding the hydrogen lower flammability limit (LFL). SRNL evaluated issues pertaining to the dissolution of the various fuels together and provided guidance for charging either the HA/LU material to the dissolved SRE solution, or vice-versa. SRNL also provided limits and controls for ensuring the neutralized solution flows properly down the waste header after neutralization. Determination of these limits and controls have been established from testing the rheological properties of the mixtures derived from the addition of 50 wt % NaOH solution to several dissolver simulant solutions.

2.0 Experimental Procedure

2.1 Dissolution

Thorium (Th) and aluminum (Al) metal were dissolved under a variety of conditions in nitric acid (Table 2-1) to measure the gas generated during dissolution as well as dissolution time. The experimental configuration for these studies was modeled after the apparatus in a recent report[3], where dissolver solution is added into a glass reaction vessel, placed onto a hot plate-stirrer, and heated to 50–100 °C. A 75 mL dissolver solution volume was selected for dissolutions based on the available mass of Th metal, the calculated total gas production, and the minimum solution needed to completely cover the one inch square thorium coupon. The vessel was purged with nitrogen or argon to remove air prior to starting dissolution by passing the purge gas through the dissolver, condenser and sample bulb. The gas port automatically closes when the gas line is removed which precludes the introduction of O_2 to the system. The reaction dissolver solution was heated to 99 ± 1 °C, at which time a coupon of 99.5 wt % Th metal of known weight and physical dimensions was immersed into the dissolver solution using a glass basket. The sample remained immersed until the Th was completely dissolved. Off-gas volume generated during the dissolution was measured and samples collected. The dissolving system utilizes Tedlar® bags to collect the off-gas and 40 mL glass sample bulbs to collect subsamples for analysis. The volume of gas collected in each bag was determined by water displacement with an accuracy of ±5 mL. Off-gas collected during the experiments was analyzed by gas chromatography to determine composition.

Table 2-1. Dissolution schemes used to determine bounding H_2 gas generation rates.

Dissolution	Metal foil used		$[HNO_3]_{Initial}$	$[F^-]$	$[Hg^{2+}]$	$[Al]_{Initial}$[2]
1[1]	–	Al	10	–	0.02	0.3
1-A	–	Al	10	–	0.002	0.3
2	Th	–	4	0.05	–	–
3	Th	–	7	0.05	–	–
4	Th	–	10	0.05	–	–
5	Th	–	7	0.05	–	0.3
3-A[3]	$Th^{4+}_{(aq)}$	Al	7	0.05	0.002	–
4-A[3]	$Th^{4+}_{(aq)}$	Al	10	0.05	0.002	–
5-A[3]	$Th^{4+}_{(aq)}$	Al	7	0.05	0.002	0.3
5-B	Th	–	7	0.01	–	0.3
6	Th	–	10	0.05	–	0.3
7	Th	Al	10	0.05	–	0.3
8	Th	Al	10	0.05	0.002	0.3
9[4]	Th	Al	10	0.05	0.002	0.3
10[4]	Th	–	7	0.05	–	0.3

1) Non-radioactive test of apparatus
2) Represents the concentration present after dissolution of FNR and part of SRE bundle
3) Dissolver solution is from Th dissolutions 3, 4 and 5. Hg added to aid in dissolution of Al.
4) Duplicate Measurement

2.2 Neutralization

SRNL personnel prepared four simulant solution stocks representing the expected composition of SRE UNF and multiple dissolver batch blends. Simulant compositions are shown in Table 2-2. These concentrations were selected from the compositions of the fuels expected to be processed at the same time, the expected order of dissolver additions, and the typical volume used in the dissolver.[2] All simulants included depleted uranium (DU) at concentrations that represent a dissolved fuel with added DU such that the isotopic ratio was reduced to 5 wt %. This provides a bounding scenario should it be determined that a further down blending is required. If necessary, DU is available in the form of UO_3 powder, with a ^{235}U concentration of approximately 0.2 wt %, dissolved to several hundred g/L U as needed and added to the dissolver solution. All simulants also included gadolinium (Gd) at 0.5 g/L to represent the Gd added as a neutron poison. Mercury has been added since it was required to aid in the dissolution of the HA/LU fuel and the L-Bundles.

Precipitation and neutralization experiments were performed on each simulant shown in Table 2-2. The acidic solution was neutralized to the pH where the first solids precipitate and did not redissolve, expected to be at a pH of ~4.5; to pH 7; to 0.8 M free hydroxide; and to 1.2 M free hydroxide. The neutralization uses 50 wt % NaOH, calculated to achieve the above neutralization points and dispensed from a 50 mL burette. The quantity of 50 wt % NaOH used to achieve excess free hydroxide included any consumed by the aluminum present in the system. To monitor the first two pH points, EMD brand pH 0–14 indicator strips were used. For samples that approximate an evaporated dissolver solution, the simulant was heated to pre-concentrate each solution to 85% of the original volume (equivalent of a change in dissolver volume of 14000 L to 12000 L due to evaporation). This simulant was then neutralized as outlined above. Samples of the neutralization to the 0.8 and 1.2 M excess were collected for rheology and density measurements.

Table 2-2. Uranium, Thorium and Aluminum content in SRE, DR-3, and FNR UNF mixed dissolver solutions.[1]

Fuel simulants	Final [U] after DU Addition (g/L)	[Th] (g/L)	[Al] (g/L)	[U] (M)	[Th] (M)	[Al] (M)
5 SRE bundle charge	29.5	19.9	5.9	0.12	0.09	0.2
10 SRE bundle charge	59.0	39.8	11.9	0.4	0.17	0.4
4 FNR + 5 SRE + 19 DR-3 bundle charge	40.1	19.9	34.3	0.17	0.09	1.3
8 SRE + 19 DR-3 bundle charge	55.9	31.8	31.4	0.24	0.14	1.2
4 FNR + 5 SRE + 19 DR-3 bundle charge[2]	46.9	23.3	40.1	1.5	0.11	1.5
8 SRE + 19 DR-3 bundle charge[2]	65.4	37.2	36.7	1.4	0.16	1.4

1) Dissolver volume chosen for calculating these concentrations is 14,000 L unless noted otherwise. Simulant prepared at a final HNO_3 concentration of 0.5 M. Silicon concentration in this simulant is approximately 0.014 M. Mercury concentration in this simulant is approximately 0.02M.
2) Represents a concentrated dissolver volume of 12,000 L. Silicon concentration increases to approximately 0.016 M.

2.3 Physical Properties

The physical properties measured in this task were solids, density and rheology. Each of these measurements or calculations is discussed in detail below. The supernate samples were obtained by letting a subsample of the slurry settle for at least 48 hours. The free liquid (supernate) was obtained by using a pipette. The concentrated solids were also analyzed to determine the density of the undissolved solids (UDS).

2.3.1 *Solids*

The measured properties for solids analyses include the total solids in the slurry and the total solids in the supernate (or soluble solids in the supernate). These properties were determined using Equation 1 and 2:

(1) $$f_{ts} = \frac{m_{dried\ slurry}}{m_{slurry}}$$

(2) $$f_{sss} = \frac{m_{dried\ supernate}}{m_{supernate}}$$

where:

$m_{slurry} = mass\ of\ slurry\ sample\ (grams)$
$m_{dried\ slurry} = mass\ of\ dried\ slurry\ at\ 105\ °C\ (grams)$
$m_{supernate} = mass\ of\ supernate\ sample\ (grams)$
$m_{dried\ supernate} = mass\ of\ dried\ supernate\ at\ 105\ °C\ (grams)$
$f_{ts} = mass\ fraction\ of\ total\ solids\ in\ slurry$
$f_{sss} = mass\ fraction\ of\ soluble\ solids\ in\ supernate$

Approximately two to four grams of a sub-sample was placed into an unglazed crucible and then placed into a forced convection oven at 95 °C for a minimum of 4 hours prior to increasing the oven temperature to 105 °C for the remainder of the analysis. The mass of the crucible and the mass of the crucible plus sub-sample were measured prior to placing it into the oven. The sample plus crucible were then measured approximately 24 and 48 hours after they were placed into the oven, where the sample was immediately taken from an oven and placed on a scale. A standard salt solution made of 20 wt % of NaCl was used to verify the operation of the oven. Triplicate samples of the slurry and supernate were measured and analyzed.

The average ($\bar{x}_j$) and standard deviation (σ_j) for each property was calculated using Equations 3 and 4 respectively. .

(3) $$\bar{x}_j = \frac{\sum_{i=1}^{n} x_i}{n}$$

(4) $$\sigma_j = \sqrt{\frac{\sum_{i=1}^{n}(x_i - \bar{x}_j)}{n(n-1)}}$$

The fraction of undissolved solids in the slurry (f_{uds}) was calculated using Equation 5 and the STDEV ($\sigma_{f_{uds}}$) was calculated using Equation 6.

(5) $$f_{uds} = \frac{f_{ts} - f_{sss}}{1 - f_{sss}}$$

(6) $$\sigma_{f_{uds}} = \left(\left(\frac{1}{1-f_{sss}}\right)^2 \sigma_{f_{ts}}^2 + \left(\frac{f_{ts}-1}{(1-f_{sss})^2}\right)^2 \sigma_{f_{sss}}^2\right)^{\frac{1}{2}}$$

2.3.2 *Density*

The densities of the slurry, supernate and concentrated slurry was measured using an Anton Paar DMA35 handheld density meter, see Figure 2-1. The accuracy of the density meter is 0.001 g/cm^3 for solutions with viscosity < 100 mPa*s and density < 2 g/cm^3. The density meter was checked prior to operation by measuring the density of water at room temperature.

The DMA35 determines the density of the fluid by measuring the shift in frequency of the oscillator U-tubes. The sample is pulled into the oscillator U-tubes using a vacuum plunger to fill the tubes. Air bubbles and settling solids can impact the measurement. Triplicate measurements of each slurry, supernate and concentrated slurry were made; their average and STDEVs were calculated.

Figure 2-1. Anton Paar DMA35 Density Meter

The average and STDEV of the concentrated slurry and supernate densities and mass fraction of undissolved solids were used to determine the average density of the UDS (ρ_{uds}) and its STDEV ($\sigma_{\rho uds}$) using Equations 7 and 8 respectively.

(7) $$\rho_{uds} = \frac{f_{uds}\rho_{sup}\rho_s}{\rho_{sup}+\rho_s(f_{uds}-1)}$$

(8) $$\sigma_{\rho_{uds}} = \frac{\left[\left(\rho_{sup}^2\rho_s-\rho_s^2\rho_{sup}\right)^2\sigma_{f_{uds}}^2+\left(\rho_s^2 f_{uds}(f_{uds}-1)\right)^2\sigma_{\rho_{sup}}^2+\left(\rho_s^2 f_{uds}\right)^2\sigma_{\rho_s}^2\right]^{\frac{1}{2}}}{\left(\rho_{sup}+\rho_s(f_{uds}-1)\right)^2}$$

2.3.3 *Particle Size Distribution*

The particle size distribution (PSD) was determined using the Microtrac X100. The Microtrac X-100 particle size analyzer uses a wet sample delivery controller (recirculator) to disperse the sample uniformly in a fluid and deliver the sample to the analyzer. This wet sample delivery controller in its basic form consists of a reservoir where the sample is introduced, a fluid pump, a valve to the drain system, and the necessary tubing connections to the analyzer. The flow through the analyzer sample cell is always from the bottom to the top. A laser beam is projected through a transparent quartz cell containing a stream of moving particles suspended in deionized water. Light from the laser strikes the particles and is scattered through various angles. The scattering angles and intensities of the scattered light are measured by two photodiode arrays producing electronic signals proportional to the measured light flux. The Microtrac proprietary mathematical software processes the signals to obtain a particle size distribution. Upon completion of the analysis, the Microtrac generates a report containing the tabular data, a histogram plot of the data, and various instrument parameters.

The volumetric particle size distribution is used. The mean volume and 90 percentile particle sizes are used to support the various calculations below. It is assumed that the densities of the various precipitated particles are the same when using the PSD data for calculations, though in reality this is mostly not the case, but it is impractical (or impossible) to measure the individual flocculated materials or compounds. If the measured PSDs are similar, the data sets were averaged to determine the percentile data, mean volume, mean area, and mean number sizes and reported.

The slurry samples were diluted using simulant salt solutions that were determined by reviewing the ICP-ES data of the various supernatants from the 14,000 L slurry batches. The salt simulants are required to provide the necessary dilution for the PSD measurement and to minimize any effect of dissolution with the undissolved solids in the actual wastes. After the salt solutions were made, they were processed through a 0.25 micron absolute filter to remove any undissolved solids greater than the filter size. The salt solutions used for the 0.8 and 1.2 M slurries are provided in Table 2-2-3.

Table 2-2-3 Salt Simulants Used for PSD Measurements

Compound/Property	1.2 M Simulant	0.8 M Simulant
DI water (g)	842.06	774.04
Aluminum Nitrate + $9H_2O$ (g)	90.92	106.43
Sodium Nitrate (g)	34.60	205.87
50 wt % Sodium Hydroxide (g)	140.72	114.07
Density (g/mL)	1.1083	1.2004

The particle size distributions of the materials processed at SRNL are expected to be larger than those of the fluids processed in 221-H. The neutralization process at the 221-H occurs in an agitated vessel, where the impellers are flat blades[4,5,6] and the addition rate of caustic solution occurs over a period of hours[7]. The flat blade design can provide a high level of shearing and dispersion of the caustic fluid during the neutralization process which was not utilized during the SRNL feed prep. Additional the slow rate of caustic addition can reduce the resulting flocculated particle size distribution.[7] Extensive work in simulant sludge preparation for DWPF simulants have shown that there are multiple variables that can impact the PSD during the neutralization process, such as mixer speed, changes in pH, caustic addition rate, and scaling.[8,9,10] In these studies, the effect of particles less than 1 micron in diameter seem to have the most drastic impact on rheology.

2.3.4 *Rheology*

The rheological properties of the dissolver simulant fluids were measured using a Haake VT550 roto-viscometer. Visual inspection of the samples showed they contained solids and the solution was viscous in nature, indicating that the MV1 bob/cup configuration would be utilized to perform the measurements. The MV1 bob/cup configuration is a concentric cylinder, where the inner cylinder rotates and the outer cylinder is fixed. The VT550 controls the rotational speed and measures both the rotational speed and measured torque on the rotating cylinder. Given the geometry of the MV1/bob/cup, the measured shear stress and shear rates are calculated by the Haake software. The shear rates are those for Newtonian fluids and if the fluid does have non-Newtonian behavior, corrections to the shear rate are not be performed. Corrections to the shear rate for non-Newtonian behavior will increase the shear rate for any given point, resulting in the decrease in the plastic viscosity, given that the fluid is shear thinning, which is the case for fluids processed at SRS. Flow curve measurements utilized an existing tank farm flow curve profile listed in Table 2-4. A National Institute of Standards and Testing (NIST) traceable Newtonian viscosity standard was used to verify the operability of the VT550 roto-viscometer on a daily basis of use, where the calculated viscosity to the flow curve is within ±10% of the NIST oil standard viscosity at 25 °C. Measurements of the fluids in this task were performed at 20 °C in duplicate. Samples were prepared by vigorously shaking the bottle to breakup flocculated material, swirling to assist in removing entrained air, loading into the cup, raising into to heating/cooling bath, trimming excess fluid and starting the measurement using the sludge flow curve profile.

Table 2-4. Sludge Flow Curve Profile Using MV1 Geometry

Shear rate and time of measurement		
Up Curve	Hold	Down Curve
0 to 600 s^{-1} linearly in 5 min	600 s^{-1} for 1 min	600 to 0 s^{-1} linearly in 5 min

The resulting up and down flow curves were linearly regressed using the following rheological models:

(9) Newtonian: $\tau = \mu\dot{\gamma}$

(10) Bingham Plastic: $\tau = \tau_o + \eta_\infty\dot{\gamma}$

where:

$\tau = measured\ shear\ stress\ (Pa)$
$\mu = viscosity\ (Pa \cdot \mathrm{s})$
$\tau_o = Bingham\ Plastic\ Yield\ Stres\ (Pa)$
$\eta_\infty = plastic\ viscosity\ (Pa \cdot \mathrm{s})$
$\dot{\gamma} = shear\ rate\ (1/s)$

The average apparent viscosity at the maximum shear rate was defined as:

(11) Apparent Viscosity at maximum shear rate: $\eta_{600\ \mathrm{s}^{-1}} = \left(\frac{\tau}{\dot{\gamma}}\right)_{600\mathrm{s}^{-1}}$

2.3.5 *Method to Determine Average Velocity and Volumetric Flow Rate*

The flow rate in the gravity waste transfer lines was determined using the energy Equation 12.[11] This energy Equation assumes the flow is turbulent and this assumption will be verified.

(12) $\frac{P_1}{g\rho_1} + z_1 + \frac{V_1^2}{2g} = \frac{P_2}{g\rho_2} + z_2 + \frac{V_2^2}{2g} + h_L$

where:

$P_i = pressure\ (\frac{lbf}{ft^2})$
$\rho_i = fluid\ density\ (\frac{lbm}{ft^3})$
$z_i = elevation\ above\ a\ datum\ (ft)$
$V_i = average\ fluid\ velocity\ (\frac{ft}{s})$
$g = gavitational\ acceleration\ (\frac{ft}{s^2})$
$h_L = head\ losses(ft)$
$i = any\ two\ points\ in\ the\ hydraulic\ system$

The average fluid velocity and hydraulic radius are given as Equation 13 and 14 respectively.

(13) $V = \frac{\dot{Q}}{A}$

(14) $R = \frac{A}{P_w}$

where:

$R = hydraulic\ radius\ (ft)$
$A = cross - sectional\ area\ of\ flow\ (ft^2)$
$P_w = wetted\ perimeter\ (ft)$
$\dot{Q} = volumemetric\ flow\ rate\ (\frac{ft^3}{s})$

The head losses associated with the waste lines include entrance, piping, elbows, and exit losses. These losses are determined using the following Equations 15, 16, 17 and 18[11,12]:

(15) Entrance: $h_{entrance} = K_{entrance}\frac{V^2}{2g} = 0.5\frac{V^2}{2g}$

(16) Exit: $h_{exit} = K_{exit}\frac{V^2}{2g} = 1\frac{V^2}{2g}$

(17) Piping: $h_{piping} = f_T\frac{L}{R}\frac{V^2}{8g}$

(18) Elbow: $h_{elbow} = K_{elbow}\frac{V^2}{2g} = f_T K_{\frac{r}{d}}\frac{V^2}{2g}$

where:

$f_T = turbulent\ friction\ factor\ (unitless)$
$L = length\ of\ piping\ (ft)$
$K_{\frac{r}{d}} = constant\ for\ specific\ pipe\ \left(\frac{r}{d}\right)\ bend\ in\ turbulent\ flow\ (see\ page\ A-29)$[12]

The total frictional loss is the sum of the above losses and the results are shown in Equation 19.

(19) $h_L = 0.5\frac{V^2}{2g} + \frac{V^2}{2g} + \sum_{i=1}^{n} f_T K_{\frac{r}{d}i}\frac{V^2}{2g} + f_T\frac{L}{R}\frac{V^2}{8g} = 1.5\frac{V^2}{2g} + \sum_{i=1}^{n} f_T K_{\frac{r}{d}i}\frac{V^2}{2g} + f_T\frac{L}{4R}\frac{V^2}{2g}$

In the case of gravity flow, $P_1 \cong P_2$ since the pressure where the waste enters the header in Building 221-H and exiting into the H Pump Pit #5 or #6 are essentially the same. It is also assumed that the pipe is partially full and the inlet and outlet velocities are the same. The differences in inlet/outlet velocities would have little impact in the overall hydraulics of the system, due to the length of piping and other minor frictional losses. Additionally, the effect of air entrainment on the hydraulics of the system or filling of the pipe was ignored. The effect of air entrainment can drastically impact the hydraulics, reducing the flowrate.[13,14,15] Equation 12 reduces to Equation 20.

(20) $z_1 - z_2 = h_L = 1.5\frac{V^2}{2g} + \sum_{i=1}^{n} f_T K_{\frac{r}{d}i}\frac{V^2}{2g} + f_T\frac{L}{4R}\frac{V^2}{2g}$

The loss coefficients used above are for turbulent flow conditions and can be determined using Reynolds number (N_{RE}), Equation 21, and the flow is considered turbulent when N_{RE} is greater than 4,000.

(21) $N_{RE} = \frac{4V\rho R}{\mu}$

where:

$\rho = density\ of\ the\ fluid\ (\frac{lbm}{ft^3})$

$$\mu = fluid\ viscosity\left(\frac{lbm}{ft \cdot s}\right)$$

The Darcy-Weisbach friction factor for fully developed turbulent flow in conduit, f_T, can be determined using the Colebrook-White Equation for filled conduit, Equation 22.[11] This Equation was solved iteratively when coupled with Equation 20.

(22) $$\frac{1}{\sqrt{f_T}} = -2log\left(\frac{k}{14.8R} + \frac{2.51}{N_{RE}\sqrt{f_T}}\right)$$

(23) $$\frac{1}{\sqrt{f_T}} = -2log\left(\frac{k}{12R} + \frac{2.51}{N_{RE}\sqrt{f_T}}\right)$$

where:

$$k = pipe\ roughness\ (ft)$$

For a Reynolds number between the 2100 and 4000, the flow is considered transitional, where the friction factor cannot be explicitly determined as shown in the Moody diagram (Figure 2-2) for Newtonian fluids[16]. If the calculated Reynolds number is in the transitional or "critical" regime, the turbulent friction factor will be used since it will yield a lower flow rate.

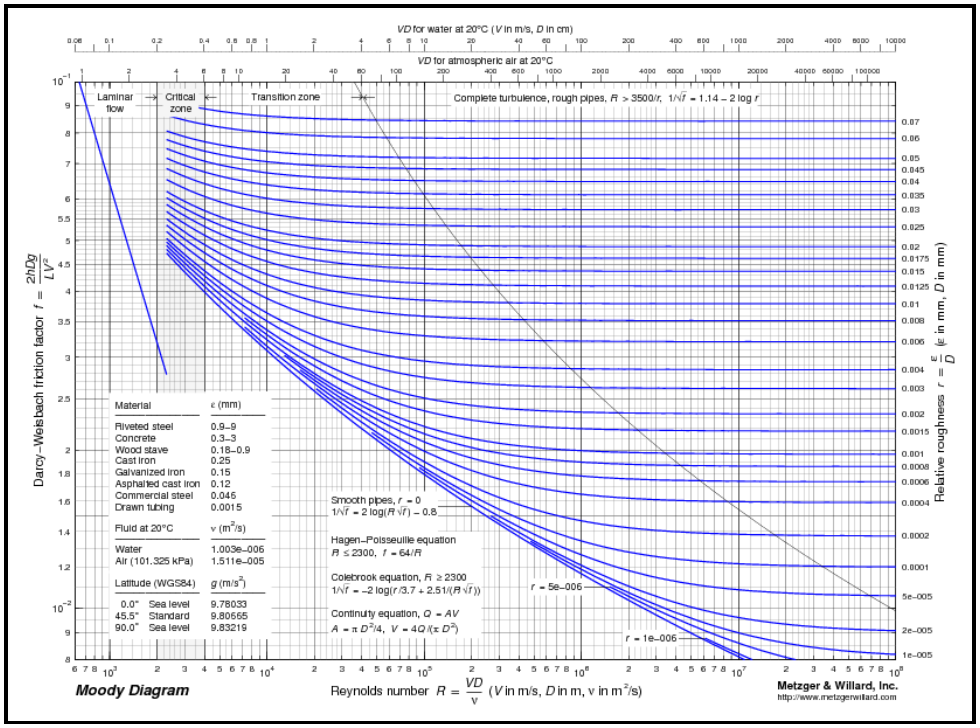

Figure 2-2. Moody Diagram

2.3.6 *Methods to Determine Non-Newtonian pipe frictional losses*

The slurries will be analyzed as a Bingham Plastic fluid. Two dimensionless parameters are required to further assess the pressure drop associated with this model and they are the Reynolds Bingham Number (Equation 24) and the Hedstrom number (Equation 25).

(24) $Re_B = \frac{4RV\rho}{\eta_\infty}$

(25) $He = \frac{16R^2\rho\tau_o}{\eta_\infty^2}$

For non-Newtonian flow, the pressure drop can be determined using the following relationship developed for a Bingham Plastic fluid.[17] Note that pipe roughness is not included in the turbulent term; hence, this calculated value could be lower than expected, but no correction will be performed. The laminar and turbulent friction factors are determined using Equations 26 and 27:

(26) $f_{BP-L} \approx \frac{16}{Re_B}\left[1 + \frac{He}{6Re}\right]\ (Laminar)$

(27) $f_{BP-T} = 10^a Re_B^b\ (Turbulent)$

where:

$f_{BP-L} = Bingham\ Plastic\ laminar\ friction\ factor$
$f_{BP-T} = Bingham\ Plastic\ Turbulent\ friction\ factor$
$a = -1.47\left[1 + 0.146e^{-2.9x10^{-5}\cdot He}\right]$
$b = -0.193$

The laminar and turbulent friction factor can be combined a single friction factor, Equation 28. Note the factor of 4. This is required to convert the Fanning friction factor to the Darcy friction factor which was used to determine the pressure drop.

(28) $f_{BP} = 4 \cdot (f_{BP-T}^m + f_{BP-L}^m)^{\left(\frac{1}{m}\right)}$

where: $m = 1.7 + \frac{40{,}000}{Re_B}$

Correcting the minor losses if the flow becomes laminar will not be performed. By not performing such a calculation, the calculated velocity will be larger since the loss coefficient is larger in laminar flow as compared to turbulent flow. Laminar minor loses can be determined using either the 2-K or 3-K method, though losses for very long radius elbows as those in these drain lines are not provided.[18]

2.3.7 *Impact of Partial Pipe Fill on Solids Suspension*

The previous calculations were based on the assumption that the pipe is full of fluid when determining the hydraulic losses for either a Newtonian or Bingham Plastic fluid. In this section, the velocity in various sections of horizontal piping is investigated to determine if the velocity is adequate to maintain the undissolved solids in suspension. The procedure consists of determining the height of fluid in the various sloped sections of piping and then using a simple correlation.

Assuming that the inlet/outlet and minor losses are ignored in sloped sections of piping and the fluid level is the same for a given pipe slope, Equation 19 reduces to Equation 29:

(29) $z_1 - z_2 = f_T \frac{L}{4R}\frac{V^2}{2g}\ (ft)$

Or solving for the slope of the pipe (S) we obtain Equation 30:

(30) $$S = \frac{z_1 - z_2}{L} = \frac{fT}{4R}\frac{V^2}{2g}\ (ft/ft)$$

The hydraulic radius for a partially filled (or full) pipe can be determined using Figure 2-3.

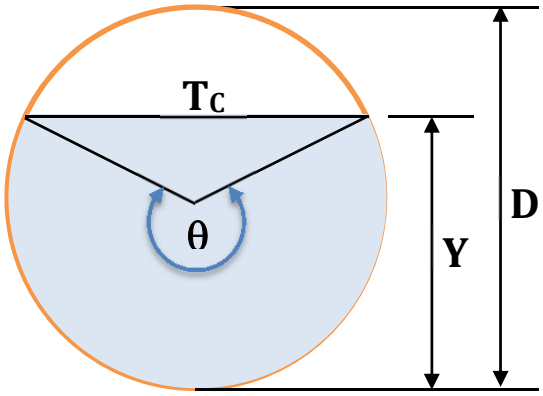

Figure 2-3. Partial Pipe Fill to Determine the Hydraulic Radius for a Given Fill Height

where:

D = diameter of pipe (ft)
Y = Fill Height (ft)
$F = Fill\ Factor = \frac{Y}{D}\ (dimensionless)$
$\theta = 2 \cdot acos(1 - 2 \cdot F)$ (radians)
$T_C = cord\ length\ at\ fill\ height = Dsin\left(\frac{\theta}{2}\right)$ (ft)
$A = cross\ sectional\ area\ of\ flow = \frac{D^2 \cdot (\theta - sin\theta)}{8}$ (ft^2)
$P_w = wetted\ perimeter = \frac{D \cdot \theta}{2}$ (ft)

The definition of the hydraulic radius is given by Equation 14 and substituting in the variables above yields Equation 31 which is the hydraulic radius for any pipe fill:

(31) $$R = \frac{\frac{D^2 \cdot (\theta - sin\theta)}{8}}{\frac{D \cdot \theta}{2}} = \frac{D \cdot (\theta - sin\theta)}{4 \cdot \theta}$$

The hydraulic radius is used in the energy Equation, Reynolds number, and friction coefficient. The friction factor for partially filled pipe for Newtonian fluids can be determined using Equation 23 and the non-Newtonian as previously described.

The energy Equation 30 in this case is solved using the goal seek option in EXCEL. The Newtonian frictional factor (Equation 23) is determined using eight iterations and the non-Newtonian friction factor is determined using Equation 28. Inputs for these calculations are the actual flowrate provided by the jet transfer pump, fluid properties, clean pipe roughness, and the pipe inside diameter.

2.3.8 *Determining Deposition Velocity and Sediment Transport*

The deposition velocity (i.e., velocity at which particles will settle out of the flow stream) will be determined assuming the particles are considered hard bodies (e.g., they are not considered flocculated material that contains interstitial fluids) and the particles are not cohesive. The assumption that these freshly made solids are hard bodies makes this calculation conservative, since the interstitial fluids would reduce the "average" density of the particle as determined using the light scattering results.

In gravity flow, the flow can be subcritical, critical or supercritical, based on the Froude number. At critical flow, Fr = 0, the specific energy is at a minimum and the velocity head is half the hydraulic depth of the channel for small slopes, but this condition is very unstable. When the channel slope is less than that for critical flow, the flow is considered subcritical (Fr < 1), resulting in a slower flow. When the channel slope is steeper than the critical slope, then the flow is faster.

The deposition velocity for open channel flow is shown in Equation 32.[16] The form of this equation is consistent with that used for completely filled piping used to transport non-cohesive solids, though the power coefficients maybe slightly different and other physical properties considered.[19]

(32) $$V_D = 1.833\left[\frac{8gR}{\rho}(\rho_S - \rho)\right]^{\frac{1}{2}}\left(\frac{d_{85}}{R}\right)^{0.158}\ \left(\frac{ft}{sec}\right)$$

where:

$V_D = deposition\ velocity$
$\rho_S = density\ of\ solid$
$d_{85} = particle\ size\ of\ the\ 85\%\ by\ volume$

Sediment transport is another model that can be used to determine how to treat the particulate material once it is in suspension and the mass flux of the particles in the flow. One of the methods is the Ackers and White model, which is based on a physical model for open channel transport process.[20,21] In this model, a dimensionless grain diameter d_{gr} is calculated (Equation 33) and if this value is between 1 and 60 the sediment is transported in suspension (as part of the fluid) and if it is greater than 60 the particles are considered coarse. If d_{gr} is less than 1, than this method does not apply since the solids tend to be cohesive and no calculation will be performed.

(33) $$d_{gr} = d_s\left[\frac{g\left(\frac{\rho_S}{\rho}-1\right)}{\nu^2}\right]^{\frac{1}{3}}\ (dimensionless)$$

(34) $$n' = 1.00 - 0.56\cdot\log\left(d_{gr}\right)\ (dimensionless)$$

(35) $$A' = \frac{0.23}{d_{gr}^{0.5}} + 0.14\ (dimensionless)$$

(36) $$m' = \frac{6.83}{d_{gr}} + 1.67\ \ (dimensionless)$$

(37) $$C = 10^{a'}\ (\mathrm{N})\ (dimensionless)$$

(38) $$a' = 2.79log\left(d_{gr}\right) - \left(log\left(d_{gr}\right)\right)^2 - 3.46\ \ (dimensionless)$$

(39) $$u_* = (g d_h S)^{0.5} \ (\frac{ft}{\sec})$$

(40) $$F = \frac{u_*^{n'}}{\left[g d_s\left(\frac{\rho_S}{\rho}-1\right)\right]^{0.5}} \cdot \left[\frac{V}{5.66 \cdot log\left(\frac{10 d_h}{d_s}\right)}\right]^{1-n} \quad (dimensionless)$$

(41) $$G = C\left(\frac{F}{A'} - 1\right)^{m'} \quad (dimensionless)$$

(42) $$X = G \cdot \frac{\rho_S}{\rho} \cdot \frac{d_s}{d_h} \cdot \left(\frac{V}{u_*}\right)^{n'} \ (\frac{lbm}{lbm})$$

where:

$d_{gr} = dimensionless\ grain\ diameter$
$n',\ A',\ m',\ C,\ a' = variou\ parameters$
$u_* = shear\ or\ friction\ velocity$
$F = Particle\ Mobility$
$G = dimensionless\ sediment\ transport\ function$
$X =$ mass of sediment transported per unit mass of fluid flow

Review of the piping drawings[22,23,24,25,26,27,28] for the waste transfer line (or waste headers) between Building 221-H and HPP#5 or HPP#6 are summarized in Table 2-5 for the data necessary to evaluate Equation 12. The waste lines running parallel to the east wall of Building 221-H consists of 10-inch headers that reduce to 3-inch schedule 40 pipe in at the transition box next to Section 4 of the building and finally discharging into HPP#5 or HPP#6. Lines WF1100 (WH#1, HL-1), WF1101 (WH#4, LL-4), and WF1102 (WH#3, LL-3) have vertical drops that occur at the transition box Building 221-H. There is no vertical drop in the 3-inch line after leaving the 10-inch header for WF1103 (WH#2, HL-2), hence this flow circuit has the lowest driving head. The slopes (vertical/horizontal distances) in the all the transfer lines has a minimum of 0.005 and a maximum of 0.29. The minimum slope was specified in reference 29.

Table 2-5. Complete Elevation, Piping Run, Elbows, Entrance and Exit Data for Waste Transfer Line between Building 221-H to HPP#5 and HPP#6

Variable		Units	Pipe Number (221-H High & Low Level Waste Header Number/ Outside Pipe or Line Number) and discharge HPP			
			(HL-1 / WF1100) HPP#6	(LL-4 / WF1101) HPP#5	(LL-3 / WF1102) HPP#5	(HL-2 / WF1103) HPP#6
Elevation Difference	$z_1 - z_2$	feet	17.1	15.3	13.9	12.8
Piping	L	feet	750.5	780.4	778.5	746.2
Entrance	$K_{entrance}$	unitless	1	1	1	1
Elbows	r/d	$K_{\frac{r}{d}}$ (unitless)	Number of elbows			
	15	40	2	2	2	1
	21	50	3	3	3	3
	2	12	1	0	0	1
	5	17	0	1	1	0
Exit	K_{exit}	unitless	1	1	1	1

All the transfer lines leaving Building 221-H initially have a slope of 0.005 and a calculation was performed to determine the velocity that this section of piping can handle. Table 2-6 provides the various lengths of piping and fittings associated with this initial section of the waste header.

Table 2-6. Initial Elevation Drop and 0.005 Sloped Piping Run, Elbows, Entrance for Waste Transfer Exiting Building 221-H

Variable		Units	Pipe Number (221-H Waste Header/ Outside Line Number) and discharge HPP			
			(HL-1 / WF1100) HPP#6	(LL-4 / WF1101) HPP#5	(LL-3 / WF1102) HPP#5	(HL-2 / WF1103) HPP#6
Elevation Difference	$z_1 - z_2$	feet	4.91	3.12	1.71	0.64
Piping	L	feet	115.5	112.2	112.3	111.2
Entrance	$K_{entrance}$	unitless	1	1	1	1
Elbows	r/d	$K_{\frac{r}{d}}$ (unitless)	Number of elbows			
	15	40	2	2	2	1
	21	50	1	1	1	1

The waste generated in Building 221-H is transferred to the 10-inch header using an S-2 steam jet[30], which can supply flow up to 30 gallon per minute (gpm).[30] The nominal flow rate provided by the S-2 steam jet is typically around 25 gpm.

Calculations for both the complete hydraulic system and that of the initial sloped section were calculated. The pipe roughness used in the calculations for a clean pipe (k = 0.00015 ft) is about 44 times smaller than for a rusted pipe (k = 0.00667 ft).[31] The pipe roughness for a rusted pipe was selected based on discussion with R. Eubanks on the operations of this header, where flushing after each transfer is not

normally performed. The actual roughness is not known for these transfer lines, but this example shows the impact that potential material buildup can have on flow.

Water and a limiting dissolver fluid (highest viscosity / lowest density) were used in the calculations to determine the velocity, Reynolds number, and flow rate. These water calculations provide an upper bound to flow rates. For the 12,000 L batched slurries that have significant non-Newtonian properties, their rheological data as well as their Newtonian fit to the flow curve will be used to determine this parameters.

Table 2-7 is a summary of the various sections of sloped piping leaving Building 221-H that are greater than 40 feet in length and their respective slopes. Slopes of 0.005 and 0.0268 ft/ft will be used in calculations to determine the velocity, fill ratio, and Reynolds number for all the characterized fluids.

Table 2-7. Sloped Piping Run

Sloped Piping Run			(HL-1 / WF1100) HPP#6	(LL-4 / WF1101) HPP#5	(LL-3 / WF1102) HPP#5	(HL-2 / WF1103) HPP#6
1	Length	ft	43.77	42.27	42.27	42.27
	Slope	ft/ft	0.0050	0.0054	0.0054	0.0054
2	Length	ft	58.25	58.25	59.75	59.75
	Slope	ft/ft	0.0050	0.0050	0.0050	0.0050
3	Length	ft	206	206	206	206
	Slope	ft/ft	0.0268	0.0268	0.0268	0.0268
4	Length	ft	177.5	177.5	179	179
	Slope	ft/ft	0.0134	0.0134	0.0131	0.0131
5	Length	ft	91.42	91.42	92.92	92.92
	Slope	ft/ft	0.0135	0.0135	0.0131	0.0131
6	Length	ft	113.08	113.08	111.08	111.08
	Slope	ft/ft	0.0150	0.0150	0.0050	0.0050
7	Length	ft	47	47	46	46
	Slope	ft/ft	0.0155	0.0155	0.0050	0.0050

2.4 Quality Assurance

Requirements for performing reviews of technical reports and the extent of review are established in manual E7 2.60. SRNL documents the extent and type of review using the SRNL Technical Report Design Checklist contained in WSRC-IM-2002-00011, Rev. 2.

3.0 Results and Discussion

3.1 Surface Area Calculations[1]

Before any off-gas generation calculations can be performed for the dissolution of various UNF assemblies in the H-Canyon dissolvers, surface area calculations per unit height need to be performed for

[1] HMI was originally selected for evaluation but was subsequently removed from planned dissolving recipes.

the L-Bundle into which the various UNF assemblies are placed. Table 3-1 shows the total surface area (inside and outside) values for the L-Bundle along with the SRE, HMI[32], and DR-3 assemblies.[2] The yellow row in Table 3-1 represents a 54 inch (4.5 ft) immersion into the dissolver and the pink row represents the approximate maximum height (11 ft) inside the L-Bundle for placing the UNF assemblies. For comparison, the MURR and L-Bundle Total Surface Area (inside and outside) values from a previous calculation[33] are shown in Table 3-1. Table 3-1 plots the total surface area data from and shows that the MURR assembly from prior dissolver campaigns has a much higher surface area per unit height value than the SRE, HMI, and DR-3 assemblies.

In a prior report for the dissolution of the MURR assemblies[34] it was shown that the total surface areas (inside and outside) of the L-Bundle and the MURR assemblies should not be used in off-gas generation calculations as actual plant data shows that the vacuum system was not overwhelmed by the dissolving of the MURR assemblies. As stated in the prior report this restriction of only using the outer surface areas is due to mass transfer limitations of nitric acid and mercury to the metal surfaces, heat transfer from the surfaces due to heat of dissolution, and the large amount of gas generated and associated bubbles at the surfaces. Since the external shape and size of the MURR assembly is comparable to the external shape and size of the SRE, HMI, and DR-3 assemblies, the same assumption for using only the outer surfaces also applies. In addition, the prior report for the MURR assemblies assumed that the peak off-gas rates for the L-Bundle and MURR assemblies occur at different times. In other words, the outer surface area of the L-Bundle is the primary contributor to the off-gas generation until it dissolves exposing the outer surface area of the assembly, which then becomes the primary off-gas contributor. Following these assumptions, only the outer surface areas of the L-Bundle and the appropriate surface areas of the new UNF assemblies (SRE, HMI, and DR-3) that were used in the off-gas calculations are shown in Table 3-2.

The details of the surface area calculations for the Disassembly L-Area Bundling Tube along with the SRE, HMI, and DR-3 (Denmark Reactor) assemblies are shown in Appendix A.

Table 3-1. L-Bundle and UNF Assemblies Total Surface Areas per Immersion Height

Assembly Immersion Depth [ft]	MURR & L-Bundle Total Surface Area [ft^2]	Outer SRE & L-Bundle Total Surface Area [ft^2]	Outer & Inner SRE & L-Bundle Total Surface Area [ft^2]	HMI-Std & L-Bundle Total Surface Area [ft^2]	HMI-Ctrl & L-Bundle Total Surface Area [ft^2]	DR-3-1 & L-Bundle Total Surface Area [ft^2]	DR-3-2 & L-Bundle Total Surface Area [ft^2]
0.000	0.77	0.65	0.65	0.65	0.65	0.65	0.65
0.083	1.74	1.13	1.15	1.16	1.16	1.23	1.23
0.167	3.16	1.42	1.45	1.47	1.54	1.58	1.58
0.250	4.57	1.71	1.75	1.77	1.84	1.93	1.93
0.333	5.99	2.00	2.06	2.08	2.14	2.28	2.28
0.417	7.41	2.29	2.36	2.38	2.45	2.64	2.64
0.500	8.83	2.59	2.66	2.69	2.75	2.99	2.99
0.583	10.25	2.88	2.96	2.99	3.06	3.34	3.34
0.667	11.66	3.17	3.26	3.29	3.36	3.69	3.69
0.750	13.08	3.46	3.56	3.60	3.67	4.04	4.04
0.833	14.50	3.76	3.87	3.90	3.97	4.40	4.40
0.917	15.92	4.05	4.17	4.21	4.27	4.75	4.75
1.000	17.34	4.34	4.47	4.51	4.58	5.10	5.10
1.083	18.76	4.63	4.77	4.82	4.88	5.45	5.45
1.167	20.17	4.92	5.07	5.12	5.19	5.80	5.80

Table 3-1. L-Bundle and UNF Assemblies Total Surface Areas per Immersion Height

Assembly Immersion Depth [ft]	MURR & L-Bundle Total Surface Area [ft^2]	Outer SRE & L-Bundle Total Surface Area [ft^2]	Outer & Inner SRE & L-Bundle Total Surface Area [ft^2]	HMI-Std & L-Bundle Total Surface Area [ft^2]	HMI-Ctrl & L-Bundle Total Surface Area [ft^2]	DR-3-1 & L-Bundle Total Surface Area [ft^2]	DR-3-2 & L-Bundle Total Surface Area [ft^2]
1.250	21.59	5.22	5.37	5.42	5.49	6.16	6.16
1.333	23.01	5.51	5.68	5.73	5.79	6.51	6.51
1.417	24.43	5.80	5.98	6.03	6.10	6.86	6.86
1.500	25.85	6.09	6.28	6.34	6.40	7.21	7.21
1.583	27.27	6.39	6.58	6.64	6.71	7.56	7.56
1.667	28.68	6.68	6.88	6.95	7.01	7.92	7.92
1.750	30.10	6.97	7.18	7.25	7.32	8.27	8.27
1.833	31.52	7.26	7.49	7.55	7.62	8.62	8.62
1.917	32.94	7.56	7.79	7.86	7.92	8.97	8.97
2.000	34.36	7.85	8.09	8.16	8.23	9.32	9.32
2.083	35.77	8.14	8.39	8.47	8.53	9.74	9.68
2.167	37.22	8.43	8.69	8.79	8.84	10.10	10.03
2.250	37.63	8.72	8.99	9.23	9.14	10.51	10.36
2.333	38.59	9.02	9.30	9.54	9.45	10.86	10.86
2.417	40.01	9.31	9.60	9.84	9.74	11.21	11.21
2.500	41.43	9.60	9.90	10.15	10.01	11.56	11.56
2.583	42.85	9.89	10.20	10.45	10.36	11.91	11.91
2.667	44.27	10.19	10.50	10.75	10.74	12.27	12.27
2.750	45.68	10.48	10.80	11.06	11.07	12.62	12.62
2.833	47.10	10.77	11.11	11.36	11.37	12.97	12.97
2.917	48.52	11.06	11.41	11.67	11.67	13.32	13.32
3.000	49.94	11.35	11.71	11.97	11.98	13.67	13.67
3.083	51.36	11.65	12.01	12.28	12.28	14.03	14.03
3.167	52.77	11.94	12.31	12.58	12.59	14.38	14.38
3.250	54.19	12.23	12.61	12.88	12.89	14.73	14.73
3.333	55.61	12.52	12.91	13.19	13.20	15.08	15.08
3.417	57.03	12.82	13.22	13.49	13.50	15.43	15.43
3.500	58.45	13.11	13.52	13.80	13.80	15.79	15.79
3.583	59.87	13.40	13.82	14.10	14.11	16.14	16.14
3.667	61.28	13.69	14.12	14.41	14.41	16.49	16.49
3.750	62.70	13.98	14.42	14.71	14.72	16.84	16.84
3.833	64.12	14.28	14.72	15.01	15.02	17.19	17.19
3.917	65.54	14.57	15.03	15.32	15.32	17.55	17.55
4.000	66.96	14.86	15.33	15.62	15.63	17.90	17.90
4.083	68.37	15.15	15.63	15.93	15.93	18.25	18.25
4.167	69.79	15.45	15.93	16.23	16.24	18.55	18.60
4.250	71.21	15.74	16.23	16.54	16.54	18.92	18.95
4.333	72.63	16.03	16.53	16.80	16.85	19.38	19.31

Table 3-1. L-Bundle and UNF Assemblies Total Surface Areas per Immersion Height

Assembly Immersion Depth [ft]	MURR & L-Bundle Total Surface Area [ft^2]	Outer SRE & L-Bundle Total Surface Area [ft^2]	Outer & Inner SRE & L-Bundle Total Surface Area [ft^2]	HMI-Std & L-Bundle Total Surface Area [ft^2]	HMI-Ctrl & L-Bundle Total Surface Area [ft^2]	DR-3-1 & L-Bundle Total Surface Area [ft^2]	DR-3-2 & L-Bundle Total Surface Area [ft^2]
4.417	74.08	16.32	16.84	17.25	17.15	19.73	19.60
4.500	74.48	16.61	17.14	17.55	17.45	20.08	19.94
4.583	75.45	16.91	17.46	17.86	17.76	20.43	20.43
4.667	76.87	17.20	17.81	18.16	18.06	20.79	20.79
4.750	78.28	17.49	17.49	18.46	18.37	21.14	21.14
4.833	79.70	17.78	17.78	18.77	18.67	21.49	21.49
4.917	81.12	18.08	18.08	19.07	18.98	21.84	21.84
5.000	82.54	18.37	18.37	19.38	19.25	22.19	22.19
5.083	83.96	18.66	18.66	19.68	19.57	22.55	22.55
5.167	85.38	18.95	18.95	19.99	19.94	22.90	22.90
5.250	86.79	19.25	19.25	20.29	20.29	23.25	23.25
5.333	88.21	19.54	19.54	20.59	20.60	23.60	23.60
5.417	89.63	19.83	19.83	20.90	20.90	23.95	23.95
5.500	91.05	20.12	20.12	21.20	21.20	24.31	24.31
5.583	92.47	20.41	20.41	21.51	21.51	24.66	24.66
5.667	93.88	20.71	20.71	21.81	21.81	25.01	25.01
5.750	95.30	21.00	21.00	22.12	22.12	25.36	25.36
5.833	96.72	21.29	21.29	22.42	22.42	25.71	25.71
5.917	98.14	21.58	21.58	22.72	22.72	26.07	26.07
6.000	99.56	21.88	21.88	23.03	23.03	26.42	26.42
6.083	100.98	22.17	22.17	23.33	23.33	26.77	26.77
6.167	102.39	22.46	22.46	23.64	23.64	27.12	27.12
6.250	103.81	22.75	22.75	23.94	23.94	27.47	27.47
6.333	105.23	23.04	23.04	24.25	24.25	27.80	27.83
6.417	106.65	23.34	23.34	24.55	24.55	28.10	28.18
6.500	108.07	23.63	23.63	24.82	24.85	28.60	28.53
6.583	109.48	23.92	23.92	25.26	25.16	28.95	28.88
6.667	110.94	24.21	24.21	25.57	25.46	29.31	29.18
6.750	111.34	24.51	24.51	25.87	25.77	29.66	29.53
6.833	112.31	24.80	24.80	26.17	26.07	30.01	30.01
6.917	113.73	25.09	25.09	26.48	26.38	30.36	30.36
7.000	115.14	25.38	25.38	26.78	26.68	30.71	30.71
7.083	116.56	25.67	25.67	27.09	26.98	31.07	31.07
7.167	117.98	25.97	25.97	27.39	27.29	31.42	31.42
7.250	119.40	26.26	26.26	27.70	27.59	31.77	31.77
7.333	120.82	26.55	26.55	28.00	27.90	32.12	32.12
7.417	122.24	26.84	26.84	28.30	28.21	32.47	32.47
7.500	123.65	27.14	27.14	28.61	28.49	32.83	32.83

Table 3-1. L-Bundle and UNF Assemblies Total Surface Areas per Immersion Height

Assembly Immersion Depth [ft]	MURR & L-Bundle Total Surface Area [ft^2]	Outer SRE & L-Bundle Total Surface Area [ft^2]	Outer & Inner SRE & L-Bundle Total Surface Area [ft^2]	HMI-Std & L-Bundle Total Surface Area [ft^2]	HMI-Ctrl & L-Bundle Total Surface Area [ft^2]	DR-3-1 & L-Bundle Total Surface Area [ft^2]	DR-3-2 & L-Bundle Total Surface Area [ft^2]
7.583	125.07	27.43	27.43	28.91	28.78	33.18	33.18
7.667	126.49	27.72	27.72	29.22	29.14	33.53	33.53
7.750	127.91	28.01	28.01	29.52	29.52	33.88	33.88
7.833	129.33	28.31	28.31	29.83	29.82	34.23	34.23
7.917	130.74	28.60	28.60	30.13	30.12	34.59	34.59
8.000	132.16	28.89	28.89	30.43	30.43	34.94	34.94
8.083	133.58	29.18	29.18	30.74	30.73	35.29	35.29
8.167	135.00	29.47	29.47	31.04	31.04	35.64	35.64
8.250	136.42	29.77	29.77	31.35	31.34	35.99	35.99
8.333	137.84	30.06	30.06	31.65	31.65	36.35	36.35
8.417	139.25	30.35	30.35	31.96	31.95	36.70	36.70
8.500	140.67	30.64	30.64	32.26	32.25	37.06	37.05
8.583	142.09	30.94	30.94	32.56	32.56	37.43	37.40
8.667	143.51	31.23	31.23	32.83	32.86	37.83	37.75
8.750	144.93	31.55	31.55	33.28	33.17	38.18	38.10
8.833	146.35	31.81	31.81	33.58	33.47	38.53	38.46
8.917	147.80	32.07	32.07	33.88	33.78	38.88	38.76
9.000	148.16	32.36	32.36	34.19	34.08	39.23	39.11
9.083	148.37	32.60	32.60	34.49	34.38	39.59	39.57
9.167	148.59	32.84	32.84	34.80	34.69	39.94	39.92
9.250	148.80			35.10	34.99	40.29	40.27
9.333	149.02			35.41	35.30	40.64	40.62
9.417	149.23			35.71	35.60	40.99	40.97
9.500	149.45			36.01	35.91	41.35	41.32
9.583	149.66			36.32	36.21	41.70	41.68
9.667	149.88			36.62	36.51	42.05	42.03
9.750	150.10			36.93	36.82	42.40	42.38
9.833	150.31			37.23	37.12	42.75	42.73
9.917	150.53			37.54	37.43	43.11	43.08
10.000	150.74			37.84	37.72	43.46	43.44
10.083	150.96			38.14	37.99	43.81	43.79
10.167	151.17			38.45		44.16	44.14
10.250	151.39			38.75		44.51	44.49
10.333	151.60			39.06			44.84
10.417	151.82			39.36			45.20
10.500	152.03			39.67			45.55
10.583	152.25			39.97			45.90
10.667	152.46			40.27			46.25

Table 3-1. L-Bundle and UNF Assemblies Total Surface Areas per Immersion Height

Assembly Immersion Depth [ft]	MURR & L-Bundle Total Surface Area [ft^2]	Outer SRE & L-Bundle Total Surface Area [ft^2]	Outer & Inner SRE & L-Bundle Total Surface Area [ft^2]	HMI-Std & L-Bundle Total Surface Area [ft^2]	HMI-Ctrl & L-Bundle Total Surface Area [ft^2]	DR-3-1 & L-Bundle Total Surface Area [ft^2]	DR-3-2 & L-Bundle Total Surface Area [ft^2]
10.750	152.68			40.58			46.60
10.833	152.89			40.85			46.96
10.917	153.11						
11.000	153.33						

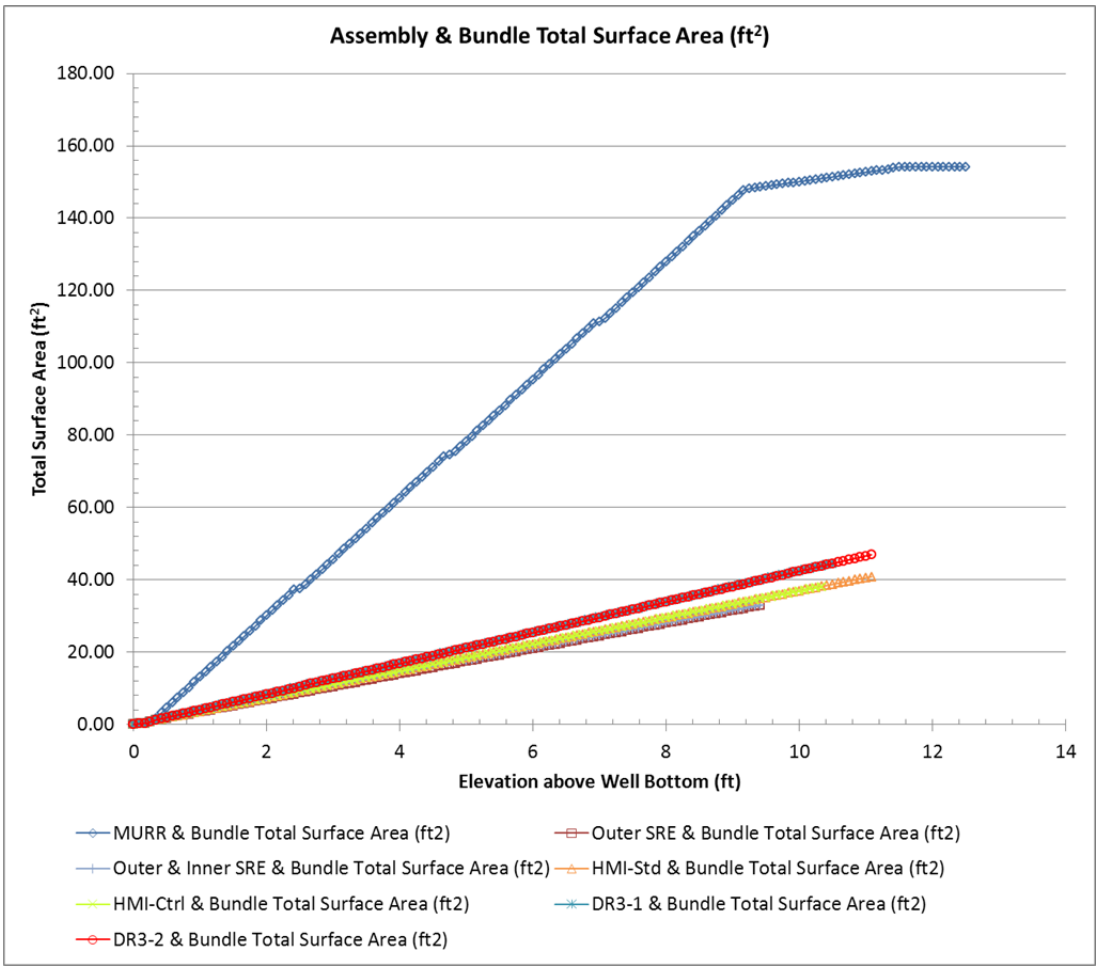

Figure 3-1. L-Bundle and Various UNF Assemblies Total Surface Areas per Immersion Height

Table 3-2. L-Bundle and UNF Assemblies Surface Areas per Immersion Height for Off-gas Calculations

Assembly Immersion Depth [ft]	L-Bundle Outer Surface Area (ft^2)	Outer SRE Surface Area (ft^2)	Inner SRE Surface Area (ft^2)	HMI-Std Surface Area (ft^2)	HMI-Ctrl Surface Area (ft^2)	DR-3-1 Surface Area (ft^2)	DR-3-2 Surface Area (ft^2)

Table 3-2. L-Bundle and UNF Assemblies Surface Areas per Immersion Height for Off-gas Calculations

Assembly Immersion Depth [ft]	L-Bundle Outer Surface Area (ft^2)	Outer SRE Surface Area (ft^2)	Inner SRE Surface Area (ft^2)	HMI-Std Surface Area (ft^2)	HMI-Ctrl Surface Area (ft^2)	DR-3-1 Surface Area (ft^2)	DR-3-2 Surface Area (ft^2)
0.000	0.44	0.00	0.00	0.00	0.00	0.00	0.00
0.083	0.67	0.13	0.03	0.17	0.17	0.24	0.24
0.167	0.78	0.21	0.04	0.26	0.33	0.37	0.37
0.250	0.89	0.29	0.04	0.35	0.42	0.51	0.51
0.333	1.00	0.36	0.05	0.44	0.50	0.65	0.65
0.417	1.11	0.44	0.06	0.53	0.59	0.78	0.78
0.500	1.22	0.52	0.07	0.61	0.68	0.92	0.92
0.583	1.33	0.59	0.08	0.70	0.77	1.05	1.05
0.667	1.44	0.67	0.09	0.79	0.86	1.19	1.19
0.750	1.55	0.74	0.10	0.88	0.95	1.33	1.33
0.833	1.65	0.82	0.11	0.97	1.03	1.46	1.46
0.917	1.76	0.90	0.12	1.06	1.12	1.60	1.60
1.000	1.87	0.97	0.13	1.14	1.21	1.73	1.73
1.083	1.98	1.05	0.14	1.23	1.30	1.87	1.87
1.167	2.09	1.13	0.15	1.32	1.39	2.01	2.01
1.250	2.20	1.20	0.16	1.41	1.48	2.14	2.14
1.333	2.31	1.28	0.17	1.50	1.56	2.28	2.28
1.417	2.42	1.36	0.18	1.59	1.65	2.41	2.41
1.500	2.53	1.43	0.19	1.67	1.74	2.55	2.55
1.583	2.64	1.51	0.19	1.76	1.83	2.69	2.69
1.667	2.75	1.58	0.20	1.85	1.92	2.82	2.82
1.750	2.85	1.66	0.21	1.94	2.01	2.96	2.96
1.833	2.96	1.74	0.22	2.03	2.09	3.09	3.09
1.917	3.07	1.81	0.23	2.12	2.18	3.23	3.23
2.000	3.18	1.89	0.24	2.20	2.27	3.37	3.37
2.083	3.29	1.97	0.25	2.29	2.36	3.56	3.50
2.167	3.40	2.04	0.26	2.40	2.45	3.71	3.64
2.250	3.51	2.12	0.27	2.63	2.54	3.90	3.75
2.333	3.62	2.19	0.28	2.72	2.62	4.04	4.04
2.417	3.73	2.27	0.29	2.80	2.71	4.17	4.17
2.500	3.84	2.35	0.30	2.89	2.76	4.31	4.31
2.583	3.95	2.42	0.31	2.98	2.89	4.45	4.45
2.667	4.05	2.50	0.32	3.07	3.05	4.58	4.58
2.750	4.16	2.58	0.33	3.16	3.16	4.72	4.72
2.833	4.27	2.65	0.34	3.25	3.25	4.85	4.85
2.917	4.38	2.73	0.34	3.33	3.34	4.99	4.99
3.000	4.49	2.81	0.35	3.42	3.43	5.13	5.13
3.083	4.60	2.88	0.36	3.51	3.52	5.26	5.26

Table 3-2. L-Bundle and UNF Assemblies Surface Areas per Immersion Height for Off-gas Calculations

Assembly Immersion Depth [ft]	L-Bundle Outer Surface Area (ft^2)	Outer SRE Surface Area (ft^2)	Inner SRE Surface Area (ft^2)	HMI-Std Surface Area (ft^2)	HMI-Ctrl Surface Area (ft^2)	DR-3-1 Surface Area (ft^2)	DR-3-2 Surface Area (ft^2)
3.167	4.71	2.96	0.37	3.60	3.61	5.40	5.40
3.250	4.82	3.03	0.38	3.69	3.69	5.53	5.53
3.333	4.93	3.11	0.39	3.78	3.78	5.67	5.67
3.417	5.04	3.19	0.40	3.87	3.87	5.81	5.81
3.500	5.15	3.26	0.41	3.95	3.96	5.94	5.94
3.583	5.25	3.34	0.42	4.04	4.05	6.08	6.08
3.667	5.36	3.42	0.43	4.13	4.14	6.21	6.21
3.750	5.47	3.49	0.44	4.22	4.22	6.35	6.35
3.833	5.58	3.57	0.45	4.31	4.31	6.49	6.49
3.917	5.69	3.65	0.46	4.40	4.40	6.62	6.62
4.000	5.80	3.72	0.47	4.48	4.49	6.76	6.76
4.083	5.91	3.80	0.48	4.57	4.58	6.89	6.89
4.167	6.02	3.87	0.49	4.66	4.67	6.98	7.03
4.250	6.13	3.95	0.49	4.75	4.75	7.13	7.17
4.333	6.24	4.03	0.50	4.80	4.84	7.38	7.30
4.417	6.35	4.10	0.51	5.03	4.93	7.51	7.39
4.500	6.45	4.18	0.52	5.12	5.02	7.65	7.51
4.583	6.56	4.26	0.55	5.21	5.11	7.78	7.78
4.667	6.67	4.33	0.61	5.29	5.20	7.92	7.92
4.750	6.78	4.41	0.00	5.38	5.29	8.06	8.06
4.833	6.89	4.49	0.00	5.47	5.37	8.19	8.19
4.917	7.00	4.56	0.00	5.56	5.46	8.33	8.33
5.000	7.11	4.64	0.00	5.65	5.52	8.46	8.46
5.083	7.22	4.71	0.00	5.74	5.62	8.60	8.60
5.167	7.33	4.79	0.00	5.82	5.78	8.74	8.74
5.250	7.44	4.87	0.00	5.91	5.91	8.87	8.87
5.333	7.55	4.94	0.00	6.00	6.00	9.01	9.01
5.417	7.65	5.02	0.00	6.09	6.09	9.14	9.14
5.500	7.76	5.10	0.00	6.18	6.18	9.28	9.28
5.583	7.87	5.17	0.00	6.27	6.27	9.42	9.42
5.667	7.98	5.25	0.00	6.35	6.35	9.55	9.55
5.750	8.09	5.33	0.00	6.44	6.44	9.69	9.69
5.833	8.20	5.40	0.00	6.53	6.53	9.82	9.82
5.917	8.31	5.48	0.00	6.62	6.62	9.96	9.96
6.000	8.42	5.55	0.00	6.71	6.71	10.10	10.10
6.083	8.53	5.63	0.00	6.80	6.80	10.23	10.23
6.167	8.64	5.71	0.00	6.88	6.89	10.37	10.37
6.250	8.75	5.78	0.00	6.97	6.97	10.50	10.50

Table 3-2. L-Bundle and UNF Assemblies Surface Areas per Immersion Height for Off-gas Calculations

Assembly Immersion Depth [ft]	L-Bundle Outer Surface Area (ft^2)	Outer SRE Surface Area (ft^2)	Inner SRE Surface Area (ft^2)	HMI-Std Surface Area (ft^2)	HMI-Ctrl Surface Area (ft^2)	DR-3-1 Surface Area (ft^2)	DR-3-2 Surface Area (ft^2)
6.333	8.85	5.86	0.00	7.06	7.06	10.62	10.64
6.417	8.96	5.94	0.00	7.15	7.15	10.70	10.78
6.500	9.07	6.01	0.00	7.20	7.24	10.99	10.91
6.583	9.18	6.09	0.00	7.43	7.33	11.12	11.05
6.667	9.29	6.17	0.00	7.52	7.42	11.26	11.13
6.750	9.40	6.24	0.00	7.61	7.50	11.39	11.26
6.833	9.51	6.32	0.00	7.69	7.59	11.53	11.53
6.917	9.62	6.39	0.00	7.78	7.68	11.67	11.67
7.000	9.73	6.47	0.00	7.87	7.77	11.80	11.80
7.083	9.84	6.55	0.00	7.96	7.86	11.94	11.94
7.167	9.95	6.62	0.00	8.05	7.95	12.07	12.07
7.250	10.05	6.70	0.00	8.14	8.03	12.21	12.21
7.333	10.16	6.78	0.00	8.22	8.12	12.35	12.35
7.417	10.27	6.85	0.00	8.31	8.22	12.48	12.48
7.500	10.38	6.93	0.00	8.40	8.28	12.62	12.62
7.583	10.49	7.01	0.00	8.49	8.35	12.75	12.75
7.667	10.60	7.08	0.00	8.58	8.51	12.89	12.89
7.750	10.71	7.16	0.00	8.67	8.66	13.03	13.03
7.833	10.82	7.23	0.00	8.75	8.75	13.16	13.16
7.917	10.93	7.31	0.00	8.84	8.84	13.30	13.30
8.000	11.04	7.39	0.00	8.93	8.93	13.43	13.43
8.083	11.15	7.46	0.00	9.02	9.02	13.57	13.57
8.167	11.25	7.54	0.00	9.11	9.10	13.71	13.71
8.250	11.36	7.62	0.00	9.20	9.19	13.84	13.84
8.333	11.47	7.69	0.00	9.29	9.28	13.98	13.98
8.417	11.58	7.77	0.00	9.37	9.37	14.12	14.12
8.500	11.69	7.85	0.00	9.46	9.46	14.26	14.25
8.583	11.80	7.92	0.00	9.55	9.55	14.41	14.39
8.667	11.91	8.00	0.00	9.60	9.63	14.60	14.52
8.750	12.02	8.11	0.00	9.83	9.72	14.73	14.66
8.833	12.13	8.15	0.00	9.92	9.81	14.87	14.80
8.917	12.24	8.19	0.00	10.01	9.90	15.00	14.88
9.000	12.35	8.27	0.00	10.10	9.99	15.14	15.02
9.083	12.45	8.29	0.00	10.18	10.08	15.28	15.26
9.167	12.56	8.32	0.00	10.27	10.16	15.41	15.39
9.250	12.67			10.36	10.25	15.55	15.53
9.333	12.78			10.45	10.34	15.68	15.66
9.417	12.89			10.54	10.43	15.82	15.80

Table 3-2. L-Bundle and UNF Assemblies Surface Areas per Immersion Height for Off-gas Calculations

Assembly Immersion Depth [ft]	L-Bundle Outer Surface Area (ft^2)	Outer SRE Surface Area (ft^2)	Inner SRE Surface Area (ft^2)	HMI-Std Surface Area (ft^2)	HMI-Ctrl Surface Area (ft^2)	DR-3-1 Surface Area (ft^2)	DR-3-2 Surface Area (ft^2)
9.500	13.00			10.63	10.52	15.96	15.94
9.583	13.11			10.71	10.61	16.09	16.07
9.667	13.22			10.80	10.69	16.23	16.21
9.750	13.33			10.89	10.78	16.37	16.34
9.833	13.44			10.98	10.87	16.50	16.48
9.917	13.54			11.07	10.96	16.64	16.62
10.000	13.65			11.16	11.04	16.77	16.75
10.083	13.76			11.24	11.09	16.91	16.89
10.167	13.87			11.33		17.05	17.02
10.250	13.98			11.42		17.18	17.16
10.333	14.09			11.51		17.32	17.30
10.417	14.20			11.60		17.45	17.43
10.500	14.31			11.69		17.59	17.57
10.583	14.42			11.77		17.67	17.71
10.667	14.53			11.86		17.83	17.84
10.750	14.64			11.95			17.98
10.833	14.74			12.00			18.11
10.917	14.85						18.25
11.000	14.97						18.39

3.2 Gas Generation

To complement the off-gas generation calculations based on the surface area of the UNF and prior literature, a series of dissolution experiments were performed. The gas generated during the dissolution of thorium has been reported in several previous reports.[35,36] In a report by Karraker, dissolution of Th metal in 10 M HNO_3 and 0.05 M fluoride results in H_2 gas generated at 3.60% by volume. In a later symposium report[36], dissolution of Th metal in 13 M HNO_3 and 0.05 M fluoride is reported to generate H_2 gas at 2.50% by volume. These data points are at the upper bounds desired for the upcoming dissolution campaigns. The previous work also was performed without any competing dissolution reactions. One potential complication for the upcoming campaign is the large quantities of aluminum present from the HA/LU fuel as well as the L-Bundles containing the used fuels. The aluminum complicates the dissolution in two main areas: 1) hydrogen generation during dissolution and 2) aluminum complexation of the fluoride necessary in the dissolution of the Th metal. Experimental conditions are listed in Table 2-1 and results are listed in Table 3-3.

Thorium metal dissolution is similar to Pu and U in that a thin oxide coating forms that protects the metal from further oxidation at ambient temperatures. After the oxide film is breached at any point(s), several different metal HNO_3 reactions can take place to dissolve the thorium or oxidize it to ThO_2. Fluoride in solution first attacks the oxide to form an oxyfluoride which can then be dissolved by HNO_3. The following Equations were derived from Karraker's work in which HF was used.[35] Current campaigns will use KF.

(43) $ThO_2 + 2\ HF \rightarrow ThOF_2 + H_2O$
(44) $ThOF_2 + 4\ HNO_3 \rightarrow Th(NO_3)_4 + 2\ HF + 2\ H_2O$

The other possible reactions of Th metal are shown in the following Equations, using different amounts of acid with only one reaction requiring as much as six moles of acid per mole of metal.

(45) $Th + 6\ HNO_3 \rightarrow Th(NO_3)_4 + NO + NO_2 + 3\ H_2O$
(46) $3\ Th + 16\ HNO_3 \rightarrow 3\ Th(NO_3)_4 + 4\ NO + 4\ H_2O$
(47) $Th + 4\ HNO_3 \rightarrow Th(NO_3)_4 + 2\ H_2$
(48) $Th + 4\ HNO_3 \rightarrow ThO_2 + 4\ NO_2 + 2\ H_2O$

Equation 45 is a minor reaction based on Karraker's report where very little NO_2 was measured in the off-gas. In the current dissolutions of thorium (Th) in 4 M, 7 M and 10 M nitric acid, little or no color was observed meaning that little NO_2/N_2O_4 gas was evolved from the solution. When Al was dissolved alone, the gas evolved was the dark red color of NO_2/N_2O_4 gas, see Figure 3-2.

Equation 46 appears to be the main reaction occurring in Th dissolution. Karraker performed dissolutions with 10–190 grams of Th in 10 M HNO_3 with 0.1 M HF. The ratio of moles of acid to moles of metal dissolved by Equation 46 is 5.33 while Karraker observed an average ratio of 5.22 ± 0.22 with NO being the primary component. This value lies within the uncertainty of his experiments, but does not exclude other reactions lowering the ratio.

Equation 47 also occurs to some extent since Karraker observed H_2 gas in his work. The quantity of H_2 produced might be expected to increase slightly as the oxidizing potential of the acid concentration decreases and due to a higher percentage of the acid being ionized at the lower acid concentration. However, as the acid concentration decreases the reaction rate decreases as well so the total volume of gas generated per minute decreases so that dilution in the off-gas system may be possible for any small increase in H_2 gas generation.

Karraker reported that the off-gas composition for his experiments was 85 vol % NO, 7.6 vol % N_2, 3.5 vol % H_2, 2.1 vol % H_2O with less than 1 vol % each of NO_2, N_2O and O_2 during his dissolutions of Th in 10 M HNO_3 with 0.1 M HF. Nitrogen and oxygen are most likely due to residual air in the samples analyzed in the experiments. That conclusion is based on each being below the detectability limit of the analytical method so it is not known for certain about the last three gases except that the three gases total the remaining 1.8 vol % of the gas composition. If the gas composition is calculated without N_2, the percentages become 92 vol % NO, 3.8 vol % H_2, 2.3 vol % H_2O with less than 1.9 vol % each of NO_2, N_2O, and O_2. The amount of H_2O in the gases is not what was produced in the reaction since much of the water would condense and drain back to the reaction vessel as during plant dissolving. However, the percentages of NO and H_2 in the off-gas are an estimate based on the contributions from Equations 46 and 47 with all other reactions contributing less than 2% to the gas volume.

Equation 48, which produces Th oxide, is a minor reaction which would be expected to occur to a slightly higher percentage at low acid concentrations due to the oxidizing potential being lower and the percent of free H^+ concentration being higher. However, Orth in his summary paper[37] on Th processing stated that some undissolved ThO_2 was present after dissolution of the metal. The dissolution rate was 4 tons per day of thorium so any of the protective layer of ThO_2 would be expected to accumulate in the dissolver with some being transferred out with the solution going to solvent extraction. This campaign has less than 2 MT of Th and will not go through solvent extraction.

Since there are multiple reactions that can occur in the solution, changes in the ratio of HNO_3 consumed per mole of Th metal dissolved should be expected to be observed even at the same acid concentration,

but especially as the HNO_3 concentration changes. Additional dissolution tests are being proposed to clarify whether the H_2 gas increases as acid concentration decreases and whether any increase is still within the safe limits for dilution.

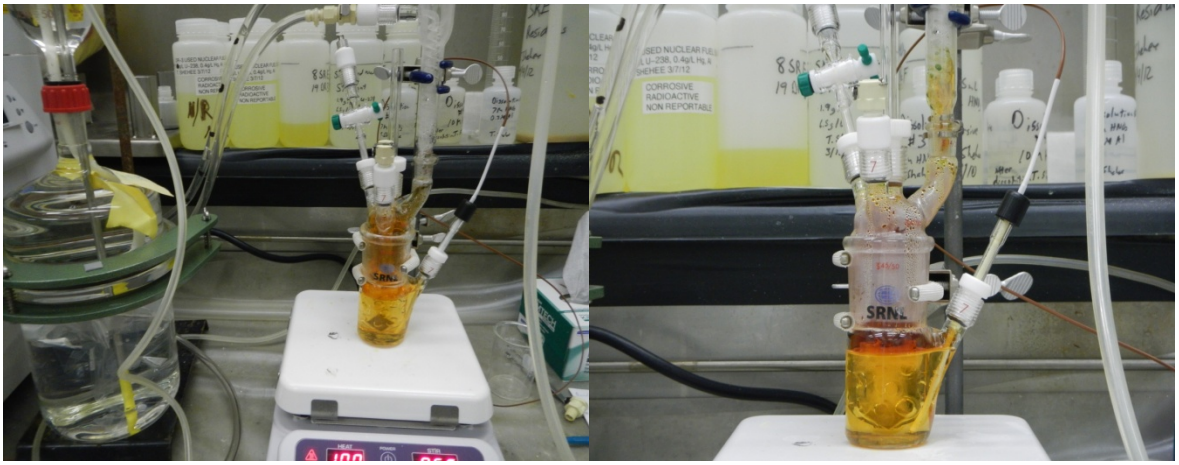

Figure 3-2. Dissolution apparatus showing the dark brown gas generated during the dissolution of an Al coupon.

Table 3-3. Initial results of dissolution studies

Dissolution	Metal foil used		Al (g)	Th (g)	Volume of off-gas (mL, ~25 °C, ~1 atm, ± 5mL)	H_2 (vol %, ± 10%)	Dissolution time (min)[5]
1[1]	–	Al	0.6702	–	Exceeded Tedlar bag volume	0.55	Not measured
1-A	–	Al	0.6334	–	70	0.31	> 125
2	Th	–	–	0.8890	51.5	1.10	33
3	Th	–	–	0.9250	60	0.18	5
4	Th	–	–	0.9180	50	0.12	3.5
5	Th	–	–	0.9140	85	1.7	4
3-A[3]	$Th^{4+}_{(aq)}$	Al	0.6317	–	283	0.28	4.5
4-A[3]	$Th^{4+}_{(aq)}$	Al	0.6482	–	24	0.86	> 25
5-A[3]	$Th^{4+}_{(aq)}$	Al	0.6241	–	270	1.4	6.75
5-B	Th	–		0.8707	75	0.5	21
6	Th	–		1.1011	58	< 0.1	4
7	Th	Al	0.9238	0.5897	126	0.9	4.5
8	Th	Al	1.0327	0.5968	142	0.6	5
9[4]	Th	Al	1.0575	0.6517	140	0.5	4.25
10[4]	Th	–		1.0880	77	0.4	5
1) Non-radioactive test of apparatus							
2) Concentration present after dissolution of FNR and part of SRE bundle							
3) Dissolver solution is from Th dissolutions 3, 4 and 5. Hg was added to aid in dissolution of Al.							
4) Duplicate Measurement							
5) Greater than symbol indicates that complete dissolution was not obtained in the indicated time period.							

3.3 Off-gas Rate Calculations

3.3.1 *Off-gas Rate Calculation Assumptions and Conditions*

The prior report[34] on the dissolution of the MURR assemblies shows that for an immersion depth of 54 inches, an initial HNO_3 of 6 M, an initial 0.002 M Hg concentration, an irradiation reduction factor of at least 50%, and a 40 scfm air purge, the peak off-gas rate from the dissolution of four L-Bundles would be 30.9 scfm and the peak off-gas generation for the four MURR assemblies in each of the four L-Bundles would be 14.1 scfm. These peak off-gas generation rates from the dissolution of the four L-Bundles and the MURR assemblies are both less than the 34.37 scfm off-gas generation limit to satisfy 60% H_2 LFL criteria with a 40 scfm air purge.

To calculate the peak off-gas rates for the dissolution of the SRE, HMI, and DR-3 assemblies in the L-Bundle, several assumptions were made as was done for the dissolution of the MURR assemblies in a prior report[34]. The off-gas rates for the FNR assemblies were not calculated in this report since it was determined in separate documents[20, 38] that the hydrogen off-gas generation from the dissolution of the L-Bundle with five FNR assemblies would be the same as dissolving the L-Bundle with four MURR assemblies.

First, the chemistry of the dissolution of the Al exterior surfaces for the L-Bundle, SRE, HMI, and DR-3 was assumed to follow the reaction:

(49) $$Al_{(s)} + 3.75\ HNO_3 \rightarrow Al(NO_3)_3 + 0.225\ NO_{(g)} + 0.15\ N_2O_{(g)} + 0.1125\ N_{2(g)} + 1.875\ H_2O_{(g)}$$

So 3.75 moles of HNO_3 acid are assumed consumed per mole of Al dissolved. This value was used to estimate how much HNO_3 remains after dissolution as well as how much Al is in solution.

Based on a collection of articles from a symposium of reprocessing irradiated fuels[36], another potential Th dissolution chemistry reaction is:

(50) $$Th_{(s)} + 5\ HNO_3 \rightarrow Th(NO_3)_4 + 2.47\ H_2O + 0.03\ H_{2(g)} + 0.25 NOx_{(g)} + 0.25\ N_{2(g)}$$

For this reaction 5 moles of HNO_3 acid are consumed per mole of thorium (Th) dissolved which matches Karraker's observation. William Prout states in this reference that in practice 5 to 5.2 moles of HNO_3 acid are consumed per mole of Th dissolved which matches earlier observations.[39] Based on these references, it was assumed that 5 moles of HNO_3 acid are consumed per mole of Th dissolved.

Since the HMI and DR-3 are High Aluminum-Low Uranium UNFs like the MURR assemblies, the same off-gas composition used for the MURR dissolution calculations[34] was used. This off-gas composition for the High Aluminum-Low Uranium assemblies is 7.0 vol % H_2, 71.4 vol % NO, and 21.6 vol % N_2O on an air, water, and nitrogen free basis where the molar ratio of NO/N_2O is 3.3. Note that this off-gas composition is based on a calculation from Weitz[40] on the LFL for H-Canyon Dissolver which points out that the reported gas compositions used to determine the 7 vol % H_2 were actually less than this value (3-5 vol % H_2) before placing on a N_2 free basis.

The same H_2 Lower Flammability Limit (LFL) criteria of 60% of the H_2 LFL value at 200 °C as was used for the MURR dissolution calculation was used for the HMI, SRE, and DR-3 dissolution calculations. This LFL at 200 °C was chosen due to the iodine reactor in the off-gas stream of H-Canyon being heated to 200 °C. These H_2 LFL values originally came from F. Scott's 28 °C data[41] and are assumed applicable for NO/N_2O molar ratios from 2 to 5. A list of these LFL values is shown in Table 3-4 which came from

the prior MURR dissolution calculations[34]. Note that the 28 °C Scott data[41] was corrected to 200 °C using a temperature correction from Dyer's work[42] where:

(51) $$LFL_T = LFL_{ref}*(1 - A*(T-T_{ref}))$$

where:

LFL_T = LFL at Temperature T (°C)
LFL_{ref} = LFL at Reference Temperature T (°C)
A = empirical coefficient (Zabetakis attenuation factor) = 0.0011
T = temperature (°C) at which LFL is to be evaluated.

So for the 28 °C Scott data the correction to 200 °C becomes:

(52) $$LFL_{200} = LFL_{28}*(1 - 0.0011*(200-28)) = LFL_{28}*0.811$$

The 200 °C H_2 LFL values and 60% of these values are shown in Table 3-4.

Table 3-4. H_2 Lower Flammability Limit from Scott and Dyer Data.

Air [vol %]	Scott H_2 LFL at 28 °C [vol %]	Dyer H_2 LFL at 200 °C [vol %]	60% of H_2 LFL at 200 °C [vol %]
0	5.62	4.56	2.73
5	6.00	4.87	2.92
10	6.10	4.95	2.97
15	6.20	5.03	3.02
20	6.30	5.11	3.07
25	6.40	5.19	3.11
30	6.50	5.27	3.16
35	6.70	5.43	3.26
40	6.80	5.51	3.31
45	6.83	5.54	3.32
50	6.70	5.43	3.26
55	6.63	5.38	3.23
60	6.50	5.27	3.16
65	6.20	5.03	3.02
70	5.70	4.62	2.77
75	5.60	4.54	2.72
80	5.20	4.22	2.53
85	4.60	3.73	2.24
90	4.30	3.49	2.09
96	4.00	3.24	1.95

In the prior MURR dissolution off-gas calculations[34], the maximum peak off-gas rate of 34.37 scfm during dissolution was calculated based on the assumed off-gas composition discussed above with a 40 scfm air purge rate to stay below the 60% of H_2 LFL at 200 °C. This same peak off-gas rate of 34.37 scfm will be used for the HMI, SRE, and DR-3 dissolutions. The reason the same flammability limit was applied to the thorium SRE assembly is that the thorium fuel is housed in an aluminum bundle tube which sits in the L-Bundle as shown in Appendix A.2. The exposed surface area of the thorium fuel inside the SRE aluminum bundle tube is about an order of magnitude smaller than the outer area of the SRE aluminum bundle tube and the aluminum L-Bundle. Using the flammability limits from the MURR

dissolution is also conservative since the off-gas composition data for dissolving pure metal thorium is less than 7 vol % H_2. The literature and experimental off-gas composition values for dissolving thorium metal only are shown in Table 3-5. The highest vol % H_2 value from the literature and from the current experiments discussed earlier is 3.6 vol % on a water free basis. Since the thorium dissolution off-gas 3.6 vol % H_2 is smaller than the Al dissolution off-gas 7 vol % H_2 and the thorium surface area is smaller than the aluminum surface area, using the Al dissolution off-gas LFL's is conservative.

Table 3-5. Off-gas Composition Values for Dissolving Thorium Metal in Solution without Th Present Initially

Data Source	Initial HNO_3 [M]	Initial F [M]	Initial Th [M]	Initial Al [M]	H_2 [vol %]	NO [vol %]	N_2 [vol %]	NO_2 [vol %]	N_2O [vol %]	O_2 [vol %]	H_2O [vol %]
Karraker[35] Water Free	10	0.05-0.1	0	0	3.6	86.8	7.8	0.6	0.6	0.6	0
Symposium[36]	10	0.05	0	0	2.5	9	13	73	2.5	0	0
Dissolution 4	10	0.05	0	0	0.1	0	99.6	0	0	0.3	0
Dissolution 6	10	0.05	0	0.3	<0.1	<0.1	27.5	0	<0.1	7.9	0
Dissolution 5-B	7	0.01	0	0.3	0.5	<0.1	5.8	0	<0.1	1.0	0
Dissolution 3	7	0.05	0	0	0.2	0	99.7	0	0	< 0.1	0
Dissolution 5	7	0.05	0	0.3	1.7	0	98.2	0	0	< 0.1	0
Dissolution 10	7	0.05	0	0.3	0.4	<0.1	9.7	0	0.9	0.8	0
Dissolution 2	4	0.05	0	0	1.1	0	87.8	0	0	11.1	0

Note: Dissolutions 1-5 in Table 2-1 used N_2 as carrier gas and the rest used argon as the carrier gas. Dissolution 2 was contaminated with air during analytical handling.

In the off-gas calculations for the dissolution of the MURR assemblies[34], the reference peak off-gas generation rate was 0.676 scfm/ft^2 at 0.001 M Hg based on testing by Caracciolo.[43] This same reference peak off-gas rate was assumed for the dissolution of the SRE, HMI, and DR-3 assemblies in the L-Bundle. Note that this High Aluminum-Low Uranium off-gas generation rate can be used for the thorium SRE assembly since the thorium SRE fuel is housed in an aluminum bundle tube which sits in the Disassembly L Area Bundling Tube (DABT) or L-Bundle. From current experiments discussed earlier, the measured off-gas generation rate for dissolving pure thorium metal is 0.004 to 0.055 scfm/ft^2 as shown in Table 3-6. After the L-Bundle is dissolved followed by the outer aluminum bundling tube of the SRE then the SRE fuel tubes will dissolve but based on the expected off-gas generation rate and the lower surface area, the prior off-gas generation rates for the exterior portions of the SRE will be bounding.

Table 3-6. Peak Off-gas Generation Rate for Thorium Dissolving Thorium Metal

Data Source	Initial HNO_3 [M]	Initial F [M]	Initial Th [M]	Initial Al [M]	Off-gas Generation [scfm/ft^2]
Dissolution 4	10	0.05	0	0	0.037
Dissolution 6	10	0.05	0	0.3	0.034
Dissolution 5-B	7	0.01	0	0.3	0.010
Dissolution 3	7	0.05	0	0	0.030
Dissolution 5	7	0.05	0	0.3	0.055
Dissolution 10	7	0.05	0	0.3	0.039
Dissolution 2	4	0.05	0	0	0.004

Additional experimental details are found in Table 2-1

Based on work by Robert Moore[44] the thorium dissolution rate is linearly proportional to the F concentration, which acts like a catalyst. For the planned dissolution of the SRE assemblies, the initial HF concentration was assumed to be 0.05 M. In the Moore reference, it states that the thorium dissolution rate is second order with respect to the initial HNO_3 concentration which means that the initial HNO_3 concentration has a bigger effect on the dissolution rate than the F concentration.

The Al dissolution rate is assumed linearly proportional to the Hg concentration as was done in the MURR dissolution calculations[34]. For the planned dissolution of the HMI, SRE, and DR-3 assemblies the initial Hg concentration was assumed to be 0.002 M.

The dissolution rate of the MURR assemblies was affected by the irradiation of the fuel assemblies by a 50% reduction due to hardening of surfaces as described in the prior dissolution calculations.[34] This 50% reduction in dissolution rate directly translates into a 50% reduction of the peak off-gas generation rate. Since the HMI and DR-3 assemblies are comparable to the MURR assemblies (High Aluminum-low Uranium), a similar 50% reduction in dissolution rate was assumed for these off-gas calculations. However, for the SRE assemblies the U^{235} burn-up is about 23% versus the about 54–65% U^{235} burn-up of the HMI and DR-3 fuels and so no reduction in dissolution rate for the SRE assemblies was assumed. This zero impact of irradiation on the dissolution of the thorium fuels is conservative or will indicate higher off-gas rates than actually expected.

For the prior dissolution calculation of the MURR assemblies[34] the impact of dissolved Al on the dissolution rate was characterized using Equation 53:

(53) $r_{Al} = 102.64*10^{-1.078*[Al]}$

where:

r_{Al} = Al dissolution rate in mg/cm^2/min
[Al] = molar concentration of dissolved Al

In the prior dissolution calculations for the MURR assemblies this correlation was used to scale down the peak dissolution rate of 52.53 mg/cm^2/min at about 0.27 M Al when calculating the impact of the dissolved Al from a prior dissolution batch. This adjustment to the dissolution rate based on dissolved Al can be expressed as:

(54) $$r_{adj} = \frac{102.64*10^{-1.078*[Al]}}{52.53}$$

where:

r_{adj} = Al dissolution rate adjustment factor for dissolved Al
[Al] = molar concentration of dissolved Al

A compilation of the thorium dissolution rate data from literature[44,36] and from the current experiments is shown in Table 3-7. A plot of the thorium dissolution rate as a function of the HNO_3 and Al concentrations is shown in Figure 3-3. This plot shows that at high HNO_3 concentrations near 13 M some dissolved Al near 0.5 M has a significant impact on the thorium dissolution rate. This plot also shows that at lower HNO_3 concentrations near 7 M the impact of dissolved Al is small and negligible when considering measurement uncertainty. For these calculations it was assumed that the SRE dissolution will

take place at an initial HNO_3 concentration less than or equal to 7 M and the impact of dissolved Al on the thorium dissolution rate is negligible.

Examining only the thorium dissolution rates in Table 3-7 with no initial dissolved Al, the thorium dissolution rate is second order with respect to the HNO_3 concentration as indicated in the literature. For this set of the data a second order fit of the thorium dissolution rates with no initial dissolved Al is shown to be:

(55) $r_{Th} = 2.7074 * [HNO_3]^2 - 32.416 * [HNO_3] + 91.425$

where:

r_{Th} = Th Dissolution Rate in $mg/cm^2/min$
$[HNO_3]$ = Molar Concentration of HNO_3

The thorium dissolution rates with no dissolved Al in Table 3-7 from the Symposium on the Reprocessing of Irradiated Fuels document[36] were interpolated from a figure on Slide 6.2 of that reference. These thorium dissolution rates were then fitted with cubic functions of the HNO_3 and thorium concentrations as shown in Figure 3-4. Table 3-8 shows the various cubic fits for the thorium dissolution rates. Note the R^2 correlation factors of these cubic fits were high (0.99 or greater) so these fits are a good approximation to the original figure in Slide 6.2 of the Symposium document.

Using these cubic fits, the thorium dissolution rates at 7 M and 10 M HNO_3 concentration with 0.05 M F and no initial Al were calculated as shown in Table 3-9. A plot of these predicted thorium dissolution rates is shown in Figure 3-5. These cubic fits can be used for any off-gas calculations for thorium metal dissolution at or below 7 M HNO_3 ignoring the impact of the dissolved Al.

Table 3-7. Thorium Dissolution Rate Data

Data Source	Initial HNO_3 [M]	Initial Al [M]	Initial F [M]	Initial Th [M]	Th Dissolution [$mg/cm^2/min$]
Moore	7	0.5	0.05	0	14.83
Moore	13	0.5	0.05	0	4.17
Moore	13	0	0.05	0.2	94.83
Moore	13	0	0.05	0.5	66.83
Moore	13	0	0.05	0.72	49.17
Moore	13	0	0.05	1	29.83
Moore	7	0	0.05	0.5	23.17
Moore	13	0	0.05	0	133.33
Dissolution 2**	4	0	0.05	0	2.19
Dissolution 3**	7	0	0.05	0	14.48
Dissolution 4**	10	0	0.05	0	20.69
Dissolution 5**	7	0.3	0.05	0	18.10
Dissolution 5-B**	7	0.3	0.01	0	3.49
Dissolution 6**	10	0.3	0.05	0	19.65
Dissolution 10**	7	0.3	0.05	0	17.03
Symposium*	2	0	0.05	0	21
Symposium*	4	0	0.05	0	38
Symposium*	6	0	0.05	0	58
Symposium*	8	0	0.05	0	84
Symposium*	10	0	0.05	0	111

Table 3-7. Thorium Dissolution Rate Data

Data Source	Initial HNO_3 [M]	Initial Al [M]	Initial F [M]	Initial Th [M]	Th Dissolution [$mg/cm^2/min$]
Symposium*	12	0	0.05	0	130
Symposium*	14	0	0.05	0	134
Symposium*	2	0	0.05	0.2	11
Symposium*	4	0	0.05	0.2	21
Symposium*	6	0	0.05	0.2	35
Symposium*	8	0	0.05	0.2	54
Symposium*	10	0	0.05	0.2	77
Symposium*	12	0	0.05	0.2	93
Symposium*	14	0	0.05	0.2	95
Symposium*	2	0	0.05	0.5	4
Symposium*	4	0	0.05	0.5	10
Symposium*	6	0	0.05	0.5	18
Symposium*	8	0	0.05	0.5	32
Symposium*	10	0	0.05	0.5	57
Symposium*	12	0	0.05	0.5	67
Symposium*	14	0	0.05	0.5	68
Symposium*	2	0	0.05	0.72	2
Symposium*	4	0	0.05	0.72	7
Symposium*	6	0	0.05	0.72	16
Symposium*	8	0	0.05	0.72	28
Symposium*	10	0	0.05	0.72	47
Symposium*	12	0	0.05	0.72	51
Symposium*	14	0	0.05	0.72	49
Symposium*	2	0	0.05	1	1
Symposium*	4	0	0.05	1	5
Symposium*	6	0	0.05	1	12
Symposium*	8	0	0.05	1	22
Symposium*	10	0	0.05	1	28
Symposium*	12	0	0.05	1	30
Symposium*	14	0	0.05	1	30

*Interpolated value from figure on Slide 6.2 from Symposium Reference, **Experiments in Table 2-1

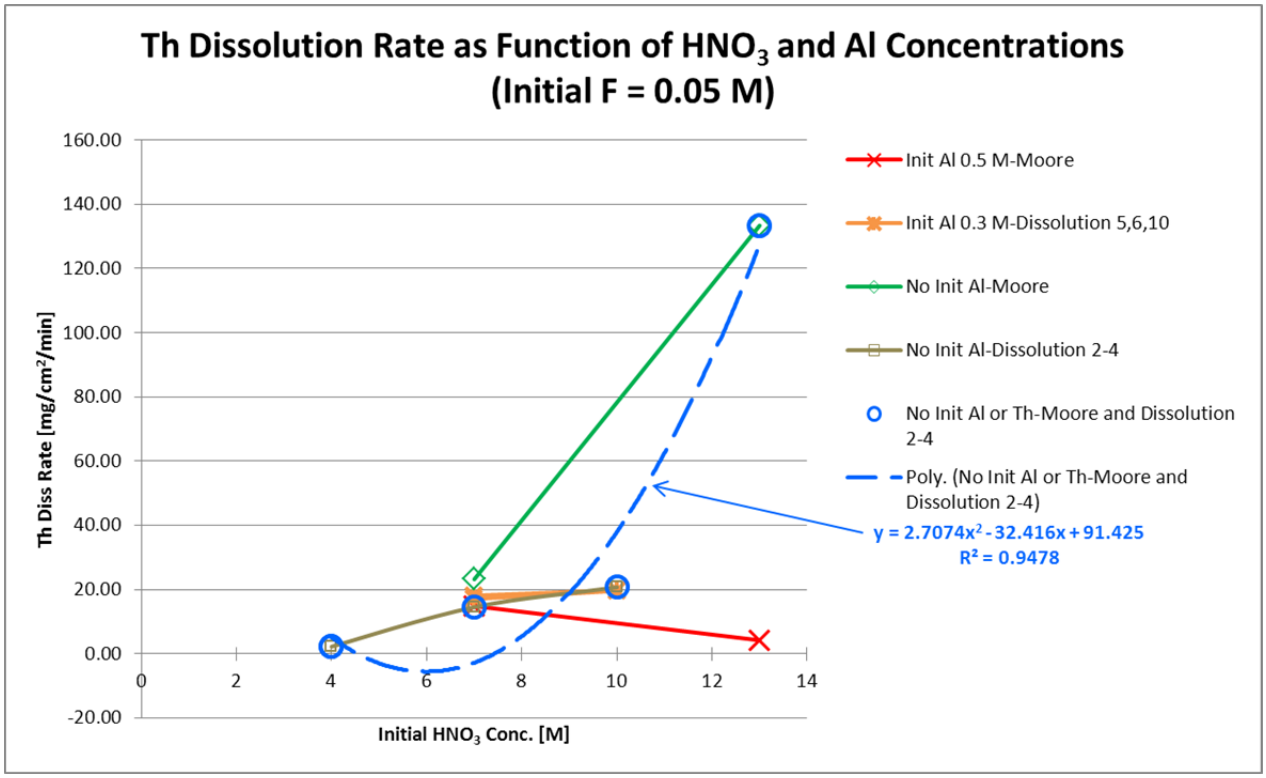

Figure 3-3. Th Dissolution Rate as function of HNO_3 and Dissolved Al

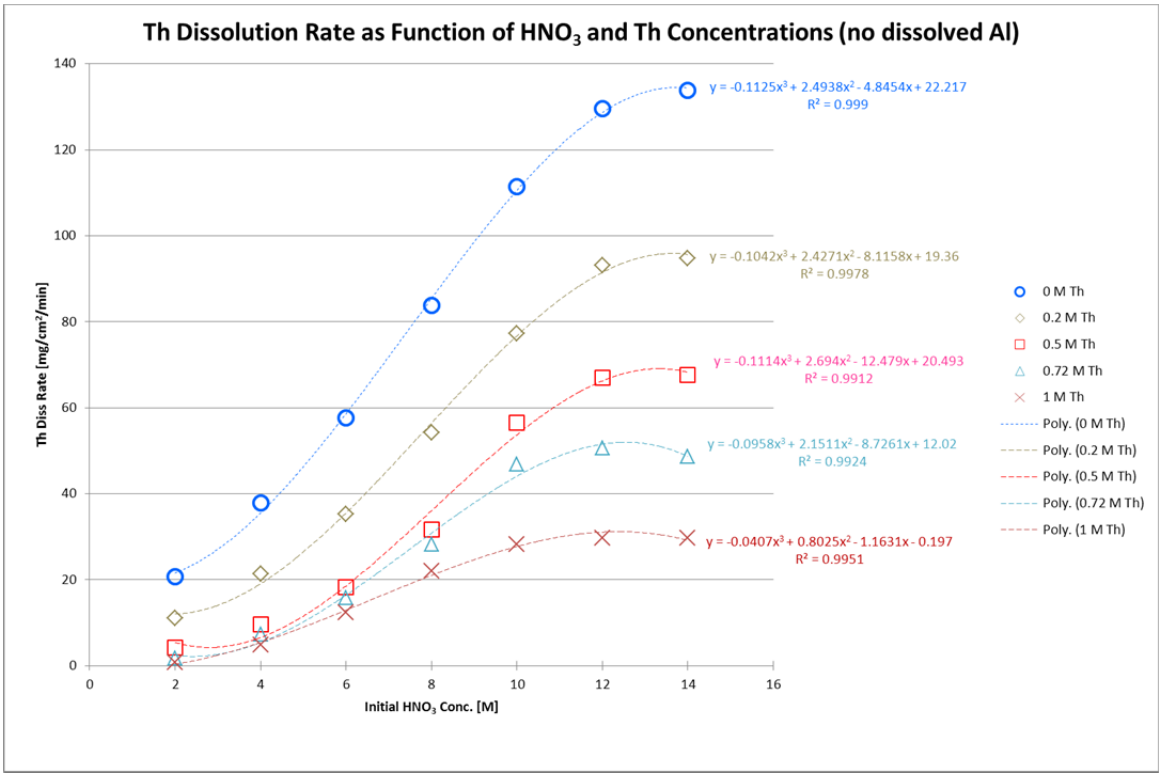

Figure 3-4. Th Dissolution Rate as function of HNO_3 and Th Concentrations

Table 3-8. Thorium Dissolution Rate Fits as function of HNO_3 and thorium Concentrations

Initial HNO_3 [M]	Initial F [M]	Initial Th [M]	Initial Al [M]	Th Dissolution Rate [mg/cm^2/min]	R^2 Correlation Factor
2-14	0.05	0	0	$r = -0.1125*[HNO_3]^3 + 2.4938*[HNO_3]^2 - 4.8454*[HNO_3] + 22.217$	0.999
2-14	0.05	0.2	0	$r = -0.1042[HNO_3]^3 + 2.4271[HNO_3]^2 - 8.1158[HNO_3] + 19.36$	0.998
2-14	0.05	0.5	0	$r = -0.1114[HNO_3]^3 + 2.694[HNO_3]^2 - 12.479[HNO_3] + 20.493$	0.991
2-14	0.05	0.72	0	$r = -0.0958[HNO_3]^3 + 2.1511[HNO_3]^2 - 8.7261[HNO_3] + 12.02$	0.992
2-14	0.05	1	0	$r = -0.0407[HNO_3]^3 + 0.8025[HNO_3]^2 - 1.1631[HNO_3] - 0.197$	0.995

Table 3-9. Predicted Thorium Dissolution Rates at 7 and 10 M HNO_3 and 0.05 M F

Initial HNO_3 [M]	Initial F [M]	Initial Th [M]	Initial Al [M]	Th Dissolution Rate [mg/cm^2/min]
7	0.05	0	0	72
7	0.05	0.2	0	46
7	0.05	0.5	0	27
7	0.05	0.72	0	23
7	0.05	1	0	17
10	0.05	0	0	111
10	0.05	0.2	0	77
10	0.05	0.5	0	54
10	0.05	0.72	0	44
10	0.05	1	0	28

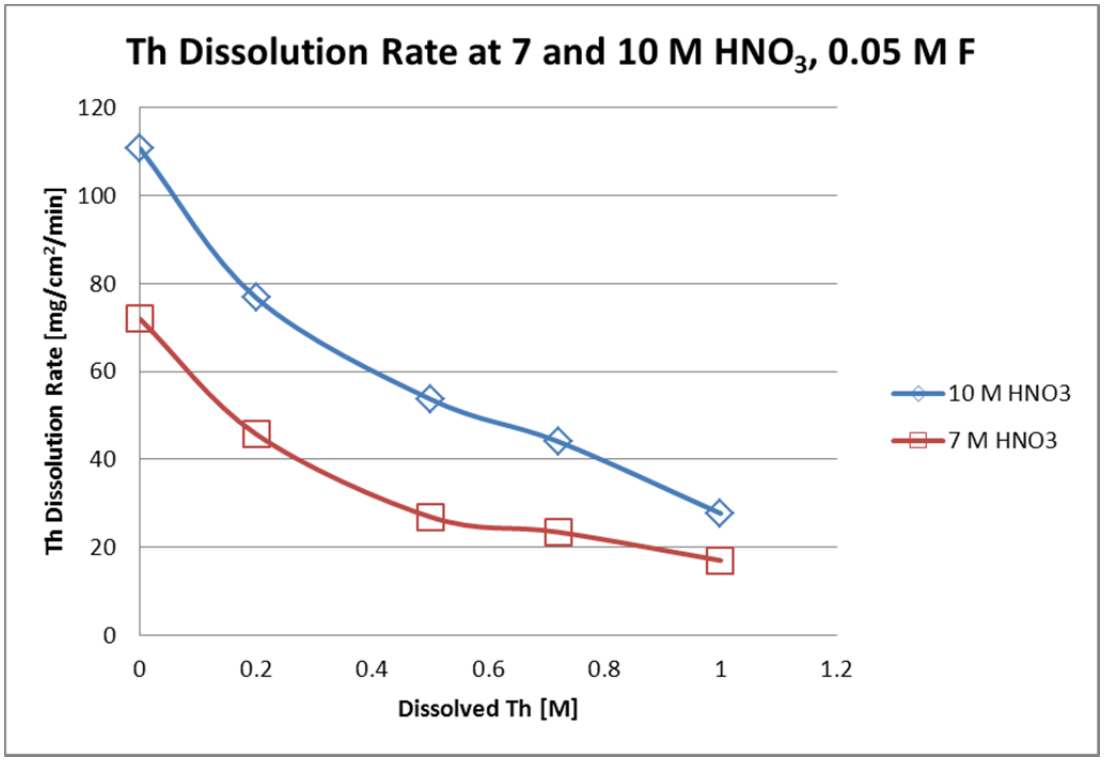

Figure 3-5. Th Dissolution Rate at 7 and 10 M HNO3, 0.05 M F as Function of Th Concentration

3.3.2 *Off-gas Rate Values for Dissolver Charging Scenarios*

Using the off-gas rate calculation assumptions and conditions defined in the prior section, the peak off-gas rates were determined to be bounded by the controls listed in the off-gas calculations for the MURR assemblies.[34] Initially, up to 4 bundles of FNR, SRE, HMI, and/or DR-3 can be charged to a solution of fresh nitric acid. After the first dissolution, the number of bundles that can be charged is dependent on the concentration of aluminum in the dissolver solution as shown in Table 8 and Figure 8 of the off-gas calculations for the MURR assemblies[34].

An example of the off-gas calculations for the initial charge of 4 bundles of SRE is shown in Table 3-10 using the dissolution terms defined in the prior section which originate from the off-gas calculations for the MURR assemblies.[34] The peak off-gas rate for processing the 4 L-Bundles of SRE assemblies is 34.80 scfm which slightly exceeds the 34.37 scfm 60% H_2 LFL at 200 °C or represents 3.26% H_2 instead of the limit of 3.2% H_2. Since the assumption of 7 vol % H_2 in the off-gas is conservative as discussed earlier or the actual off-gas values were less than the base average 7 vol % and no credit is taken for the reduction in rate due to irradiation of the SRE assemblies (23%), the 34.80 scfm peak off-gas is acceptable. After the 4 outer L-Bundles dissolve, the peak off-gas rate for processing the 4 outer bundling tubes of the SRE assemblies themselves is 22.54 scfm labeled as **Peak Off-Gas for Assembly Area 1** in Table 3-10. If there is a possibility of a hole or cut in any of the 4 outer bundling tubes of the SRE assemblies inside the 4 L-Bundles then the off-gas rate based on the inside exposed fuel area of the SRE assemblies assuming it reacts like Al would be 2.82 scfm labeled as **Peak Off-gas for Assembly Area 2.** If one uses the thorium dissolution off-gas rates discussed earlier then the peak off-gas rates for the exposed inside fuel tubes will be much smaller. This example calculation demonstrates that the dissolving of the outer L-Bundle will generally dictate how many bundles are processed per dissolver charging scenario as shown in the prior off-gas calculations for the MURR assemblies.[34]

Table 3-10. Example Off-Gas Rates for Dissolver Batching Scenario with 4 SRE L-Bundles

Dissolver Batches	Fuel Type	L-Bundles	Assemblies per Bundle	Initial HNO_3 [M]	Final HNO_3 [M]	Initial Al Conc [M]	Final Al Conc [M]	Initial Th Conc [M]	Final Th Conc [M]	Moles of HNO3 consumed per mole of Al dissolved	Moles of HNO3 consumed per mole of Th dissolved	Hg [M] (assume constant)	F [M] (assume constant)	Exposed Metal
1	SRE	4	1	2.40	1.23	0.00	0.22	0.00	0.07	3.75	5.00	0.0020	0.05	Al

Ref. Peak Off-gas Rate [scfm/ft^2]	Ref. Peak Off-gas Rate Hg conc. [M]	Scale for Ref. Peak Off-gas Rate based on Diss Al	Scale for Ref. Peak Off-gas Rate based on Irradiation	Scale for Ref. Peak Off-gas Rate based on Catalyst Conc	Corrected Peak Off-gas Rate [scfm/ft^2]	Immersion Depth [in]	Immersion Depth [ft]	Bundle Outer Surface Area (ft^2)	Peak Off-gas for Bundle Outer Area [scfm]	Assembly Surface Area 1 [in^2]	Peak Off-gas for Assembly Area 1 [scfm]	Assembly Surface Area 2 [in^2]	Peak Off-gas for Assembly Area 2 [scfm]
0.676	0.001	1	1	1.99	1.35	54	4.5	25.8	34.80	16.7	22.54	2.1	2.82

3.4 Fuel Simulant Neutralization

Neutralization experiments using 50 wt % sodium hydroxide targeted 4 neutralization points. The acidic solution was neutralized to the pH where the first solids precipitate and do not redissolve, pH of ~4.5; to pH 7; to 0.8 M free hydroxide, and to 1.2 M free hydroxide. The four data points were chosen after evaluating a previous neutralization study that used these points and are a good fit for these neutralization experiments.[45] Figure 3-6 below shows the samples at several of these points.

Precipitation occurs with the first addition of 50 wt % NaOH. The first and second target pH points proved difficult to achieve since they both fell near the equivalence point of the reaction. The pH for each point was monitored with a broad range pH test strip. At pH 7, it is notable that the material becomes a very thick slurry as shown in Figure 3-6C. This precipitate is thick enough that the beaker can be turned upside down without spilling any material. The very thick precipitate, previously observed, is due to the major component of the precipitate at pH 7 which is $Al(OH)_3$ solid. With the addition of additional sodium hydroxide, the reaction quickly moves past this point and the aluminum forms a more soluble species, presumed to be the anionic $Al(OH)_4^-$. [46]

The quantity of NaOH added to achieve a 0.8 and 1.2 M excess OH^- was calculated. The amount required to complex all Al in the simulant was accounted for in the calculation. The slurry produced at the final neutralization point for both 0.8 and 1.2 M excess OH^- was visually similar. These points are represented in Figure 3-6D.

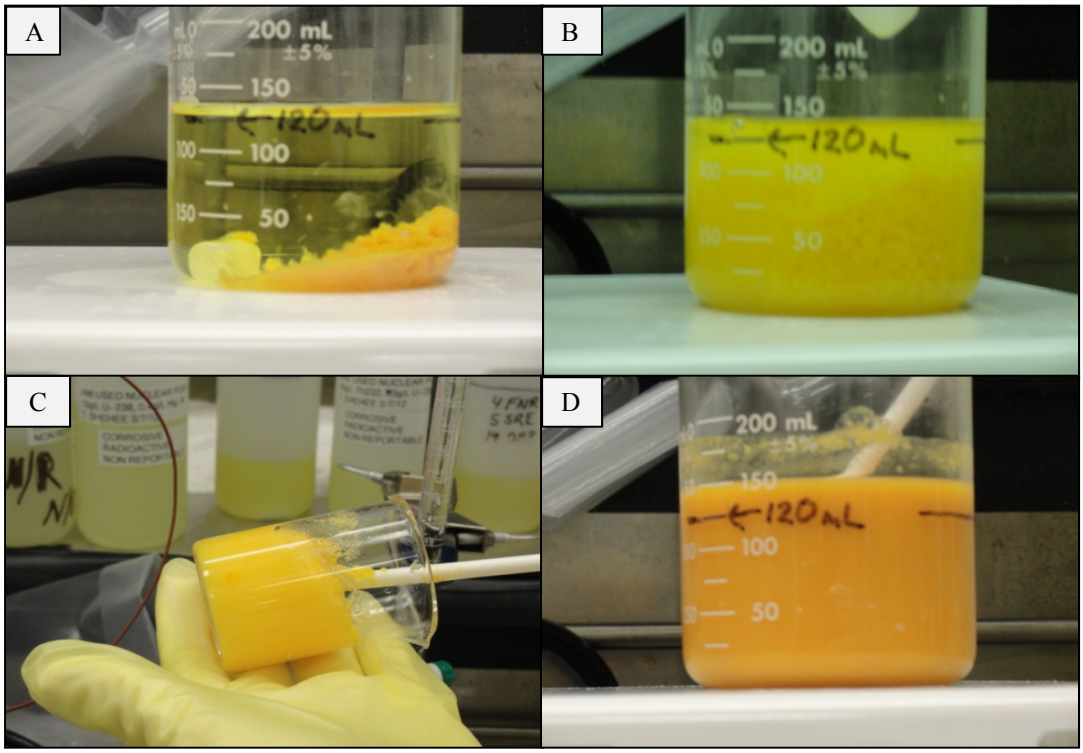

Figure 3-6. Neutralization of simulated dissolver batch. A) after addition of a few mL 50 wt % NaOH showing initial precipitation; B) neutralization at pH~4.5; C) neutralization at pH 7; D) neutralization with excess 50 wt % NaOH.

3.5 Physical Properties

The density and mass fraction of the supernate, solids in the slurry, and the undissolved solids in the 14,000 L dissolver fluids are provided in Table 3-19. Note that the sample names follow the format #F#S#D-M where the # indicates the number of L-Bundles containing the F (FNR or Ford Nuclear Reactor), S (SRE or Sodium Reactor Experiment), or D (DR-3 or Denmark Reactor) fuel, and M indicates the amount of free hydroxide molarity at the end of neutralization (0.8M or 1.2M). (Note: These solutions may also contain DU to lower the ^{235}U isotopic percentage.) Tables 3-13 through 3-14 provide Equations used for flow calculations. The rheological data for the 14,000 L dissolver fluids are provided in Table 3-20 with data fitted to the Newtonian and Bingham Plastic models as well as the apparent viscosity at 600 s^{-1}. These tables provide the average physical property values and the 95% confidence level of the average physical property values.

For the 14,000 L dissolver fluids, subsamples were pulled, allowed to settle for 24 hours, decanted and the resulting slurries analyzed for density and total solids to see if there was an effect on slurry concentration in the determination of the undissolved solids properties. These results are provided in Table 3-11 and they clearly show that by concentrating the slurry via settling decanting, the UDS density deceases and the confidence level decreased, in all cases. A reason for the larger calculated densities and errors is the denominator in Equations 7 and 8, $\rho_{sup} + \rho_s(f_{uds} - 1)$. For a low UDS slurry, the density of the supernate and slurry have values that are close to each other and are made closer by further reducing the slurry density when considering the UDS fraction. This difference can be very small, thereby increasing the UDS density and error.

Table 3-11. Undissolved Solids Density Determination Using Concentrated 14,000 L Dissolver Fluids

Identification	As-Received Slurry				Concentrated Slurry			
	Slurry		UDS		Slurry		UDS	
	Density (g/ml)	TS fraction	Density (g/cm^3)	STDEV	Density (g/ml)	TS fraction	Density (g/cm^3)	STDEV
4FS19D-0.8M	1.3057	0.3322	14.9481	4.7964	1.3336	0.3907	2.647	0.090
4FS19D-1.2M	1.3103	0.3527	3.5842	0.2617	1.3347	0.3750	3.301	0.147
8S19D-0.8M	1.3180	0.3422	8.8419	0.5403	1.3495	0.4033	2.763	0.041
8S19D-1.2M	1.3207	0.3418	10.4840	1.3970	1.3687	0.3993	3.429	0.074
5SRE-0.8M	1.1477	0.1751	7.2870	0.8528	1.1769	0.2031	5.686	0.512
5SRE-1.2M	1.1601	0.1840	7.0746	0.4654	1.2070	0.2285	5.029	0.390
10SRE-0.8M	1.2397	0.2686	5.2041	0.2903	1.2487	0.3030	2.691	0.147
10SRE-1.2M	1.2517	0.2741	5.7577	0.2181	1.2862	0.3188	3.352	0.199

During the rheological measurements of 14,000 L dissolver fluids, all the SRE samples started to visually phase separate, where a clear liquid (supernate) was observed on the top surface of the rotating bob. This behavior was not the case for the other 14,000 L dissolver fluids or for the 12,000 L dissolver fluids.

All the flow curves were fitted to both Newtonian (N) and Bingham Plastic (BP) rheological models. A representative flow curve for the 14,000 L and 12,000 L dissolver fluids are shown in Figure 3-7, fitted to both the N and BP models. The 14,000 L flow curve shows that using a Newtonian fit the data is very

similar to the BP fit; hence, the Newtonian results will be used to assess these fluids in the various calculations in this document. For the more viscous 12,000 L dissolver fluids, the Newtonian model can also be used, but with caution and depending on the condition of flow (e.g. laminar, turbulent). If the flow is turbulent, the Newtonian model is used for the pressure drop calculations, given that turbulent losses maybe greater for Newtonian fluids given that pipe roughness is not considered in the non-Newtonian case.

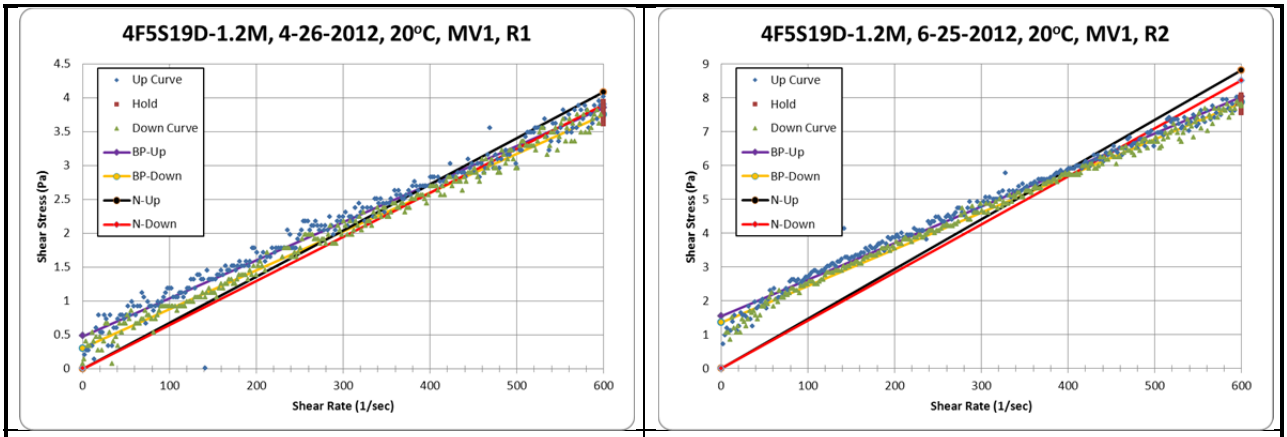

4F5S19D, 14000L, 35.27 wt % TS	4F5S19D, 12000L, 38.90 wt % TS

Figure 3-7. Flow Curves for 14,000 and 12,000 L 4F5S19D Slurries

Particle size distributions were obtained for the 12,000 L dissolver fluids and the distributions are shown in Figure 3-8 and have similar PSD profiles. The volume percentiles, mean values and the average and standard deviations are provided in Table 3-12. The deposition velocity correlation (Equation 32) uses the 85th percentile data and since this data is not available, the 90th percentile data will be used and is conservative. The mean volume of 19.3 microns is used to determine if the slurry can be treated as a non-cohesive slurry and, if so, its mass flux is determined.

Table 3-12. Particle Size Distribution, Percentiles and Mean Values

Parameter		Microns					
		4F5S19D 0.8M	4F5S19D 1.2M	8S19D 0.8M	8S19D 1.2M	Average Value	STDEV
Volume Percentiles Distribution	10	1.58	1.64	2.15	1.75	1.78	0.26
	20	3.75	3.77	4.91	4.10	4.13	0.55
	25	5.08	4.83	6.16	5.21	5.32	0.58
	40	9.16	7.99	10.43	8.85	9.11	1.01
	50	12.82	10.79	14.57	12.49	12.67	1.55
	60	16.77	14.57	19.60	16.91	16.96	2.06
	70	21.00	19.12	25.94	22.28	22.09	2.88
	75	23.56	21.89	30.00	25.72	25.29	3.51
	90	39.23	37.46	50.34	43.57	42.65	5.73
	95	56.58	52.11	67.83	56.92	58.36	6.68
Mean Values	Volume	19.33	16.74	22.02	18.88	19.24	2.17
	Number	0.46	0.40	0.49	0.45	0.45	0.04
	Area	4.21	3.92	4.93	4.40	4.36	0.43

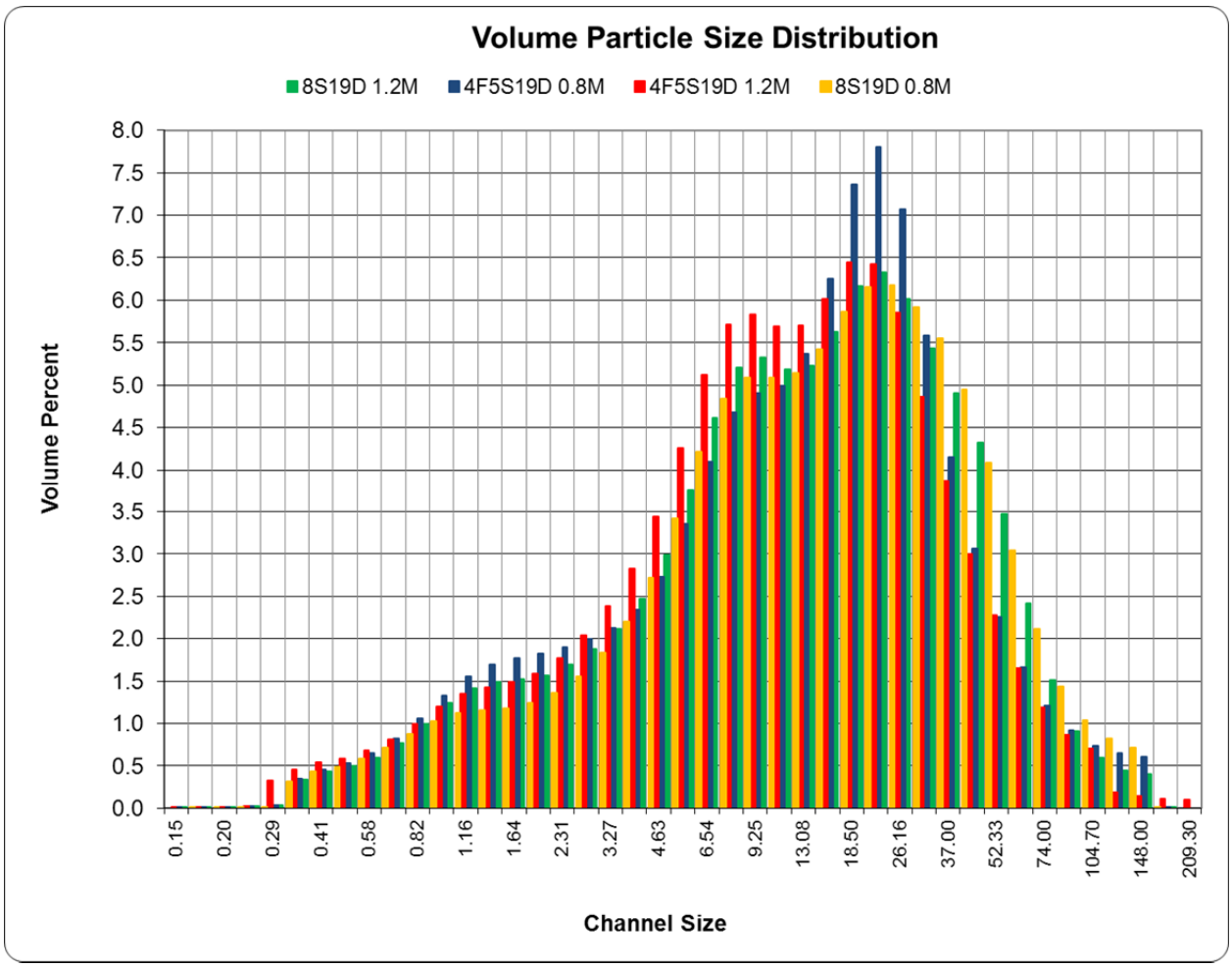

Figure 3-8. Particle Size Distribution of 12,000 L Dissolver Batch Fluids

3.6 Flow Data

The properties of water with a density of 62.4 *lbm/ft*^{3} (specific gravity (SG) = 1) and viscosity of 1 cp = 0.00674 *lbm/ft·sec* and a dissolver fluid (slurry) with a SG of 1.148 and viscosity of 14.5 cp were used with the Equations shown in Table 3-13 represents the energy Equation for the complete waste transfer line associated with the 3-inch piping between Building 221-H and the HPP. Table 3-14 represents the energy Equation for the 3-inch header in Building 221-H that includes only the initial section of the waste transfer line having a slope of 0.005 $ft_{vertical}/ft_{horizontal}$ leaving Building 221-H.

Table 3-13. Energy Equations for Velocity Determination for Waste Transfer Lines Between Building 221-H and HPP

WH#/Line Number	Energy Equation
WH #1/WF1100 (HPP#6)	$17.1 = \frac{V^2}{2g}(1.5 + 3216 f_T)$
WH #4/WF1101 (HPP#5)	$15.3 = \frac{V^2}{2g}(1.5 + 3340 f_T)$
WH #3/WF1102 (HPP#5)	$13.9 = \frac{V^2}{2g}(1.5 + 3332 f_T)$
WH #2/WF1103 (HPP#6)	$12.8 = \frac{V^2}{2g}(1.5 + 3159 f_T)$

Table 3-14. Energy Equations for Velocity Determination for Initial Section of the Waste Transfer Lines Leaving Building 221-H with Slope of 0.005

WH#/Line Number	Energy Equation
WH #1/WF1100	$4.91 = \frac{V^2}{2g}(1.5 + 588 f_T)$
WH #4/WF1101	$3.12 = \frac{V^2}{2g}(1.5 + 575 f_T)$
WH #3/WF1102	$1.71 = \frac{V^2}{2g}(1.5 + 575 f_T)$
WH #2/WF1103	$0.64 = \frac{V^2}{2g}(1.5 + 531 f_T)$

Table 3-15. Average Velocity, Reynolds Number, and Flow rate for Waste Transfer Lines Between Building 221-H and HPP

Line	Dissolver Slurry 14.5 cP, 1.148 g/mL						Water 1 cP, 1 g/mL					
	Pipe roughness						Pipe roughness					
	0.0015 ft			0.006667 ft			0.0015 ft			0.006667 ft		
	V (ft/s)	N_{RE}	Q (gpm)	V (ft/s)	N_{RE}	Q (gpm)	V (ft/s)	N_{RE}	Q (gpm)	V (ft/s)	N_{RE}	Q (gpm)
WF1100	3.07	5848	70.7	2.78	5216	64.1	4.22	99903	97.3	3.15	74586	72.6
WF1101	2.81	5260	64.7	2.57	4807	59.1	3.89	92154	89.7	2.92	69198	67.4
WF1102	2.65	4975	61.2	2.43	4559	56.1	3.69	87435	85.1	2.78	65912	64.2
WF1103	2.61	4896	60.2	2.40	4490	55.2	3.64	86094	83.8	2.75	64994	63.3

Table 3-16. Average Velocity, Reynolds Number, and Flow rate for Initial Section of the Waste Transfer Lines Leaving Building 221-H With Slope of 0.005

Line	Dissolver Fluid 14.5 cP, 1.148 g/mL						Water 1 cP, 1 g/mL					
	Pipe roughness						Pipe roughness					
	0.0015 ft			0.006667 ft			0.0015 ft			0.006667 ft		
	V (ft/s)	N_{RE}	Q (gpm)	V (ft/s)	N_{RE}	Q (gpm)	V (ft/s)	N_{RE}	Q (gpm)	V (ft/s)	N_{RE}	Q (gpm)
WF1100	3.84	7192	88.4	3.47	6507	80.0	5.10	120636	117.4	3.84	90990	88.6
WF1101	2.99	5612	69.0	2.74	5139	63.2	4.03	95380	92.8	3.09	73090	71.2
WF1102	2.12	3964	48.7	1.97	3685	45.3	2.90	68716	66.9	2.27	53831	52.4
WF1103	1.25	2334	28.7	1.18	2212	27.2	1.76	41646	40.5	1.43	33825	32.9

The deposition velocity for the 90th percentile particle, the dimensionless grain diameter, and the pipe fill ratio (based on inside diameter of pipe), velocity and Reynolds number for the minimum and maximum pipe slopes are provided in Table 3-17 for a nominal 25 gpm flowrate for all the dissolver batches using the values inTable 3-19 and Table 3-20. For the 14,000 L dissolver batches all the fluids were treated as Newtonian and for the 12,000 L dissolver batches all the fluids were treated as Newtonian and non-Newtonian in determining the fill ratio, velocity and Reynolds number. For the non-Newtonian cases, if the slope was inadequate, a slope that can process 25 gpm of fluid is provided. A calculation was performed using water to determine the transfer velocity required to exceed the deposition velocity when using water and this was 57.5 gpm.

Table 3-17. Deposition, Dimensionless Grain Diameter, Fill Ratio, Velocity and Reynolds Number for the Minimum and Maximum Pipe Slopes at 25 gpm

Dissolver Batch	Sample	Deposition Velocity (ft/s)	d_{gr}*	25 GPM Sloped Data						
					Slope = 0.005 ft/ft			Slope = 0.0268 ft/ft		
				Model**	Fill Ratio	Vel. (ft/sec)	Re	Fill Ratio	Vel. (ft/sec)	Re
	Water	4.44	0.56	N	0.548	1.93	48406	0.331	3.76	65827
14,000 L	4FS19D-0.8M	3.71	0.19	N	0.606	1.71	10738	0.354	3.42	15021
	4FS19D-1.2M	3.71	0.16	N	0.617	1.67	8597	0.359	3.36	12092
	8S19D-0.8M	3.67	0.20	N	0.599	1.73	12254	0.352	3.45	17091
	8S19D-1.2M	3.68	0.18	N	0.611	1.70	9737	0.356	3.39	13653
	5SRE-0.8M	4.08	0.24	N	0.591	1.76	14669	0.348	3.50	20378
	5SRE-1.2M	4.04	0.25	N	0.589	1.77	15278	0.348	3.51	21206
	10SRE-0.8M	3.87	0.17	N	0.616	1.68	8796	0.359	3.36	12365
	10SRE-1.2M	3.83	0.11	N	0.606	1.71	10679	0.355	3.42	14941
12,000 L	4FS19D-0.8M	3.69	0.11	N	0.658	1.56	4449	0.375	3.16	6380
				NN	0.0098 (slope required)			0.330	3.78	10193
	4FS19D-1.2M	3.66	0.10	N	0.666	1.53	3937	0.379	3.13	5670
				NN	0.0092 (slope required)			0.327	3.82	8347
	8S19D-0.8M	3.77	0.12	N	0.645	1.59	5395	0.370	3.22	7688
				NN	0.0061 (slope required)			0.321	3.92	10711
	8S19D-1.2M	3.69	0.16	N	0.621	1.66	8040	0.361	3.34	11329
				NN	0.549	1.93	11047	0.315	4.02	15466

* d_{gr} = dimensionless grain diameter
** Model can be either Newtonian (N) or Non-Newtonian (NN) to determine the fill ratio, velocity or Reynolds number.

Additional calculations were performed on the 1st section of piping to determine if there is a potential for the fluids to start accumulating into their respective header in Building 221-H. The energy equations in Table 3-14 and the physical properties of the 12,000 L 4FS19D-0.8M fluid are used and the results are provided in Table 3-18.

Table 3-18. Maximum Flow using the Most non-Newtonian Solution, 12000 L 4FS19D-0.8M

Line	Flow (gpm)
WF1100 (WH 1)	109.8
WF1101 (WH 4)	86.0
WF1102 (WH 3)	52.4
WF1103 (WH 2)	1.7

Table 3-19. Supernate, Slurry, and Undissolved Density and Solids Fraction Data, 14,000 L and 12,000 L Dissolver Batch Fluids

Sample	Supernate				Slurry				Undissolved Solids in Slurry			
	Density (g/mL)		solids fraction		Density (g/mL)		solids fraction		Density (g/mL)		solids fraction	
	Avg.	STDEV.	Avg.	STDEV.	Avg.	STDEV.	Avg.	STDEV.	Avg.	STDEV.	Avg.	STDEV.
14,000 L Dissolver Batch Fluids												
4FS19D-0.8M	1.230	0.000	0.2871	0.0010	1.306	0.001	0.3322	0.0005	2.647	0.090	0.0633	0.0015
4FS19D-1.2M	1.238	0.000	0.2931	0.0001	1.310	0.000	0.3527	0.0023	3.301	0.147	0.0843	0.0032
8S19D-0.8M	1.221	0.000	0.2810	0.0003	1.318	0.001	0.3422	0.0003	2.763	0.041	0.0850	0.0006
8S19D-1.2M	1.229	0.000	0.2857	0.0001	1.321	0.001	0.3418	0.0005	3.429	0.074	0.0786	0.0006
5SRE-0.8M	1.096	0.000	0.1292	0.0007	1.148	0.000	0.1751	0.0005	5.686	0.512	0.0526	0.0010
5SRE-1.2M	1.111	0.000	0.1410	0.0004	1.160	0.000	0.1840	0.0003	5.029	0.390	0.0500	0.0006
10SRE-0.8M	1.157	0.000	0.2002	0.0001	1.240	0.001	0.2686	0.0001	2.691	0.147	0.0855	0.0002
10SRE-1.2M	1.172	0.000	0.2113	0.0001	1.252	0.001	0.2741	0.0002	3.352	0.199	0.0797	0.0003
12,000 L Dissolver Batch Fluids												
4F5S19D-0.8	1.257	0.003	0.3291	0.0002	1.335	0.001	0.3991	0.0000	2.856	0.128	0.1044	0.0004
4F5S19D-1.2	1.292	0.001	0.3471	0.0011	1.351	0.002	0.3890	0.0003	4.071	0.357	0.0642	0.0017
8S19D-0.8	1.232	0.000	0.2796	0.0003	1.297	0.000	0.3362	0.0003	3.363	0.053	0.0785	0.0006
8S19D-1.2	1.256	0.001	0.3126	0.0003	1.321	0.004	0.3680	0.0003	3.207	0.321	0.0806	0.0006

Table 3-20. Rheological Data, 14,000 L and 12,000 L Dissolver Batch Fluids

Sample	Newtonian Fluid Viscosity (cP)				Apparent Viscosity At Maximum Shear rate cP		Bingham Plastic							
							Up Curve				Down Curve			
	Up Curve		Down Curve				Yield Stress (Pa)		Plastic Viscosity (cP)		Yield Stress (Pa)		Plastic Viscosity (cP)	
	Avg.	STDEV	Avg.	STDEV	Avg.	STDEV.	Avg.	STDEV	Avg.	STDEV	Avg.	STDEV	Avg.	STDEV
14,000 L Dissolver Batch Fluids														
4F5S19D-0.8	5.5	0.2	5.3	0.3	5.3	0.2	0.12	0.16	4.80	0.02	-0.01	0.02	5.11	0.06
4F5S19D-1.2	6.8	0.0	6.5	0.1	6.4	0.0	0.45	0.05	5.67	0.07	0.28	0.04	5.77	0.03
8S19D-0.8	4.9	0.2	4.6	0.3	4.7	0.1	0.24	0.08	4.33	0.04	-0.01	0.11	4.59	0.01
8S19D-1.2	6.1	0.1	5.5	0.3	5.6	0.3	0.17	0.20	5.17	0.26	0.05	0.02	5.39	0.35
5SRE-0.8	3.6	0.1	3.1	0.2	3.3	0.2	0.35	0.07	2.68	0.30	0.05	0.03	3.01	0.16
5SRE-1.2	3.5	0.8	3.1	0.7	3.4	0.4	0.40	0.26	2.56	0.15	0.10	0.27	2.82	0.06
10SRE-0.8	6.3	0.2	5.8	0.2	5.8	0.2	0.63	0.04	4.77	0.31	0.20	0.02	5.29	0.29
10SRE-1.2	5.3	0.4	4.9	0.5	4.9	0.4	0.54	0.11	3.96	0.10	0.14	0.14	4.52	0.12
12,000 L Dissolver Batch Fluids														
4F5S19D-0.8	12.8	0.2	12.2	0.0	11.2	0.1	1.66	0.00	8.67	0.19	1.11	0.06	9.41	0.11
4F5S19D-1.2	14.6	0.2	14.2	0.0	13.0	0.1	1.49	0.08	10.81	0.00	1.37	0.01	10.80	0.06
8S19D-0.8	10.4	0.2	10.0	0.2	9.5	0.2	0.92	0.09	8.14	0.01	0.61	0.03	8.48	0.16
8S19D-1.2	7.3	0.1	7.1	0.0	6.8	0.2	0.51	0.22	5.80	0.17	0.43	0.25	6.00	0.00

4.0 Conclusions

Dissolution time for Th was fast (<5 min) in 7 and 10 M HNO_3 when 0.05 M F^- was present. At 10 M HNO_3, dissolution of Al proved to be extremely slow when 0.002 M Hg was used as is expected to be used in the dissolver. Dissolution was longer than 2 hours without reaching a complete dissolution. Conversely, when dissolved in one of the dissolver solutions from the earlier Th dissolution which started at 7 M HNO_3, the aluminum dissolved in 4.5 to 7 minutes.

Hydrogen gas generation was generally low for thorium dissolutions. The highest raw volume percent of 1.10% in a Th dissolution came when the initial nitric acid concentration was low (4 M) and there was no initial aluminum present in the solution. With aluminum pre-dissolved at about 0.3 M, an initial nitric acid solution of 7 M produced about 1.70% H_2 raw measured volume percent. These values are lower than those observed in literature and are less than those shown in several of the Al dissolutions.

Neutralization of the simulants showed considerable formation of solid material. This material was still fluid at both neutralization points for the idealized dissolver batch composed of 4 FNR, 5 SRE, and 19 DR-3 L-Bundles or a batch made of 8 SRE and 19 DR-3 L-Bundles. The density of the material only increased upon further NaOH addition to achieve 1.2 M excess.

The surface area calculations for the L-Bundles along with the SRE, HMI, and DR-3 assemblies were completed. When comparing the total surface areas of these UNF assemblies with that of the prior processed MURR assemblies as shown in Figure 3-1, the outer surface areas of the SRE, HMI, and DR-3 assemblies are less. Since the off-gas generation rate from dissolving the L-Bundle with the assemblies inside is surface area dependent, dissolving the SRE, HMI, and DR-3 UNF in the H-Canyon is feasible and is bounded by the analyses provided in the prior off-gas calculations for MURR Assemblies.[34]

The literature revealed that about 5 moles of HNO_3 are needed to dissolve 1 mole of thorium versus 3.75 mole of HNO_3 to dissolve 1 mole of aluminum. The literature and experiments showed that the highest vol % H_2 in the off-gas from the dissolution of thorium metal was 3.6 wt % on a water free basis whereas the nominal vol % H_2 in the off-gas from the dissolution of aluminum metal was 7 wt % on a water free basis. The thorium dissolution experiments and literature reviewed showed that at lower HNO_3 concentrations (< 7 M) the dissolved Al has a negligible impact on the dissolution of thorium but this is not true at high HNO_3 concentrations (around 10 M). The amount of HNO_3 and dissolved thorium in solution has a significant impact on the thorium dissolution rate. The thorium dissolution rate is approximately second order with respect to the HNO_3 concentration as shown in Figure 3-3. The HNO_3 concentration also has a big impact on the aluminum dissolution as seen for the MURR and other High Aluminum-Low Uranium assemblies. The thorium dissolution rate, at a constant HNO_3 concentration, drops as the amount of dissolved thorium increases as shown in Figure 3-5. The Al dissolution rate follows a similar behavior as the amount of dissolved aluminum increases as seen in the prior calculations for the dissolution of the MURR assemblies.[34]

There was concern about the off-gas generation from the SRE assemblies which have thorium fuel sources unlike the HMI and DR-3 which have High Aluminum-Low Uranium fuel sources. However, since the SRE assemblies are encased in an external aluminum bundling tube which is then encased in the aluminum L-Bundle, the peak off-gas rates are based on the same Al dissolution chemistry used for the MURR, HMI, and DR-3 assemblies. Should the inner thorium fuel tubes of the SRE assemblies become exposed, the experimental off-gas generation rates per unit surface area of thorium is 0.03 to 0.05 scfm/ft^2 which is low compared to the off-gas generation rates per unit surface area of aluminum of 0.676 scfm/ft^2. As a conservative measure, when the off-gas generation rates were calculated for the inner thorium fuel sources for the SRE assemblies, the Al dissolution off-gas rate was used and the off-gas generation was

still small compared to the off-gas generation from dissolving the exterior L-Bundle and the exterior bundling tube of the SRE assemblies.

The peak off-gas rates for the FNR, SRE, HMI and DR-3 were determined to be bounded by the controls listed in prior calculations for the dissolution of the MURR assemblies.[34] Initially, up to 4 bundles of FNR, SRE, HMI, and/or DR-3 can be charged to a solution of fresh nitric acid. After the first dissolution, the number of bundles that can be charged is dependent on the concentration of aluminum in the dissolver solution as shown in Figure 8 and Table 8 of prior calculations for the dissolution of the MURR assemblies[34]. Since there is conservatism built into these calculations, the proposed dissolver scenarios discussed above should be safe with respect to the H_2 LFL.

The simulated 14,000 L dissolver batch fluids were visually very fluid in nature. The simulated 12,000 L dissolver batch fluid were also very fluid but could be modeled as a Bingham Plastic fluid. The density of the slurries ranged from 1.148 to 1.335 g/mL. The undissolved solids fraction concentrations in the slurries were between 0.05 to 0.1044 and the average densities of these solids ranged between 2.65 to 5.7 g/cm^3, though it is expected that the average density is around 3.5 g/cm^3. The rheological data indicated that the 12,000 L dissolver fluids have non-Newtonian properties and were analyzed using both Newtonian and Bingham Plastic rheological models. There are slight differences in the viscosities as determined using the Bingham Plastic model, Newtonian model, or the apparent viscosity at the maximum shear rate for the 14,000 L batches, but these differences start to become slightly larger for the 12,000 L batches. A viscosity of 14.5 cP and density of 1.148 g/mL were used to assess the hydraulics of the various waster lines. The analysis assumed that the lines were full of fluid with no air entrainment. The flow calculations showed that the initial section of the waste lines leaving Building 221-H had a minimum flow rate of 27.2 gpm associated with WF1103 (WH#2) waste line and is due to this line having essentially no vertical drop as compared to the other waste lines. The flow calculations showed that the other waste lines provide a flow of at least 45.3 gpm. These calculated flow rates were for dirty piping. For clean piping, the calculated flow rates are slightly larger. The calculations showed that the waste lines leaving Building 221-H could handle the 25 to 30 gpm flow that the jet pumps provide, other than waste line WF1103 (WH#2) for the condition where the waste header would not backup into Building 221-H. A calculation was performed using the most non-Newtonian fluid (12,000 L 4F5S19D-0.8 M) for all the headers and only WF1103 (WH#2) was determined to backup. The effect of pipe roughness impacts the flow rates and in this example the flow rates could be reduced by over 20% based on clean pipe conditions.

Critical velocities and dimensionless grain diameters were calculated. The dimensionless grain diameters were all less than 1, indicating that all these fluids should be treated as cohesive slurries. The critical velocity calculation ranged between 3.5 to 4.1 ft/s, indicating that some of the particles will settle to the bottom of the pipe. This critical velocity range is consistent with previous calculations performed for F-Canyon transfers.[7] There is not sufficient data or literature to make a determination if and how much material can potentially settle. Issues such as the actual floc size, shape and composition are not known and the effect of the fine particles on hindering the settling of the larger particles would impact such calculations. Given a range of pipe slopes in the transfer lines, the steepest slopes have transfer velocities of the same values of the critical velocities, given the 25 gpm. Shallower slopes have lower transfer velocities.

5.0 Recommendations

The processing of fuels described in this document will occur in 3 phases. Due to a desire to begin processing to deploy a SRE flowsheet as quickly as possible, SRNL has provided a flowsheet for H-Canyon to charge HA/LU bundles (SRNL-STI-2012-00279 Rev. 0) as part of Phase 1. In June 2010, SRNL issued a flowsheet report (SRNL-STI-2010-00005) for dissolution of MURR UNF. This flowsheet can also be used for the dissolution of HA/LU plate fuels such as FNR fuel. No issues have been identified by SRNL which would preclude H-Canyon from charging the FNR fuel and subsequent charging and blending with SRE and DR-3 UNF (Phase 2). Phase 3 will begin with charging SRE fuel bundles to a fresh dissolver solution followed by a number of DR-3 bundles. Charging recommendations per phase are shown below.

5.1 Phase 1–2

In Phase 1, SRNL proposes the following flowsheet for charging of HA/LU fuel to support the initial SRE flowsheet.

- 6–7 M HNO_3
- 0.5 g/L Gd
- 0.002 M Hg
- 48 to 72 hour dissolution

The dissolver would be prepared with the nitric acid and gadolinium solution. Mercury catalysts will be added to the dissolver to a concentration of 0.002 M. A total of 4 bundles of Ford Nuclear Reactor (FNR) each with 5 assemblies could be charged to the dissolver at an immersion depth of 54 inches as described in the MURR dissolution flowsheet.[34] The mercuric nitrate catalyst could be added at the rate specified in the report for the first charge. Subsequent charges would not require additional mercury catalyst. The generation of hydrogen during dissolution would be bounded by the MURR analysis. Dissolution time should be 48 - 72 hours.

For Phase 2, the number of bundles of SRE fuel to be charged to the dissolver solution from Phase 1 will be based on the methodology explained in the dissolution of the MURR assemblies[34] which depends on several factors including the immersion depth, the amount of dissolved aluminum, the amount of irradiation of the assemblies, and the amount of catalyst present. Prior to addition of the SRE UNF bundles to the dissolver, fluoride should be added to achieve a concentration of 0.05 M. The fluoride acts as a catalyst and is required in the dissolution of Th metal. Following the dissolution of the SRE bundles, the number of DR-3 fuel bundles charged to the dissolver will be based on the methodology explained for the dissolution of the MURR assemblies just like the SRE assemblies.

5.2 Phase 3

In Phase 3, SRNL proposes the following flowsheet for charging of SRE fuel to support the final SRE flowsheet.

- 6–7 M HNO_3
- 0.05 M F^-
- 0.5 g/L Gd
- 0.002 M Hg
- 48 to 72 hour dissolution

The dissolver would be prepared with the nitric acid, fluoride, and gadolinium solution. Fluoride acts as a catalyst and is required in the dissolution of Th metal in the SRE fuel. The mercuric nitrate catalyst

should be added at the rate specified in the MURR dissolution flowsheet[34] for the first charge. Subsequent charges will not require additional mercury or fluoride catalyst. The number of bundles of SRE fuel that can be charged to the dissolver will be determined using the methodology explained in the dissolution of the MURR assemblies[34] which depends on several factors including the immersion depth, the amount of dissolved aluminum, the amount of irradiation of the assemblies, and the amount of catalyst present. The generation of hydrogen during dissolution will be bounded by the MURR analysis. Dissolution time should be 48–72 hours. Following dissolution of the SRE bundles, the number of DR-3 fuel bundles charged to the dissolver will be based on the methodology explained for the dissolution of the MURR assemblies just like the SRE assemblies.

5.3 Additional DR-3 Fuel

L-Area has identified several bundles of HEU DR-3 which are pitted. These bundles are also high aluminum fuels; however, the fuel core is composed of either U-Al_x or U_3O_8-Al, (cermet fuel) not the U_3Si_2-Al alloy of the LEU DR-3 material. U-Al_x or U_3O_8-Al fuels have been evaluated at the Savannah River Laboratory for processing by H-canyon.[34,43,47] The Perkins report determined that the dissolving behavior of the U_3O_8-Al fuel was similar to that of a U-Al_x alloy fuel with fast dissolution rates in HNO_3-$Hg(NO_3)_2$ solutions.[47]

The U-Al_x DR-3 fuel elements basically have the same dimensions as the LEU DR-3 evaluated in the report; therefore, surface area per unit height will not change. As an example, one U-Al_x DR-3 assembly with 4 fuel tubes has dimensions for Tube 1: 62.5 x 6.395 x 0.146 [cm], Tube 2: 62.5 x 7.375 x 0.146 [cm], Tube 3: 62.5 x 8.355 x 0.146 [cm], and Tube 4: 62.5 x 9.335 x 0.146 [cm]. Of note, several assemblies such as 12/049, 12/050, 12/051 do not have a Fuel Tube 1. This configuration will give a slightly higher surface area per unit height but this variance should not be a significant effect on the amount of off-gas since the L-area Bundle is the primary surface source.

The U-Al_x alloy of the specific HEU DR-3 fuel elements will not affect the off-gas calculations since the off-gas generation source term for the MURR, FNR, SRE, and DR-3 assemblies comes from the work of Caracciolo.[43] The Caracciolo off-gas rates were based on 16 wt % U-84 wt % Al fuel cores with an average 8.4 wt % U when taking into account the complete fuel element including the Al cladding. The specific U-Al_x cited in the Appendix A for this fuel has about 6 wt % U in the complete fuel element including Al cladding which is not considerably different from the Caracciolo fuels.

Another difference of this HEU U-Al_x DR-3 fuel is that 5 DR-3 assemblies are stacked one on top of another versus having 4 DR-3 assemblies stacked one on top of another inside a L-Area Bundle tube. This will not affect the surface area per unit height other than extending the surface area one more assembly in terms of height and thus will not affect the peak off-gas rate other than taking longer to dissolve.

Several of the pitted fuel assemblies are composed of a U_3O_8-Al fuel core. These fuel elements basically have the same dimensions as the LEU DR-3 evaluated in this report so surface area per unit height should not change significantly. Example dimensions of these assemblies are 62.5 x 6.38 x 0.151 cm, 62.5 x 7.36 x 0.151 cm, 62.5 x 8.34 x 0.151 cm, and 62.5 x 9.32 x 0.151 cm for fuel tubes 1, 2, 3, and 4, respectively.

Similar to the UAl_x fuels, the U_3O_8-Al version of the HEU DR-3 fuel elements will not affect the off-gas calculations since the off-gas generation source term for the MURR, FNR, SRE, and DR-3 assemblies

comes from the work of Caracciolo.[43] The Caracciolo off-gas rates were based on 16 wt % U-84 wt % Al fuel cores with average 8.4% U in the complete fuel element including Al cladding.

The specific U_3O_8-Al fuel cited in the Appendix A for this HEU DR-3 fuel element has about 29 wt % U in the complete fuel element including Al cladding which is significantly different than the 8.4 wt % U Caracciolo value.[43] However, the Caracciolo report states that for the average 14.6 wt % U Type 1B fuel elements the dissolution time was 16 h versus ~32 h for the average 8.4 wt % U Type 1A fuel elements, but the 8.4 wt % U Type 1A fuel elements gave a peak off-gas rate of 5 scfm while the 14.6 wt % U Type 1B fuel elements gave a peak off-gas rate of 3.2 scfm. In other words, a higher wt % U fuel element may dissolve faster but the peak off-gas rate is lower, probably due to the increased foaming at the metal-nitric acid surfaces. The work of W. C. Perkins discusses the dissolving of U_3O_8-Al fuel elements with about 60 wt % U_3O_8 and 40 wt % Al in the fuel core and about 40 wt % Al cladding in the entire fuel element which is equivalent to 31 wt % U in the complete fuel element including Al cladding.[47] For the Perkins U_3O_8-Al fuel elements the dissolution rate is about 0.7 lb(h*ft) for a 0.001 M Hg and a 0.7 M Al dissolver solution which matches rates shown in Caracciolo for 16 wt % U-84 wt % Al fuel cores. [43, 47]

Based on the Caracciolo and Perkins references, the U_3O_8-Al fuel cores should not behave differently in terms of the dissolution and amount of off-gas produced than the U_3Si_2-Al DR-3 already discussed in the report.

5.4 Flowrate recommendations

It is recommended that Waste Header #1, 4, or 3 (transfer lines WF1100 , WF1101, or WF1102 respectively) be used if there is a potential for the fluid to have a Bingham Plastic yield stress of larger than 1 Pa such as those of the 12,000L dissolver batch fluids. If transfer line WF1103 is used for such fluids, the fluid will back up in to the header in Building 221-H. The 10-inch header associated with Waste Header #2 (WF1103) may backup and provide the necessary head for 25 gpm, but this was not analyzed.

The deposition velocity was calculated between 3.5 to 4.1 ft/s. Given a discharge rate of 25 gpm, only the steepest transfer lines have a potential to mitigate settling of solids. Intermittent flushing with inhibited water is recommended in minimizing undissolved solids buildup at the maximum achievable flow rate with a minimum of at least 3 waste line volumes or an acceptable drop rate in the waste header liquid level is observed.

6.0 Lessons Learned

6.1 Recent Offgas Rate and Concentration Experiments

The technical basis that has been used for dissolution was established using early experimental work performed to develop a recovery process for highly enriched U fuels discharged from SRS reactors.[48] The earlier dissolutions were performed by Caracciolo using unirradiated U-Al alloy tubular fuel assemblies[43] and by Schlea using both unirradiated and irradiated coupons from U-Al alloy fuel[49].

New dissolution experiments performed to evaluate the use of AFS-2 column waste solution for UNF dissolutions challenged current assumptions regarding the potential to exceed 60% of the H_2 lower flammability limit (LFL) in the dissolver off-gas during fuel dissolution.[50] To resolve differences in the previous data that were used for the technical basis, additional experiments were performed to more

closely represent the fuels to be dissolved in H-Canyon. This recent work included a dissolution study of L-Bundle alloy comprised of Al-6061 and experiments that dissolved U-Al alloys.

One of the main differences observed in the technical basis data[43,48,49] and the recent dissolution experiments[50] related to the H_2 off-gas concentration. In the earlier work, the H_2 concentration was highest during the initial part of the dissolution and subsequently decreased to a much lower constant value. In the more recent work, the H_2 concentration with Al-1100 and L-Bundle Al-6061 coupons was observed to be the lowest during the earliest part of the dissolution and generally increased to a constant (or a higher) value during the remaining dissolution. In contrast, when a U-Al alloy was dissolved under the same conditions as Al-1100 and Al-6061 alloys, the off-gas profiles were similar to the original experimental work by Caracciolo, exhibiting high H_2 concentrations initially which decreased with time.

Hydrogen flammability calculations were performed using the recent experimental data[50] to determine the conditions that H-Canyon can safely dissolve SRE/DR-3 fuel in L-Bundles with respect to the H_2 levels during the projected peak off-gas rates. To stay under the 60% LFL for H_2, the charges of L-Bundles containing SRE shall be limited to four, where the Hg is gradually added to the dissolver per the restrictions of Procedure 221-H-4101 after reaching temperature to the recommended 0.012–0.015 M.[51] In order to process the L-Bundles of DR-3 fuel, a minimum of 0.17 M Al must be in solution. This minimum dissolved Al could be reached by first dissolving SRE fuel or by adding $Al(NO_3)_3$ to the dissolver solution. The number of L-Bundles of DR-3 fuel that could be charged successively to the H-Canyon dissolver is dependent on the concentration of U in the U-Al alloy and the dissolved Al concentration. The number of bundles increases as the Al concentration increases in the dissolving solution. The technical basis and recommendations for the dissolution flowsheet provided for DR-3 fuel is applicable to other UNF similar to the University of Missouri Research Reactor (MURR) fuel as discussed in the recent report[50] and memo [52]. H-Canyon is following the revised flowsheet recommendation of SRNL[50,52] as new experiments are being performed to determine an applicable flowsheet that does not require dissolved Al to be present initially.

6.2 Solids formation

Of concern during any dissolution campaign at the H-Canyon is the precipitation of a fissile solid. During the preparation of this original flowsheet, no solids occurred or were expected based on the report by Rodrigues.[53] However, the report documents the dissolution of a UAl_x fuel which yielded 410 mg/L Si in solution when dissolved and the presence of an amorphous solid.[53] This was interpreted to mean that at the calculated Si concentrations in the desired dissolver batches, the Si concentration would be lower than solubility limit observed in the report and thus would not precipitate.[53] During the flowsheet testing described within Rev. 0 and Rev. 1 of this report, Si was added to simulants in the form of sodium metasilicate to achieve a target concentration of ~ 391 mg/L.[58,54]

However, when nearing end of dissolution of the first batch of the SRE campaign in H Canyon, solids were observed in the 6.4 Dissolver samples. The batch included four bundles of FNR, five bundles of SRE and ten bundles of DR3 fuels at the point when solids were first observed. Dissolution of the batch was completed after observation of solids with the addition of nine DR3 bundles for a total of 19 DR3 bundles processed. A sample of the observed solids was transferred to SRNL for identification early in November 2012.[55]

During flowsheet testing, Si was added to simulants in the form of sodium metasilicate to achieve a concentration of ~ 391 mg/L. Based on the work of Rodrigues,[53] this concentration was deemed obtainable and was not expected to precipitate. All simulants were filtered prior to use with the filter being closely inspected. No large precipitate was observed on the filter media. Silicon was not a focus of the flowsheet development work and therefore the Si data was not scrutinized during the initial

documentation. Subsequent inspection of ICP-ES data for the flowsheet development work after observation of solids in the H Canyon dissolver shows that the measured [Si] in the simulants was lower than the targeted [Si] of ~ 391 mg/L indicating that the sodium metasilicate did not completely dissolve.

Scanning electron microscopy (SEM) with elemental analysis by energy-dispersive X-ray spectroscopy (EDS) and inductively coupled plasma emission spectroscopy (ICP-ES) of an alkali fusion[56] digested sample was chosen to help identify the unknown solid from the Canyon dissolver. The results are reported in terms of micrograms of element per gram of dry solids compound. The bulk of the material found in the H-Canyon dissolver 6.4 is amorphous silica. The minor component includes Fe, Ni, Zr, and Mo in the matrix. Iron, nickel, and chlorine are consistent with corrosion products associated with stainless steel.

Figure 6-1, reproduced from reference 57, plots calculated solubility curves for Si with respect to temperature and nitric acid concentration based on equations evaluating silica chemistry.[57] The maximum concentrations of Si found in the Rodrigues work are shown as individual points labeled as to the fuel type dissolved.[53] Expected concentrations for Si from the dissolution of 10 and 19 DR3 bundles at 12000 L (upper point) and 14000 L (lower point) are also displayed. Nitric acid concentrations for these points are estimated and a 10% error is shown. The highest concentration for silicon in the SRE flowsheet testing, 120 mg/L (labeled as "Experimental [Si] in Figure 6-1; 391 mg/L was the target concentration), was found in one of the concentrated samples from the flowsheet development work.[55]

Figure 6-1 shows that the calculated [Si] in the H Canyon batches is above the solubility limits of silica.[57] Historical work at SRS shows silica to be soluble to concentrations above the 10 DR3 charge concentration and still larger than a 19 DR3 bundles charge assuming no evaporation.[53] It is expected that some evaporation will occur in the dissolver. If the dissolver volume drops to ~12000 L without adding additional acid to make up the drop, the calculated [Si] concentration would be higher than the concentration observed in all previous work. In Figure 6-1, the data points show the calculated [Si] for a 10 and 19 DR3 batch. The lower data point corresponds to a 14000 L batch and the upper point represents a 15% drop in dissolver volume. Iler stated that dissolved aluminum would lower the solubility of SiO_2.[57] Aluminum was present at up to 0.98 M in the evaluation of silicide fuels by Rodrigues compared to a maximum of 1.3 M in the present batch in H-Canyon.[58,53,54]

The solids found in the current dissolver batch **do not contain fissile material** as determined by SEM/EDS. The previous revisions of this flowsheet work relied on the Rodrigues site report[53] to evaluate the potential for solids formation in the planned dissolver batches. The Rodrigues report[53], as well as observation of no solids in simulants prior to neutralization during experiments for flowsheet testing, provided no indication that a silica solid should be expected. Silicon concentration calculated to be present on dissolution of 10 – 19 DR3 fuel bundles in the expected H-Canyon dissolver volumes very closely falls within the realm of conditions evaluated by Rodrigues and appears to be only slightly outside of the system described by Iler at 105 °C.[53,57]

Using the literature, it is now evident that a certain amount of solids is to be expected after complete dissolution of a silicide fuel.

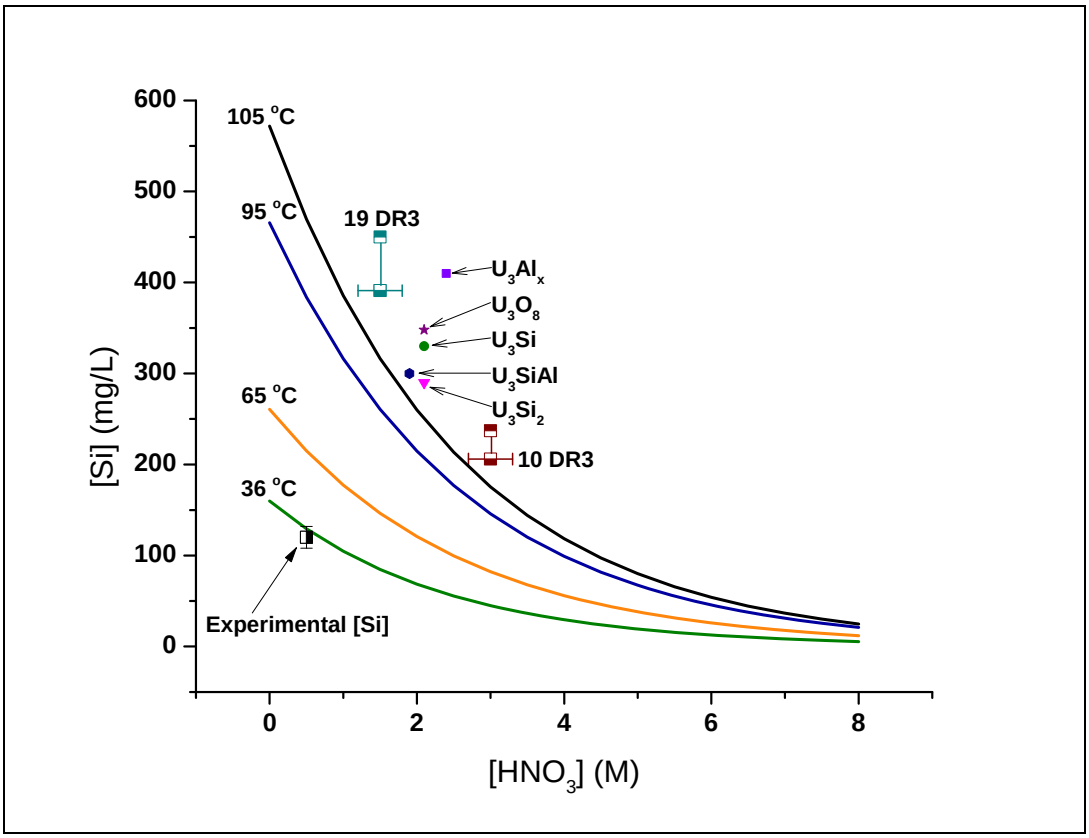

Figure 6-1. Concentration of silicon calculated to be present at several temperatures with respect to nitric acid concentration, experimental [Si], and calculated based on batch size.

6.3 Confirmatory analysis – rheology

Due to concerns that arose after issuing the SRE flowsheet (SRNL-STI-2012-00279, Rev. 1)[58], the document entitled "Confirmatory Analysis on the Physical Properties of the Actual Solution Matrix Tank 16.3 and 16.4 Containing SRE product – By Calculation"[59] was created to addresses the first action item raised in SRNL-L3100-2014-00101[60]:

"A confirmatory analysis– i.e., calculation and SME review – should be conducted prior to discard of the current contents of Tank 16.3/16.4 or prior to resumption of dissolution operations, whichever occurs first."

The major points of that calculation are summarized in the following paragraphs.

The primary concern discussed in this statement is that potential plugging of the transfer line or backing up into the 10-inch header could occur due to the viscosity being too high. This document will show that backing up or plugging of the transfer line is not expected. However, with respect to undiluted batches the supernate salt molarity will be larger, which will increase carrier fluid viscosity. While the slurries are still expected to flow freely, there are not enough data to definitively rule out the potential of backing up in the header. Processing of the batches without water dilution is permitted. If backing up into the header occurs, it is recommended the waste line be flushed with water and the remaining neutralized batch be diluted using at least the minimal water addition.

A calculation was performed in the memorandum[59] using the analytical contents of Tanks 16.3 and 16.4 and the batching requirements as specified by procedures used in H-Canyon[61,62] and comparing these

results to the Sodium Reactor Experiment (SRE) physical data generated by SRNL[63]. The neutralization of these acid streams from Tanks 16.3/16.4 occurs in Tank 16.1 (or equivalent tank for neutralization). Historical test data performed at TNX[63] was also used to support this comparison.

The results from the calculation performed are summarized in Table 1 of the memorandum[59] (shown here as Table 6-1) for 16 waste streams. The first 10 rows are SRNL data: eight rows are the SRE data for the 14,000 liter batches[62], the next row is the Tank 16.4 sample analyzed in 2013[64,65], the next row is the TNX data[63]. The final nine rows are the Tank 16.1 materials with different water content as determined in the memorandum[59] using plant procedures[60,61]. The calculated results in Table 6-1 and statement made in the memorandum of the 16 waste streams are repeated below.

- Tank 16.1 streams contain the least amount of undissolved solids (UDS) in the slurries.
- Tank 16.1 streams have low concentrations of precipitated thorium hydroxide, i.e., < 20 g/L.
- A higher concentrated thorium hydroxide (60 g/L) slurry was processed at TNX at 75 gpm under gravity flow conditions simulating plant design without plugging using an average slope for the 3" pipe and nominal slope for the 10 inch header. This stream has the least amount of soluble salts but the highest concentration of thorium hydroxide. Testing at TNX showed this stream not to be problematic with settling and resuspension.
- Tank 16.1 streams have the lowest concentration of precipitated sodium diuranate as compared to SRNL data, with two exceptions, i.e., a Tank 16.4 analysis done in 2013 and the TNX test where uranium was not used.
- Tank 16.1 streams precipitated aluminum hydroxide concentrations were zero and less than the multi bundled SRNL streams. This concentration was assumed in this memorandum upon characterization of the Tank 16.4 analysis performed in 2013.
- Tank 16.1 streams have the greatest concentration of precipitated gadolinium hydroxide.
- Tank 16.1 streams are generally denser than the other streams. This is due to having more soluble salts ($NaNO_3$, $NaAl(OH)_4$, NaOH) via H-canyon procedures.
- Both SRNL simulated 4 FNR+5SRE+19 DR-3 waste streams most resemble that of the Tank 16.1 streams. These SRNL streams have higher UDS content but lower sodium hydroxide molarity as compared to the Tank 16.1 streams.
- The viscosities of the soluble components in the supernate are provided in Table 5 of SRNL-L3100-2014-00118, Rev. 1.
- The remaining Tank 16.1 streams in Table 6-1 are the maximal concentration values from SRE/DR3 batches to be processed in the near future.[66] These batches have no dilution additions from $Gd(NO_3)_3$ addition or flush water to the acidic stream and the maximum concentration values are provided given the three batches to be processed.
- Dilution from steam jet operations from the acidic tanks to Tank 16.4 and further dilution from Tank 16.1 to the 10 inch header is not considered.
- For the Tank 16.1 slurries, it is not expected that any combination of soluble salt blends with the low UDS concentration will exceed 14.5 cP.

SRNL prepared SRE samples were analyzed for flowability[62] for the waste gravity drain systems used in H-canyon to discharge the waste to the tank farm. The flowability was assessed for a Newtonian fluid having a viscosity of 14.7 cP and density of 1.148 g/mL. Given these properties, waste headers 1, 3, and 4 were determined to easily handle the expected flow rate. Fluids with a lower viscosity or higher density will flow at even higher rates. In the case for non-Newtonian SRE slurries (12,000L samples), a Bingham Plastic yield stress of 1.66 Pa, plastic viscosity of 8.7 cP could backup into the 10 inch header in H-canyon. The gravity drains lines are sensitive for a fluid having a defined yield stress.

Table 6-1. Physical Properties of Thorium Based Neutralized and pH Adjusted Fuel in the Slurry – Reproduced from Reference 59

	Waste Stream	Density (g/ml)	Percent UDS	Undissolved Solids Concentration (g/L)				Soluble Solids (M)			Newtonian	Bingham Plastic	
				$Na_2U_2O_7$	$Th(OH)_4$	$Al(OH)3$	$Gd(OH)_3$	$NaNO_3$	$NaAl(OH)_4$	NaOH	Viscosity (cP)	Yield Stress (Pa)	Plastic Viscosity (cP)
SRNL	5 SRE bundle charge - 1.2M NaOH excess	1.160	5.05	34.50	22.58	0.76	0.70	1.55	0.18	0.47	3.31	0.25	2.69
	5 SRE bundle charge - 0.8M NaOH excess	1.148	5.15	34.84	22.80	0.77	0.70	1.56	0.19	0.29	3.34	0.20	2.85
	10 SRE bundle charge - 1.2M NaOH excess	1.252	8.69	64.46	42.19	1.42	0.65	2.47	0.34	0.39	5.09	0.34	4.24
	10 SRE bundle charge - 0.8M NaOH excess	1.240	8.77	64.49	42.21	1.42	0.65	2.47	0.34	0.38	6.06	0.41	5.03
	4 FNR + 5 SRE + 19 DR-3 bundle charge - 1.2M NaOH excess	1.310	8.52	38.89	18.73	53.49	0.58	3.72	0.24	1.06	6.62	0.36	5.72
	4 FNR + 5 SRE + 19 DR-3 bundle charge - 0.8M NaOH excess	1.306	8.74	39.73	19.13	54.63	0.59	3.80	0.25	0.67	5.39	0.05	4.96
	8 SRE + 19 DR-3 bundle charge - 1.2M NaOH excess	1.321	9.90	53.02	29.31	47.88	0.57	3.67	0.22	1.39	5.78	0.11	5.28
	8 SRE + 19 DR-3 bundle charge - 0.8M NaOH excess	1.318	10.54	53.02	29.31	47.88	0.57	3.90	0.23	0.29	4.75	0.12	4.46
Tank 16.1	Tank 16.4 analyzed in 2013	1.374	1.37	5.85	12.99	0.00	0.00	3.91	0.82	2.90			
	TNX(4X dilution with water)	1.125	7.20	0.00	60.01	0.24	0.00	1.18	0.28	0.00			
	Tank 16.4 contents + no water	1.372	1.75	5.64	15.81	0.00	2.50	3.55	0.69	3.10			
	Tank 16.4 contents + minimum target water	1.342	1.64	5.19	14.56	0.00	2.30	3.27	0.63	2.85			
	Tank 16.4 contents + target water	1.299	1.48	4.54	12.72	0.00	2.01	2.86	0.55	2.49			
	Tank 16.3 contents + no water	1.364	2.10	5.95	19.35	0.00	3.35	3.01	0.62	2.56			
	Tank 16.4 contents + minimum target water	1.341	2.00	5.59	18.16	0.00	3.15	2.82	0.58	2.40			
	Tank 16.4 contents + target water	1.294	1.79	4.80	15.61	0.00	2.71	2.43	0.50	2.07			
	Max SRE/DR3 batch values + no water	1.382	2.30	5.85	25.40	0.00	0.47	4.23	0.89	3.24			
	Max SRE/DR3 Batch values + minimum target water	1.344	2.12	5.27	22.85	0.00	0.42	3.81	0.80	2.91			
	Max SRE/DR2 Batch values + target water	1.294	1.89	4.51	19.57	0.00	0.36	3.26	0.68	2.50			

Note: Tan-Pinkish shaded data are the Tank 16.1batches that have the minimal water dilution

7.0 References

1. (a) Parkins, W.E., *Power Reactors - The Sodium Reactor Experiment*, Proceedings of the International Conference on the Peaceful Uses of Atomic Energy, Geneva, United Nations - New York: Geneva, 1955, p 27. (b) Pickett, C. E. *Recommended Disposition of SRE Fuel*, CBU-HCP-2004-00078, Savannah River Site, 2004, p 3.
2. Clifton, Jr., W. H. *Flowsheet Evaluation for the Dissolving of Sodium Reactor Experiment Used Nuclear Fuel*, TTR, NMMD-HTS-2012-3193, Savannah River Nuclear Solutions, Aiken, SC, January 30, 2012.
3. Rudisill, T. S.; Pierce, R. A. *Dissolution of Plutonium Metal in 8-10 M Nitric Acid*, SRNL-STI-2012-00043, Rev. 0, Savannah River National Laboratory, Aiken, SC, 2012, p 58.
4. D129820, Bldg 221 F/H Savannah River Plant Standard 6'- 0" DIA. X 6'-0" Cell Tank.
5. D127605, Bldg 221 F/H, Stirrers for 6'- 0" Diameter Cell Tank.
6. W146044, SRS 200 AREA, BLDG 221 F/G, 3 H.P. Agitator Assembly For 6' – 0" Dia X 6' – 0" Cell Tank.
7. Lambert, D. P., et. al. *Determining the Cause for Low Flowrates During Am/Cm Simulant Testing in F Area*, WSRC-TR-2002-00569, Rev. 0, April 29, 2003.
8. Newell, J. D., et. al. *Continuously Stirred Tank Reactor Parameters That Affect Sludge Batch 6 Simulant Properties*, SRNL-STI-2009-00603, May 2010.
9. Koopman, D. C., et. al. *Rheology Improvements During Preparation of 40-Inch Heel Case Simulants for Sludge Batch 4*, WSRC-STI-2006-00068, October 2006.
10. Koopman, D. C., et. al. *Impact of Preparation Methods and Scale Factors on Sludge Batch 4 Simulant Properties*, WSRC-STI-2006-00088, November 2006
11. Haestad Methods, Chapter 1, "Basic Hydraulic Principles", http://www.aces.edu/waterquality/streams/Fact%20Sheets/Hydraulic%20Basics.pdf, 2002.
12. Crane Technical Paper No. 410, *Flow of Fluids Through Valves, Fittings, and Pipe*, 1988.
13. Steimke, J. L., et al. *Engineering Development Laboratory (EDL) Draining Tests and Transfer Path Review*, SRT-WHM-2004-00017, Savannah River Laboratory, Aiken, SC, December 30, 2004.
14. Lauchlan, C. S., et al. *Air in Pipelines – A literature Review*, HR Wallingford, SR649, Rev. 2.0, April 2005.
15. Pozos, O., et al. *Air Entrapped in Gravity Pipeline Systems*, Journal of Hydraulic Research, Vol. 48, No. 3, pp. 338-347, 2010.
16. Mathworks, Inc., Natick, Massachusetts, Matlab Central File Exchange, http://www.mathworks.com/matlabcentral/fileexchange/7747.
17. Abulnaga, B. *Slurry Systems Handbook*, Chapter 6, McGraw-Hill, 2002.
18. Darby, R., *Chemical Engineering Fluids Mechanics*, Chapter 6, 2nd, Mercel Dekker, 2001.
19. Turian, R. M., HSU, F. L., Ma, T. W., *Estimation of the Critical Velocity in Pipeline Flow of Slurries*, Powder Technology, Volume 51, pp. 35-47, 1987.
20. Blevins, R. D. *Applied Fluid Dynamics Handbook*, Chapter 8, Kreiger Publishing Company, 2003.
21. Yang, C. T. *Erosion and Sedimentation Manual*, Chapter 3 – Noncohesive Sediment Transport, U.S. Department of the Interior, Bureau of Reclamation, November 2006.
22. W715433, SRP BLDG 21H Replace Waste HDRS Transition Box Sections & Details Process, Instruments & Elect., Rev. 15.
23. W712040, SRP Bldg. 241H Replace Waste Header WF1100 & WF1101 221-H-HPP5 & HPP6, Piping Flexibility Analysis, Sheet 1, Rev. 7.

24. W712042, SRP Bldg. 241H Replace Waste Header WF1102 & WF1103 221-H-HPP5 & HPP6, Piping Flexibility Analysis, Sheet 3, Rev. 7.
25. W712648, SRP Bldg. 241H Replace Waste Header WF1102 & WF1103 221-H-HPP5 & HPP6, Piping Flexibility Analysis, Sheet 4, Rev. 2.
26. W712649, SRP Bldg. 241H Replace Waste Header WF1100 & WF1101 221-H-HPP5 & HPP6, Piping Flexibility Analysis, Sheet 2, Rev. 2.
27. D178553, Waste Line Details, Rev. 4.
28. D179291, Waste Line Details, Rev. 8.
29. Proctor, J. F. *Savannah River Plant Replace Waste Headers, Wr 860604 Basic Design Data*, 132220, October 3, 1978.
30. S1-2-669, Jet Jumper.
31. Darby, R., *Chemical Engineering Fluid Mechanics*, Marcel Dekker, Inc., 2nd Edition, 2001.
32. Jessee, L. *Cropping of HMI (BER-II) Fuel Assemblies (U)*, M-CLC-L-00285, Rev. 1, Savannah River Nuclear Solutions, Aiken, SC, September 28, 2009.
33. Laurinat, J. E. *Calculation of Surface Area for Dissolution of MURR Fuel*, X-CLC-H-00800, Rev. 0, Savannah River Nuclear Solutions, Aiken, SC, December 17, 2009.
34. Kyser, E. A. *Dissolution of Irradiated MURR Fuel Assemblies*, SRNL-STI-2010-00005, Revision 2, Savannah River National Lab, Aiken, SC, June 2010.
35. Karraker, D. G. *Dissolution of Thorium in Mixtures of HNO_3 and HF*, DP-399, Savannah River Laboratory, Aiken, SC, 1959, p 15.
36. Blanco, R. E. *Dissolution and Feed Adjustment*, Symposium on the Reprocessing of Irradiated Fuels, Book 1, United States Atomic Energy Commission, Brussels, Belgium, May 20-25, 1957, p. 22-44.
37. Orth, D. A., *SRP Thorium Processing Experience*, DPSPU 78-30-3, American Nuclear Society Meeting, San Diego, CA, E. I. du Pont de Nemours & Co., Savannah River Laboratory, Aiken, SC, June 18-23, 1978.
38. Clifton, Jr., W. H., *KUR. RECH-I. FNR. and HOR UNF Campaign Validation*, SRNS-EI100-2010-00021, Rev. 0, Savannah River Nuclear Solutions, Aiken, SC, October 13, 2010.
39. Prout, W. E., Symonds, A. E. *Recovery of Thorium and Uranium-233 from Irradiated Thorium Oxide and Metal*, DP-1036, E. I. du Pont de Nemours & Co., Savannah River Laboratory, Aiken, SC, January 1967.
40. Weitz, F. R. *H-Canyon Dissolver Hydrogen Dilution Calculations using Off-gas Specific Lower Flammability Limit (LFL)*, X-CLC-H-00473, Westinghouse Savannah River Company, Aiken, SC, October 2, 2003.
41. Scott, F. E. , Zabetakis, M. G. *Flammability of Hydrogen-Air-Nitrogen Oxide Mixtures*, AECU-3178 or BM-3507, United States Department of the Interior; Bureau of Mines, Pittsburg, PA, 1956.
42. Dyer, W. G., Williams, J. C. *Impact of Temperature on Hydrogen Lower Flammability Limit for Separations, Facilities*, WSRC-TR-2003-00313, Rev 0, Westinghouse Savannah River Company, Aiken, SC, July 2003.
43. Caracciolo, V. P. *Dissolver for Uranium-Aluminum Alloy Tubes*, DP-398, E. I. du Pont de Nemours and Company, Savannah River Laboratory, Aiken, SC, September 1959.
44. Moore, R. L., Goodall, C. A., Hepworth, J. L., Watts, Jr., R. A. *Nitric Acid Dissolution of Thorium*, Hanford Atomic Products Operation, General Electric Co., Richland, Wash. May 1957.
45. Taylor-Pashow, K.M.L. *Neutralizations of High Aluminum Low Uranium Used Nuclear Fuel Solutions Containing Gadolinium as a Neutron Poison*, SRNL-STI-2011-00316, June 2011.

46. Russell, A. S., Edwards, J. D., Taylor, C. S. *Solubility and Density of Hydrated Aluminas in NaOH Solutions*, J. of Metals, **1955**, 1123-1128.
47. Perkins, W. C. *Dissolving Uranium Oxide Fuel Aluminum*, DP-1337, E. I. du Pont de Nemours and Company, Savannah River Laboratory, Aiken, SC, Nov. 1973.
48. Kyser, E. A. *Dissolution of Irradiated MURR Fuel Assemblies – Effect of Increased Purge Rate and Catalyst Concentration on the Batch Size*, SRNL-STI-2010-00205, Savannah River National Laboratory, Aiken, SC, July 2010.
49. Schlea, C. S. *The Dissolution of Uranium-Aluminum Alloy*, DP-629, E. I. du Pont de Nemours and Company, Savannah River Laboratory, Aiken, SC, September 1961.
50. Almond, P. M., Daniel, W. E, Rudisill, T. S. *Flowsheet Modifications for Sodium Reactor Experiment, and Denmark Reactor-3 Used Nuclear Fuel Processing*, SRNL-STI-2014-00228, Revision 0, Savannah River National Laboratory, Aiken, SC, June 2014.
51. *Operation of 6.4D to Dissolve Used Nuclear Fuel*, 221-H-4101, Rev 62, September 2012.
52. Almond, P. M. *Application of Flowsheet Modifications for Denmark Reactor-3 Used Nuclear Fuel Processing to Fuels Similar to the University of Missouri Research Reactor Fuel*, SRNL-L3100-2014-00162, Rev 0, Savannah River National Laboratory, Aiken, SC, September 2014.
53. Rodrigues, G. C., *Reprocessing RERTR Fuels*; DP-MS-83-76.
54. Daniel, W. E.; Hansen, E. K.; Shehee, T. C. *Preliminary Flowsheet Evaluation for the Dissolving and Neutralization of Sodium Reactor Experiment Used Nuclear Fuel*; SRNL-STI-2012-00279 Rev 0, June 2012.
55. Shehee, T. C. *Flowsheet Options for Remediation of Solids in Dissolver used for Dissolution of Sodium Reactor Experiment and Silicide Used Nuclear Fuels,* SRNL-STI-2012-00752 Rev. 0, Savannah River National Laboratory, Aiken, SC, Dec, 2012.
56. SRNL Manual: L16.1 Analytical Development Procedure: ADS - 2502 Revision: 6.
57. Iler, R. K. *The Occurrence, Dissolution and Deposition of Silica,* The Chemistry of Silica – Solubility, Polymerization, Colloid and Surface Properties, and Biochemistry; Wiley & Sons: New York, 1979; Chapter 1.
58. Daniel, W. E., Hansen, E. K., Shehee, T. C. *Flowsheet Evaluation for the Dissolving and Neutralization of Sodium Reactor Experiments Used Nuclear Fuel*, SRNL-STI-2012-00279 Rev. 1, October 2012.
59. Hansen, E. K. *Confirmatory Analysis on the Physical Properties of the Actual Solution Matrix Tank 16.3 and 16.4 Containing SRE product – By Calculation*, SRNL-L3100-2014-00118, Rev. 1, June 2014.
60. Fink, S. D. *Extent of Condition Review: SRE Fuel Processing – pH Adjustment ("Neutralization") and Discard – Batches 1-3*, SRNL-L3100-2014-00101, Rev. 0, May 22, 2014.
61. *Transferring Waste Stream HCAN-SW-25 From Tank 16.4 to Tank 16.1*, 221-H-4871-SW-25, Rev. 0, 5/8/2014.
62. *Receiving Waste Steam HCAN-SW-25 from Tank 16.4 in Tank 16.1, Neutralizing in Tank 16.1, and Discarding to Tank 51, Sludge Batch 9*, 221-H-4872-SW-25, Rev. 0, 5/8/2014.
63. Goodlet, C. B. *Chemical Processing of Irradiated Thorium Handling of Frist Cycle Aqueous Wastes*, DPST-64-134, January 27, 1964.
64. Travel Copy 64557, Rev. 8, Ronnye Eubanks, 7/17/2013C.
65. Coleman email, N*eutralization of recent 16.4 sample*, 8/8/2013.
66. Separate Email from K. Usher and B. Clifton and batch concentration, *Re: Fw: SRE discard of material left to be processed*, 2:30 P.M., 6/11/2014.

Appendix A. Surface Area Calculations

A.1. Disassembly L-Area Bundling Tube Surface Area Calculations

The surface area per unit height of the L-Bundle as described in the SRNS drawing C-CS-L-0962 revision 7 was derived. A sketch of the L-Bundle is shown in Figure A-1. The various parts of the L-Bundle have been color coded and the dimensions of these parts are shown in Table A-1.

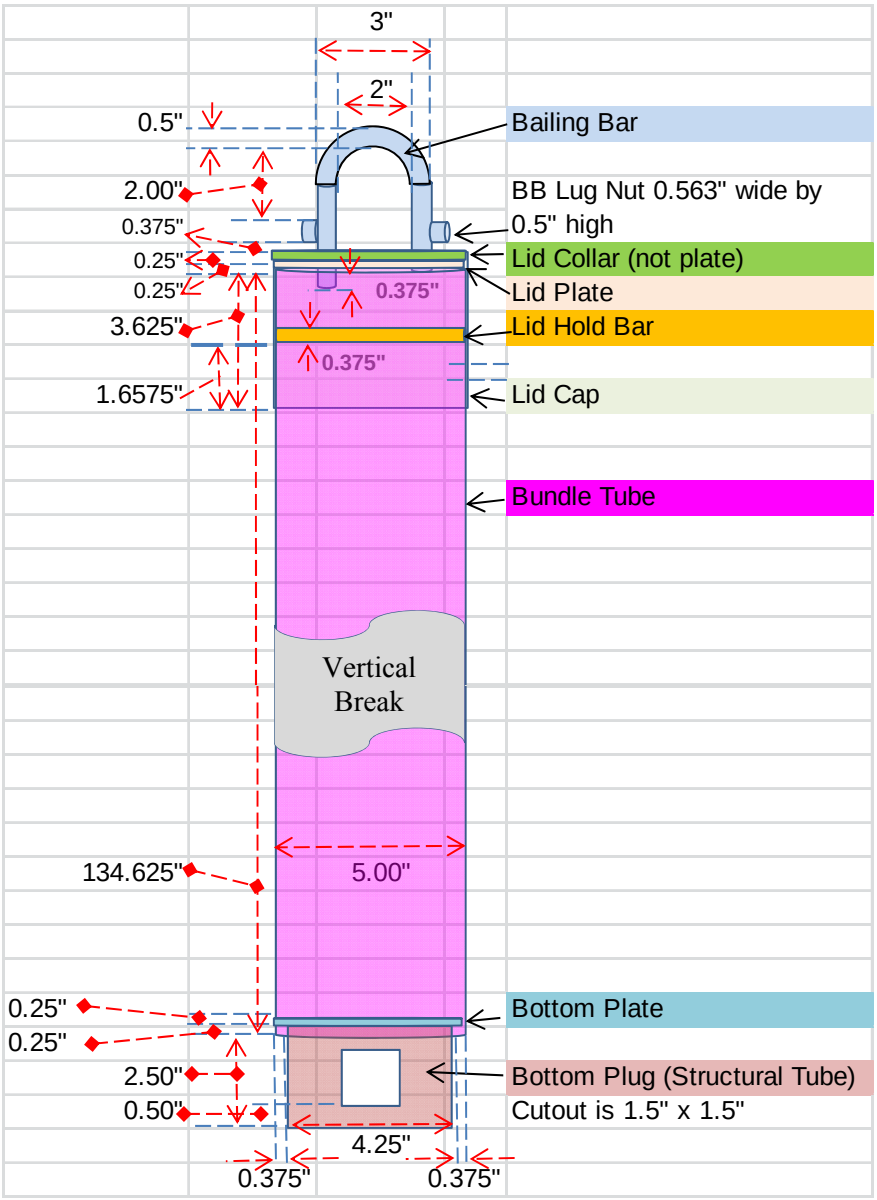

Figure A-1. Sketch of Disassembly L-Area Bundling Tube (DABT) or L-Bundle

Table A-1. Disassembly L-Area Bundling Tube Parts and Dimensions

L-Bundle Part	Outer Diameter (OD) [in]	Wall [in]	Length (vertical height) [in]	Comments
Bailing Bar	0.500	0.500*	8.552	Believe correct bail bar length as 1.875 in. slot in bundle tube for holding bar and treat holding bar separate.
Lid Collar	5.080	0.052	0.250	Since calls collar treat as annular ring on top of lid plate.
Lid Plate	4.976	NA	0.250	Has eight equally space 0.25 in. OD holes plus two 0.5 in. OD holes for bail bar.
Lid Hold Bar	0.375	NA	5.000	Welded to lid to go into 1.875 in. slot on bundle tube.
Lid Cap	5.080	0.052	4.125	Note length (or height) includes 0.25 in. tall lid plate and 0.25 in. tall collar.
Bundle Tube	5.000	0.052	134.625	None
Bottom Plate	4.896	NA	0.250	Has 8 equally space 0.25 in. OD holes. Note that bottom plate sits 0.25 in up from bottom of bundle tube.
Bottom Plug (Structural Tube)	4.250	0.250	2.750	Two 180° apart 1.5 in. x 1.5 in. slots in Bottom Plug 0.5 in. off bottom. Bottom Plug recessed 0.25 in. up into Bundle Tube where contacts Bottom Plate giving exposed 2.5 in. below bundle tube

NA=Not Applicable, *Solid Thickness

Starting from the bottom of the L-Bundle and going up vertically the exposed inner and outer surface area of L-Bundle is calculated as shown in Table A-2. This table details the surface area calculations for specific sections of the L-Bundle in terms of height from its bottom. The first column is called the *Scaling Factor for Height h* or the area per unit height for each section of the L-Bundle. The second column is the *Height h* of each section of the L-Bundle. The third column is the *Constant* area term for each section of the L-Bundle like the previous section's surface area or a specific surface area at the boundary between sections. The fourth column is the *Cumulative Surface Area* term which is the total area up to the specific height of each section which is calculated as the *scaling factor for height* times *height h* plus the *constant*. The fifth and sixth columns are the *from* and *to* height respectively from the bottom of the L-Bundle. These *from* and *to* columns can be used to find the specific surface area at a specific height if desired. The seventh column is the *Description* of the particular section of the L-Bundle where the surface area calculation applies. The eighth column is *Surface Area Sums* in the particular section of the L-Bundle. The [ ] in the *Area Sums* reflect calculation values used in the *Scaling Factor for Height h* and *Constant* columns as shown by the formulae where h terms go into the *Scaling Factor for Height h* and *Constant* terms go into the *Constant* term. Using the logic outlined here, the total inner and outer surface area for the L-Bundle for the full 141 inch height was 4335.83 in^2 giving an overall scaling factor for the L-Bundle of 30.75 in^2/in or 2.56 ft^2/ft.

Table A-2. Inner and Outer Surface Area Calculation for DABT or L-Bundle

Scaling Factor for Height h [in^2/in]	Height h [in]	Constant [in^2]	Cumulative Surface Area [in^2]	From [in]	To [in]	Description	Surface Area Sums
25.13	0.50	3.14	15.71	0	0.5	from bottom of structural tube (bottom plug or BP) up to start of 1.5" cutouts	[Bottom Annular Ring of BP] + [Outside Circumference Area of BP] + [Inside Circumference Area of BP] = $[\pi/4*(4.25^2 - 3.75^2)] + [\pi*4.25*h] + [\pi*3.75*h]$
23.63	1.50	15.71	51.16	0.5	2	from bottom of 1.5" cutouts on bottom plug up to top of 1.5" cutouts on BP	[Outside Circumference Area of BP] + [Inside Circumference Area of BP] - [Outside Face Area of Cutouts] - [Inside Face Area of Cutouts] + [Inside Edge Area of Cutouts] = $[\pi*4.25*h] + [\pi*3.75*h] – [1.5*h] – [1.5*h] + [2*(1.5*0.25 + h*0.25*2)]$
25.13	0.50	51.91	64.47	2	2.5	from top of 1.5" cutouts on BP up to bottom of Bundle Tube	[Outside Circumference Area of BP] + [Inside Circumference Area of BP] + [Top Inside Edge Area of Cutouts] = $[\pi*4.25*h] + [\pi*3.75*h] + [2*(1.5*0.25)]$
29.06	0.25	65.28	72.55	2.5	2.75	from bottom of Bundle Tube up to bottom of bottom plate	[Outside Circumference area of Bundle Tube] + [Inside Circumference area of BP] + [bottom annular ring of Bundle Tube] = $[\pi*5*h] + [\pi*4.25*h] + [\pi/4*(5^2 – 4.896^2)]$
21.99	0.25	87.84	93.34	2.75	3	from bottom of bottom plate up to top of bottom plate	[Inside Surface area of 0.25" holes] + [Outside Circumference area of Bundle Tube] + [bottom surface area of bottom plate] = $[8*(\pi*0.25*h)] + [\pi*5*h] + [\pi/4*4.896^2 – 8*\pi/4*0.25^2 - \pi/4*(4.25^2 – 3.75^2)]$
31.09	130.50	111.77	4168.91	3	133.5	from top of bottom plate up to bottom of lid where overlaps Bundle Tube	[Inside Circumference area of Bundle Tube] + [Outside Circumference area of Bundle Tube] + [top surface area of bottom plate] = $[\pi*4.896*h] + [\pi*5*h] + [\pi/4*4.896^2 – 8*\pi/4*0.25^2]$
31.34	1.66	4168.91	4220.86	133.5	135.16	from bottom of lid where overlaps Bundle Tube up to bottom of holding bar	[Outside Circumference area of Lid] + [Inside Circumference area of Bundle Tube] = $[\pi*5.08*h] + [\pi*4.896*h]$
51.36	0.19	4220.86	4230.49	135.16	135.35	from bottom of holding bar up to middle of holding bar	[Outside Circumference area of Lid] + [Inside Circumference area of Bundle Tube] + [circumference area of holding bar] - [end face areas of holding bar against lid] = $[\pi*5.08*h] + [\pi*4.896*h] + [2*5*0.375*\cos^{-1}(1 - 8/3*h)] - [2*0.375*\{0.375*\cos^{-1}(1 - 8/3*h) – (0.375 – h)*\sin(\cos^{-1}(1 - 8/3*h))\}]$

Table A-2. Inner and Outer Surface Area Calculation for DABT or L-Bundle

Scaling Factor for Height h [in^2/in]	Height h [in]	Constant [in^2]	Cumulative Surface Area [in^2]	From [in]	To [in]	Description	Surface Area Sums
41.29	0.19	4230.49	4238.23	135.35	135.53	from middle of holding bar up to top of holding bar	[Outside Circumference area of Lid] + [Inside Circumference area of Bundle Tube] + [circumference area of holding bar] - [end face areas of holding bar against lid] = $[\pi*5.08*h] + [\pi*4.896*h] + [2*5*0.375*(\pi/2 - \cos^{-1}(h/0.375))] - [1/2*0.375*0.375*(\pi/2 - \cos^{-1}(h/0.375)) + h*\sqrt{0.375^2 - h^2}]$
31.34	1.21	4238.23	4276.23	135.53	136.745	from top of holding bar up to bottom of bail bar in bundle tube	[Outside Circumference area of Lid] + [Inside Circumference area of Bundle Tube] = $[\pi*5.08*h] + [\pi*4.896*h]$
32.91	0.38	4276.43	4288.77	136.75	137.12	from bottom of bail bar in bundle tube up to bottom of lid plate	[Outside Circumference area of Lid] + [Inside Circumference area of Bundle Tube] + [circumference area of bail bar] + [end face area of bail bar] = $[\pi*5.08*h] + [\pi*4.896*h] + [\pi*0.5*h] + [\pi*(0.5/2)^2]$
22.24	0.25	4307.82	4313.38	137.12	137.37	from bottom of lid plate up to top of lid plate (don't count bail bar holes since bail bar fills)	[inside surface area of 0.25" holes] + [Outside Circumference area of Lid] + [bottom surface area of lid plate] = $[8*\pi*0.25*h] + [\pi*5.08*h] + [\pi*(4.976/2)^2 - 8*\pi*(0.25/2)^2]$
34.73	0.25	4313.38	4322.07	137.37	137.62	from top of lid plate (don't count bail bar holes since bail bar fills) up to top of 0.052 thick lid collar	[inside Circumference area of lid collar] + [Outside Circumference area of lid collar] + [Circumference area of bail bar] = $[\pi*4.976*h] + [\pi*5.08*h] + [2*\pi*0.5*h]$
3.14	0.38	4322.89	4324.07	137.62	138	from top of 0.052" thick lid collar to bottom of bail bar lugs	[circumference area of bail bar] + [top annular ring SA of lid collar] = $[2*\pi*0.5*h] + [\pi*(5.08/2)^2 - \pi*(4.976/2)^2]$
4.91	0.25	4324.07	4325.29	138	138.25	from bottom of bail bar lugs up to middle of bail bar lugs	[circumference area of bail bar] + [circumference area of lug] (note [end area of lug exposed] - [end area of lug against bail bar] cancel one another and circumference area of bail bar covered by lug is greater than the end area of lug exposed) = $[2*\pi*0.5*h] + [0.5*0.563*\cos^{-1}(1 - h/0.25)]$

Table A-2. Inner and Outer Surface Area Calculation for DABT or L-Bundle

Scaling Factor for Height h [in^2/in]	Height h [in]	Constant [in^2]	Cumulative Surface Area [in^2]	From [in]	To [in]	Description	Surface Area Sums
4.91	0.25	4325.29	4326.52	138.25	138.5	from middle of bail bar lugs up to top of bail bar lugs	[circumference area of bail bar] + [circumference area of lug] (note [end area of lug exposed] - [end area of lug against bail bar] cancel one another and circumference area of bail bar covered by lug is greater than end area of lug exposed) = $[2*\pi*0.5*h] + [0.563*(\pi/2 - \cos^{-1}(h/0.25))*0.5]$
3.14	1.00	4326.52	4329.66	138.5	139.5	from top of bail bar lugs up to start of arc on bail bar	[circumference area of bail bar] = $[2*\pi*0.5*h]$
4.11	1.50	4329.66	4335.83	139.5	141	from start of arc on bail bar up to top of bail bar	[fraction of bail bar arc SA covered] (note treat circumference area of arc as 2 straight pieces each with half length of 180° arc with diameter of 2.5") = $[h/1.5*\pi/2*2.5*\pi*0.5]$

In a prior set of dissolution calculations for the MURR assemblies, only the external area of L-Bundle was used. For the SRE, HMI, and DR-3 assemblies documented in this report, the predicted clearances between the outermost dimension of these assemblies and the inner diameter of the L-Bundle (4.896 in.) are shown in Table A-3**.** Based on the MURR assemblies dissolution calculations[34] and its references, any surfaces separated by 2 to 9.7 mm are considered too close to be included in the surface area calculations due to the gas layer forming on the "close" surfaces. Based on the clearances described in Table A-3 and the general shape of the assemblies, it was decided to ignore the internal surface parts of the L-Bundle so a set of calculations were performed where only the outer surface area parts of the L-Bundle were counted and the internal surface area parts were not counted but shown as strike through in Table A-4 for completeness. Using the logic outlined here, the total outer surface area for the L-Bundle for the full 141 inch height was 2236.74 in^2 giving an overall scaling factor for the L-Bundle of 15.86 in^2/in or 1.32 ft^2/ft.

Table A-3. Clearances between L-Bundle and SRE, HMI, and DR-3 Assemblies

Assembly	Assembly Outermost Dimension	Clearance between Bundling Tube Inner Wall and Assembly Outermost Dimension	
	[in]	[in]	[mm]
SRE	3.50	0.698	17.7
HMI	3.37	0.763	19.4
DR-3	3.819	0.539	13.7

Table A-4. Outer Surface Area Calculation for DABT or L-Bundle

Scaling Factor for Height h [in^2/in]	Height h [in]	Constant [in^2]	Cumulative Surface Area [in^2]	From [in]	To [in]	Description	Surface Area Sums
13.35	0.50	3.14	9.82	0.00	0.50	from bottom of structural tube (bottom plug or BP) up to start of 1.5" cutouts	[Bottom Annular Ring of BP] + [Outside Circumference Area of BP] + ~~[Inside Circumference Area of BP]~~ = [π/4*(4.25^2 - 3.75^2)] + [π*4.25*h] + ~~[π*3.75*h]~~
13.35	1.50	9.82	29.85	0.50	2.00	from bottom of 1.5" cutouts on bottom plug up to top of 1.5" cutouts on BP	[Outside Circumference Area of BP] + ~~[Inside Circumference Area of BP]~~ - [Outside Face Area of Cutouts] - ~~[Inside Face Area of Cutouts]~~ + [Inside Edge Area of Cutouts] = [π*4.25*h] + ~~[π*3.75*h]~~ – [1.5*h] – ~~[1.5*h]~~ + [2*(1.5*0.25 + h*0.25*2)]
13.35	0.50	30.60	37.27	2.00	2.50	from top of 1.5" cutouts on BP up to bottom of Bundle Tube	[Outside Circumference Area of BP] + ~~[Inside Circumference Area of BP]~~ + [Top Inside Edge Area of Cutouts] = [π*4.25*h] + ~~[π*3.75*h]~~ + [2*(1.5*0.25)]
15.71	0.25	38.08	42.01	2.50	2.75	from bottom of Bundle Tube up to bottom of bottom plate	[Outside Circumference area of Bundle Tube] + ~~[Inside Circumference area of BP]~~ + [bottom annular ring of Bundle Tube] = [π*5*h] + ~~[π*4.25*h]~~ + [π/4*(5^2 – 4.896^2)]
21.99	0.25	57.30	62.80	2.75	3.00	from bottom of bottom plate up to top of bottom plate	[Inside Surface area of 0.25" holes] + [Outside Circumference area of Bundle Tube] + [bottom surface area of bottom plate] = [8*(π*0.25*h)] + [π*5*h] + [π/4*(4.896^2 – 8*π/4*0.25^2 - π/4*(4.25^2 – 3.75^2)]
15.71	130.50	81.23	2131.12	3.00	133.50	from top of bottom plate up to bottom of lid where overlaps Bundle Tube	~~[Inside Circumference area of Bundle Tube]~~ + [Outside Circumference area of Bundle Tube] + [top surface area of bottom plate] = ~~[π*4.896*h]~~ + [π*5*h] + [π/4*4.896^2 – 8*π/4*0.25^2]
15.96	1.66	2131.12	2157.57	133.50	135.16	from bottom of lid where overlaps Bundle Tube up to bottom of holding bar	[Outside Circumference area of Lid] + ~~[Inside Circumference area of Bundle Tube]~~ = [π*5.08*h] + ~~[π*4.896*h]~~
15.96	0.19	2157.57	2160.56	135.16	135.35	from bottom of holding bar up to middle of holding bar	[Outside Circumference area of Lid] + ~~[Inside Circumference area of Bundle Tube] + [circumference area of holding bar] – [end face areas of holding bar against lid]~~ = [π*5.08*h] + ~~[π*4.896*h] + [2*5*0.375*$\cos^{-1}$(1 – 8/3*h)] – [2*0.375*{0.375*$\cos^{-1}$(1 – 8/3*h) – (0.375 – h)*sin($\cos^{-1}$(1 – 8/3*h))}]~~

Table A-4. Outer Surface Area Calculation for DABT or L-Bundle

Scaling Factor for Height h [in^2/in]	Height h [in]	Constant [in^2]	Cumulative Surface Area [in^2]	From [in]	To [in]	Description	Surface Area Sums
15.96	0.19	2160.56	2163.56	135.35	135.53	from middle of holding bar up to top of holding bar	[Outside Circumference area of Lid] + ~~[Inside Circumference area of Bundle Tube] + [circumference area of holding bar] - [end face areas of holding bar against lid]~~ = [π*5.08*h] + ~~[π*4.896*h] + [2*5*0.375*(π/2 - $\cos^{-1}$(h/0.375))] - [1/2*0.375*0.375*(π/2 - $\cos^{-1}$(h/0.375)) + h*$\sqrt{0.375^2 - h^2}$]~~
15.96	1.21	2163.56	2182.91	135.53	136.75	from top of holding bar up to bottom of bail bar in bundle tube	[Outside Circumference area of Lid] + ~~[Inside Circumference area of Bundle Tube]~~ = [π*5.08*h] + ~~[π*4.896*h]~~
17.53	0.38	2183.10	2189.68	136.75	137.12	from bottom of bail bar in bundle tube up to bottom of lid plate	[Outside Circumference area of Lid] + ~~[Inside Circumference area of Bundle Tube]~~ + [circumference area of bail bar] + [end face area of bail bar] = [π*5.08*h] + ~~[π*4.896*h]~~ + [π*0.5*h] + [π*$(0.5/2)^2$]
22.24	0.25	2208.73	2214.29	137.12	137.37	from bottom of lid plate up to top of lid plate (don't count bail bar holes since bail bar fills)	[inside surface area of 0.25" holes] + [Outside Circumference area of Lid] + [bottom surface area of lid plate] = [8*π*0.25*h] + [π*5.08*h] + [π*$(4.976/2)^2$ – 8*π*$(0.25/2)^2$]
34.73	0.25	2214.29	2222.98	137.37	137.62	from top of lid plate (don't count bail bar holes since bail bar fills) up to top of 0.052 thick lid collar	[inside Circumference area of lid collar] + [Outside Circumference area of lid collar] + [Circumference area of bail bar] = [π*4.976*h] + [π*5.08*h] + [2*π*0.5*h]
3.14	0.38	2223.80	2224.98	137.62	138.00	from top of 0.052" thick lid collar to bottom of bail bar lugs	[circumference area of bail bar] + [top annular ring SA of lid collar] = [2*π*0.5*h] + [π*$(5.08/2)^2$ – π*$(4.976/2)^2$]
4.91	0.25	2224.98	2226.20	138.00	138.25	from bottom of bail bar lugs up to middle of bail bar lugs	[circumference area of bail bar] + [circumference area of lug] (note [end area of lug exposed] - [end area of lug against bail bar] cancel one another and circumference area of bail bar covered by lug is greater than the end area of lug exposed) = [2*π*0.5*h] + [0.5*0.563*$\cos^{-1}$(1 – h/0.25)]

Table A-4. Outer Surface Area Calculation for DABT or L-Bundle

Scaling Factor for Height h [in^2/in]	Height h [in]	Constant [in^2]	Cumulative Surface Area [in^2]	From [in]	To [in]	Description	Surface Area Sums
4.91	0.25	2226.20	2227.43	138.25	138.50	from middle of bail bar lugs up to top of bail bar lugs	[circumference area of bail bar] + [circumference area of lug] (note [end area of lug exposed] - [end area of lug against bail bar] cancel one another and circumference area of bail bar covered by lug is greater than end area of lug exposed) = $[2*\pi*0.5*h] + [0.563*(\pi/2 - \cos^{-1}(h/0.25))*0.5]$
3.14	1.00	2227.43	2230.57	138.50	139.50	from top of bail bar lugs up to start of arc on bail bar	[circumference area of bail bar] = $[2*\pi*0.5*h]$
4.11	1.50	2230.57	2236.74	139.50	141.00	from start of arc on bail bar up to top of bail bar	[fraction of bail bar arc SA covered] (note treat circumference area of arc as 2 straight pieces each with half length of 180° arc with diameter of 2.5") = $[h/1.5*\pi/2*2.5*\pi*0.5]$

A.2. Sodium Reactor Experiment (SRE) Surface Area Calculations

The surface area per unit height of the Sodium Reactor Experiment (SRE) shipping can as described in the SRNS drawing EX-N704-000065 was derived. A sketch showing the side view of the SRE is shown in Figure A-2. The numbers along the right side of the drawing show the various layers of fuel slugs stacked end to end. A sketch showing the top cross-section of the SRE is in Figure A-3 where the red circles represent the 0.75 in. outer diameter fuel slugs, the green circles represent the 1 in. outer diameter aluminum spacer tubes, and the blue circles are the 1.125 in. outer diameter aluminum spacer tubes. A sketch of the lifting bail on top of the SRE shipping can is shown in Figure A-4. The various parts of the SRE have been color coded and the dimensions of these parts are shown in Table A-5.

Table A-5. Sodium Reactor Experiment (SRE) Shipping Can Parts and Dimensions

L-Bundle Part	Outer Diameter (OD) [in]	Wall [in]	Length (vertical height) [in]	Comments
Lifting Bail	3.44	0.75*	5.750	Detail dimension in Figure A-4
Lid Top	5.080	0.052	0.250	Whole Lid overlaps flush with top of Bundle Tube so count as part of Bundle Tube Height. Indicate Lid Top Thickness for potential inside surface area calculations.
External Bundle Tube	3.500	0.125	110.250	No holes or cuts in external bundle tube.
Large Internal Aluminum Spacer Tubes	1.125	0.028	103.000	Two of these.
Small Internal Aluminum Spacer Tubes	1.000	0.028	103.000	Five of these.
Internal Fuel Slug	0.750	NA	6.000	Stacked end to end in internal aluminum spacer tubes. Maximum number per SRE shipping can is 119.
Bottom Plate	3.250	NA	0.500	Bottom plate recessed up into external bundle tube except for 0.12" exposed.

NA=Not Applicable, *Leg Thickness

The SRE shipping can has no holes or cuts in the external bundle tube. For this reason the surface area calculations only consider the external surfaces. Starting from the bottom of the SRE and going up vertically the exposed outer surface area is calculated as shown in Table A-6. This table details the external surface area calculations for specific sections of the SRE in terms of height from its bottom. The same terms and structure as defined for the L-Bundle above are used in this table. Using the logic outlined in Table A-6, the total outer surface area for the SRE for the full 110.245 inch height was 1198.21 in^2 giving an overall outer scaling factor for the SRE of 10.87 in^2/in or 0.91 ft^2/ft.

If one wanted to evaluate the additional area from the internal parts of the SRE assembly, the calculations in Table A-6 would need to be augmented. After careful examination of the internal spacing between the aluminum spacer tubes and the fuel slugs, most of the internal clearances are less than 9.7 mm (~3.18–9.65 mm) but there was a small portion of two of the one inch aluminum space tubes (No. 3 and 4) and a small portion of the main bundle tube with a clearance of about 12.2 mm. Therefore the internal area that would possibly be exposed if there were cuts or holes in the SRE main bundling tube is not significant but is quantified in Table A-7. Note that the internal surface area terms that are not counted in the calculation are shown as strike through in Table A-7 for completeness. The additional inner surface area for the SRE for the full 110.245 inch height was 153.34 in^2 giving an overall inner scaling factor for the SRE of 1.47

in^2/in or 0.12 ft^2/ft. If the outer scaling factor of 0.91 ft^2/ft is combined with the inner scaling factor of 0.12 ft^2/ft the total inner and outer scaling factor becomes 1.03 ft^2/ft.

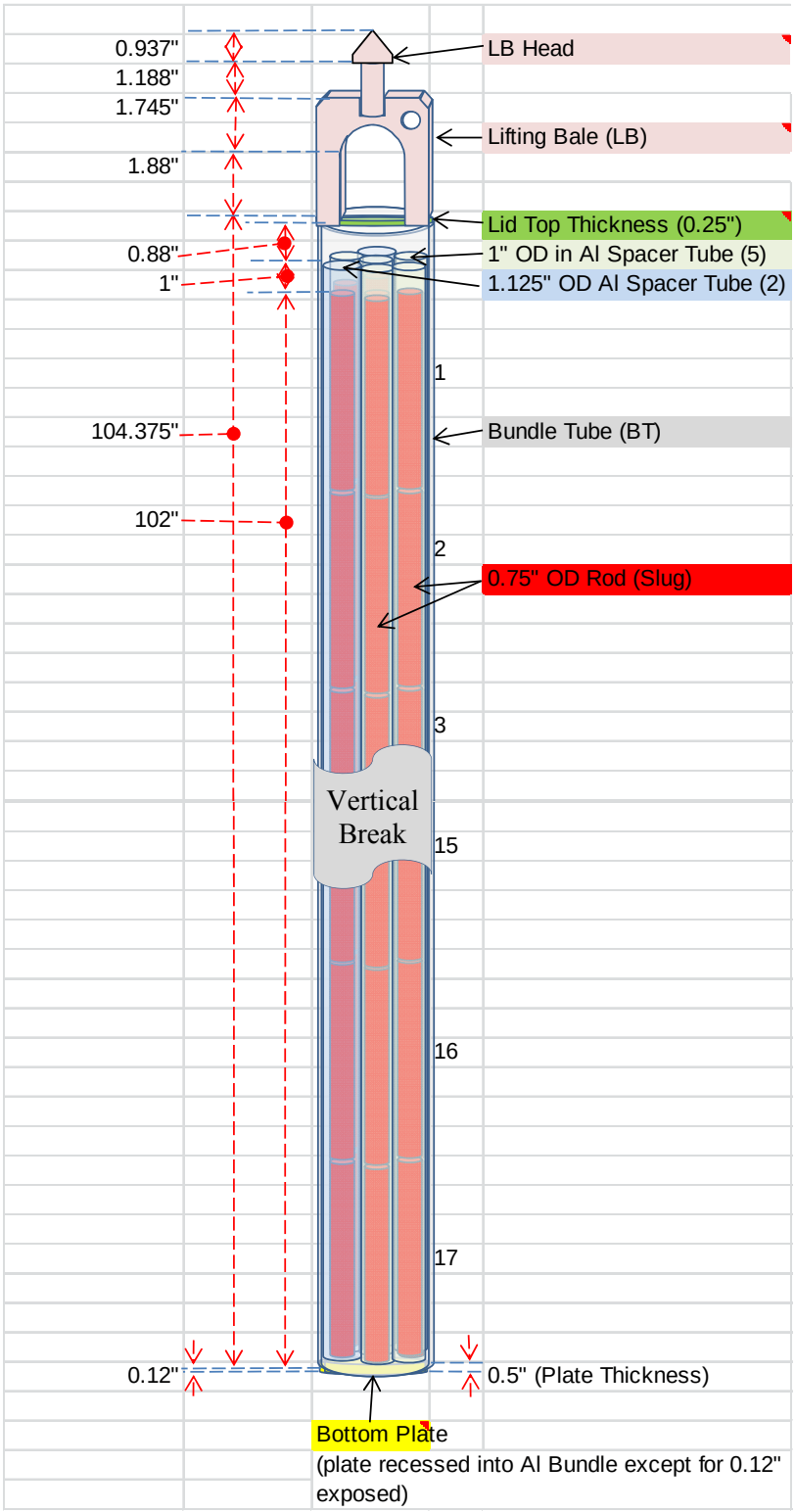

Figure A-2. Sketch of Sodium Reactor Experiment (SRE) Shipping Can

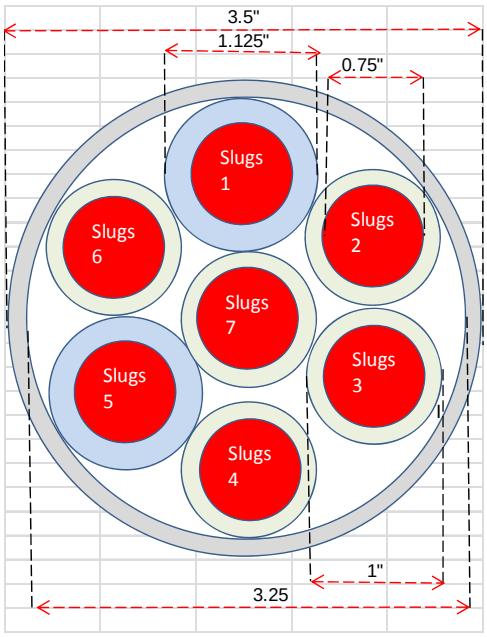

Figure A-3. Sketch of Cross-section of Sodium Reactor Experiment (SRE) Shipping Can

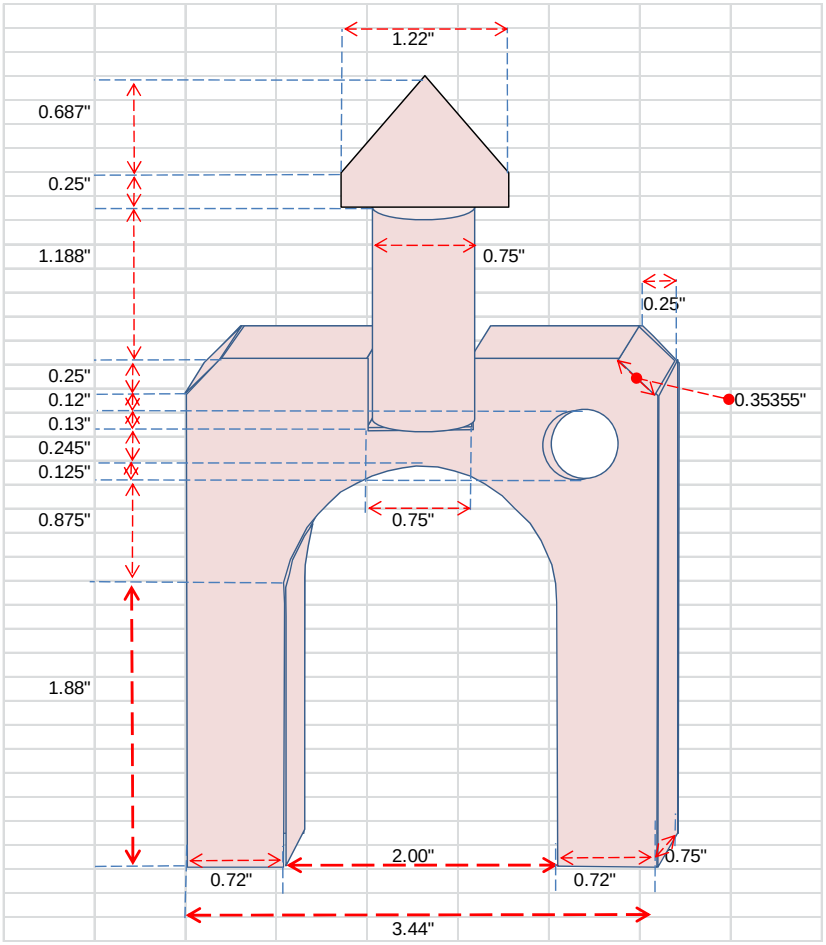

Figure A-4. Sketch of Lifting Bail of Sodium Reactor Experiment (SRE) Shipping Can

Table A-6. Outer Surface Area Calculation for SRE

Scaling Factor for Height h [in^2/in]	Height h [in]	Constant [in^2]	Cumulative Surface Area [in^2]	From [in]	To [in]	Description	Surface Area Sums
10.21	0.12	8.30	9.52	0.00	0.12	From bottom of bottom plate up to start of external Bundle Tube.	[Circumference area of bottom plate] + [Surface area of bottom plate] = $[\pi*3.25*h] + [\pi*(3.25/2)^2]$
11.00	104.38	9.52	1157.18	0.12	104.50	From start of external Bundle Tube up to top of lid. Ignores small 0.125" high 45° chamfer in lid and lid counted as part of external Bundle Tube since sits flush with outside wall of external Bundle Tube.	[Circumference area of external Bundle Tube and Lid] = $[\pi*3.5*h]$
5.88	1.88	1164.62	1175.68	104.50	106.38	From start of exposed Lifting Bale (LB) legs in Al lid up to start of arc in LB.	[(front/back faces of LB leg + right/left faces of LB leg)*No. of LB Legs] + [surface area of top of lid] = $[2*(2*0.72*h + 2*0.75*h)] + [\pi*((3.5-0.75)/2)^2 + 2*0.75]$
6.80	0.88	1175.68	1181.63	106.38	107.25	from start of arc in Lifting Bale (LB) up to start of 0.5" diameter hole in right side of LB	[inside SA of LB arc] + [outside right/left faces of LB legs] + [front/back faces of LB legs] = $[2*0.75*\sin^{-1}(h)] + [2*0.75*h] + [2*\{h*3.44 - \sin^{-1}(h) - h*\sqrt{1-h^2}\}]$
26.03	0.13	1181.63	1184.88	107.25	107.38	from start of 0.5" diameter hole in right side of LB up to top of arc in LB	- [face area of hole] + [inside area of hole] + [outside right/left faces of LB legs] + [front/back faces of LB legs] + [inside SA of LB arc] = $-[0.25^2*\cos^{-1}(1-4*h) - (0.25-h)*0.25*\sin(\cos^{-1}(1-4*h))] + [2*0.75*\cos^{-1}(1-4*h)] + [h*0.75*2] + [2\{h*3.44 - h/0.125*0.04179\}] + [h/0.125*0.50536*0.75*2]$
14.18	0.13	1184.88	1186.66	107.38	107.50	from top of arc in LB up to middle of 0.5" diameter hole in right side LB	[front/back faces of LB legs] + [outside right/left faces of LB legs] -[face area of hole in new section] + [inside area of hole in new section] = $[2*h*3.44] + [2*h*0.75] - [(0.25^2*\cos^{-1}(1 - 4*(h + 0.125)) - h*(0.25 - h - 0.125)*0.25*\sin(\cos^{-1}(1 - 4*(h + 0.125))) - (0.25^2*\cos^{-1}(1 - 4*0.125) - (0.25 - 0.125)*0.25*\sin(\cos^{-1}(1 - 4*0.125)))] + [2*0.75*\cos^{-1}(1 - 4*(h + 0.125)) - 2*0.75*\cos^{-1}(1-4*0.125)]$

Table A-6. Outer Surface Area Calculation for SRE

Scaling Factor for Height h [in^2/in]	Height h [in]	Constant [in^2]	Cumulative Surface Area [in^2]	From [in]	To [in]	Description	Surface Area Sums
9.46	0.12	1186.66	1187.79	107.50	107.62	from middle of 0.5" diameter hole in right side LB up to bottom of notch in LB	[front/back faces of LB legs] + [outside right/left faces of LB legs] -[face area of hole in new section] + [inside area of hole in new section] = [2*h*3.44] + [2*h*0.75] –[0.25^2*$\sin^{-1}$(4*h) + h*$\sqrt{0.25^2 - h^2}$)] + [2*0.75*0.25*sin-1(4*h)]
11.00	0.13	1187.79	1189.22	107.62	107.75	from bottom of notch in LB up to top of 0.5" diameter hole on right side LB	[front/back faces LB legs] + [outside right/left faces LB legs]-[face area of hole in new section] + [inside area of hole in new section] + [notch area bottom exposed] + [head circumference area] + [notch side area exposed] = [3.44*h - 0.75*h] + [0.75*h] – [h/0.13*0.04057] + [h/0.13*0.4013] + [0.75^2*(1- π /4)] + [0.75*π*h] + [2*h*0.75]
7.30	0.12	1189.22	1190.10	107.75	107.87	from top of 0.5" diameter hole on right side LB up to 45° chamfer start on LB	[front/back faces LB legs] + [outside right/left faces LB legs] + [head circumference area] + [notch side area exposed] = [3.44*h - 0.75*h] + [0.75*h] + [0.75*π*h] + [2*h*0.75]
7.48	0.25	1190.10	1191.97	107.87	108.12	from 45° chamfer start on LB up to top of LB	[front/back faces LB legs] + [head circumference area] + [notch side area exposed]-[chamfer missing face area] + [chamfer side area] = [3.44*h - 0.75*h] + [0.75*π*h] + [2*h*0.75] – [$0.5*h^2$] + [0.75*h*$\sqrt{2}$]
2.36	1.19	1191.97	1194.77	108.12	109.31	from top of LB up to start of conical section of head	[head circumference area] = [0.75* π*h]
6.74	0.25	1194.77	1196.45	109.31	109.56	from start of conical section of head up to top of flat sided portion of conical section	[area on underside of conical section] + [flat section of conical section side area] = [π*$(1.22/2)^2$ - π*$(0.75/2)^2$] + [1.22*π*h]
2.56	0.69	1196.45	1198.21	109.56	110.25	from top of flat sided portion of conical section up to conical apex	[conical surface area] = [π*0.61*0.91873 - π*0.66396*$(0.687-h)^2$/0.74777^2]

Table A-7. Internal Surface Area Calculation for SRE

Scaling Factor for Height h [in^2/in]	Height h [in]	Constant [in^2]	Cumulative Surface Area [in^2]	From [in]	To [in]	Description	Surface Area Sums
0.00	0.50		0.00	0.00	0.50	from outside bottom plate up to top of bottom plate	Already accounted for in external calculation.
1.35	102.00	3.09	140.66	0.50	102.50	from top of bottom plate up to top of fuel slugs inside Al tubes	[circumference area of inside main Al canister] + [circumference area of outside Al tubes 1-7] + ~~[circumference area of inside Al tubes 1-7]~~ + ~~[circumference area of outside fuel slugs 1-7]~~ + [bottom surface area of fuel slugs 1-7] assumes fuel slugs flush top to bottom and contact points between inside Al tubes and Al canister and fuel slugs negligible and anything closer than 9.7 mm ignore = [0.29647*1.625*h] {only portion > 9.7 mm} + [2*(0.86689*0.5)*h] {only portion > 9.7 mm} + [7*π *$(0.75/2)^2$]
1.35	1.00	143.75	145.10	102.50	103.50	from top of fuel slugs inside Al tubes to top of Al tubes	[circumference area of inside main Al canister] + [circumference area of outside Al tubes 1-7] + ~~[circumference area of inside Al tubes 1-7]~~ + [top surface area of fuel slugs 1-7] assumes fuel slugs flush top to bottom and contact points between inside Al tubes and Al canister and fuel slugs negligible = [0.29647*1.625*h] {only portion > 9.7 mm} + [2*(0.86689*0.5)*h] {only portion > 9.7 mm} + [7*π *$(0.75/2)^2$]
9.42	0.88	145.10	153.34	103.50	104.38	from top of Al tubes to top inside of lid	[circumference area of inside Al lid] = [3.00*π*h]

A.3. Hahn-Meitner-Institut (HMI) Surface Area Calculations

There were two types of Hahn-Meitner-Institut (HMI) assemblies, a standard and control assembly. The surface area calculations for the standard HMI assembly will be described first followed by the control assembly.

A.3.1. Standard HMI Assembly Surface Area Calculations

The standard HMI assembly is described in the SRNS drawings 2598-100, 101, 102, 104, 105, 300, 303, 304, and 305. The standard HMI assemblies described in these drawings were then cropped by SRNS as described in the calculation sheet M-CLC-L-00285[32]. A sketch showing the side view of the standard HMI assembly is shown in Figure A-5. An enlarged sketch of the standard HMI assembly with the front side plate removed is shown in Figure A-6. The various parts of the standard HMI assembly have been color coded and the dimensions of these parts are shown in Table A-8.

Table A-8. Standard HMI Assembly Parts and Dimensions

HMI Part	Height [in]	Length (width) [in]	Depth[in]	Comments
Side Plate	3.37	28.48	0.18	Front and Back Side Plates
External Fuel Plate	0.06	27.30	2.79	2 External Plates
External Fuel Plate Core	0.06	24.02	2.79	2 External Plates
Internal Fuel Plate	0.05	24.61	2.79	21 Internal Plates
Internal Fuel Plate Core	0.05	24.02	2.79	21 Internal Plates

Since the original standard HMI assembly was cropped, some internal surfaces will be exposed when placed in the L-Bundle. Starting from the bottom of the standard HMI assembly and going up vertically the exposed surface area is calculated as shown in Table A-9. This table as the earlier ones details the surface area calculations for specific sections of the standard HMI assembly in terms of height from its bottom. The same terms and structure as defined for the L-Bundle and SRE above are used in this table. Note that the clearances between the internal and external fuel plates are about 2.1 mm and so these internal surfaces should not be counted in the surface area calculations. Using the logic outlined in Table A-9, the total surface area for the standard HMI assembly for the full 26 inch height was 345.71 in^2 giving an overall outer scaling factor for the standard HMI assembly of 13.30 in^2/in or 1.11 ft^2/ft.

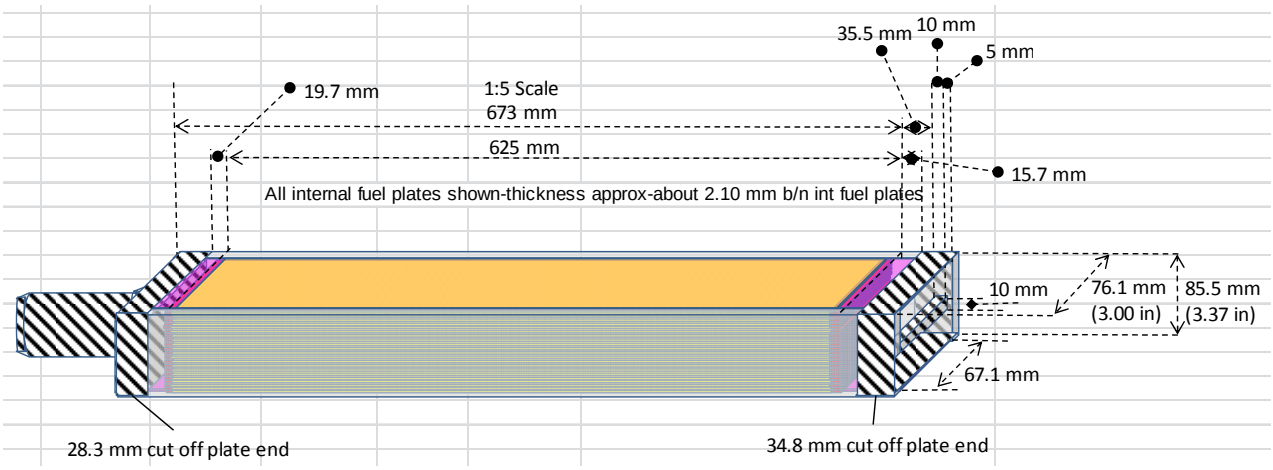

Figure A-5. Sketch of Standard HMI Assembly with Cropped Sections Cross Hatched

Figure A-6. Sketch of Standard HMI Assembly with Side Plate Removed

Table A-9. Surface Area Calculation for Standard HMI Assembly

Scaling Factor for Height h [in^2/in]	Height h [in]	Constant [in^2]	Cumulative Surface Area [in^2]	From [in]	To [in]	Description	Surface Area Sums
25.45	0.62	1.50	17.23	0.00	0.62	from start of cropped end up to start of internal fuel plates	[bottom edges of side plates] + [bottom edges of outer fuel plates] + [outside side plates] + [inside side plates] + [outside outer fuel plates] + [inside outer fuel plates]= [2*0.177*3.366] + [2*0.059*2.642] + [3.366*h*2] +[3.366*h*2] + [2.996*h*2] + [2.996*h*2]
12.72	24.61	19.99	333.09	0.62	25.22	from start of internal fuel plates up to top of internal fuel plates (note ignore inside area between internal fuel plates and outer fuel plates since they are about 2.1 mm apart)	[bottom edge area of internal plates] + [outside side plates] + [outside outer fuel plates] = [21*0.05*2.62] + [3.366*h*2] + [2.996*h*2]
12.72	0.78	335.84	345.71	25.22	26.00	from top of internal fuel plates up to cropped end	[top edge area of internal plates] + [outside side plates] + [outside outer fuel plates] = [21*0.05*2.62] + [3.366*h*2] + [2.996*h*2]

A.3.2. Control HMI Assembly Surface Area Calculations

The control HMI assembly is described in the SRNS drawings 2598-400, 401, 402, 403, 405, 201, 202, 203, 205, and 207. The control HMI assemblies described in these drawings were then cropped by SRNS as described in the calculation sheet M-CLC-L-00285[32]. A sketch showing the side view of the control HMI assembly is shown in Figure A-7. An enlargement of the cylindrical cropped end of the control HMI assembly is shown in Figure A-8. An enlarged sketch of the standard HMI assembly with the front side plate removed is shown in Figure A-9. The various parts of the standard HMI assembly have been color coded and the dimensions of these parts are shown in Table A-10.

Table A-10. Control HMI Assembly Parts and Dimensions

HMI Part	Height [in]	Length (width) [in]	Depth[in]	Comments
Side Plate	3.37	31.79	0.18	Front and Back Side Plates
Outer Absorber Plate	0.06	31.75	2.79	2 Outer Plates on Top and Bottom
Inner Absorber Plate	0.05	29.90	2.79	2 Inner Plates on Top and Bottom
Internal Fuel Plate	0.05	24.61	2.79	17 Internal Plates
Internal Fuel Plate Core	0.05	24.02	2.79	17 Internal Plates
Cylindrical End -1	2.969 (OD)	0.197	NA	Cylindrical end closest to fuel plates (see Figure A-8)
Cylindrical End - 3	2.402 (OD)	0.689	NA	Cylindrical end furthest from fuel plates (see Figure A-8)

OD = Outer Diameter, NA=Not Applicable

Since the original control HMI assembly was cropped, some internal surfaces will be exposed when placed in the L-Bundle. Starting from the bottom of the control HMI assembly and going up vertically the exposed surface area is calculated as shown in Table A-11. This table as the earlier ones details the surface area calculations for specific sections of the control HMI assembly in terms of height from its bottom. The same terms and structure as defined for the L-Bundle, SRE, and HMI-standard above are used in this table. Note that the clearances between the internal fuel plates and outer/inner absorber plates are about 2.1 mm and the clearance between the outer/inner absorber plates is about 6 mm so these internal surfaces should not be counted in the surface area calculations. Using the logic outlined in Table A-11, the total surface area for the control HMI assembly for the full 30.3 inch height was 399.72 in^2 giving an overall outer scaling factor for the control HMI assembly of 13.19 in^2/in or 1.10 ft^2/ft.

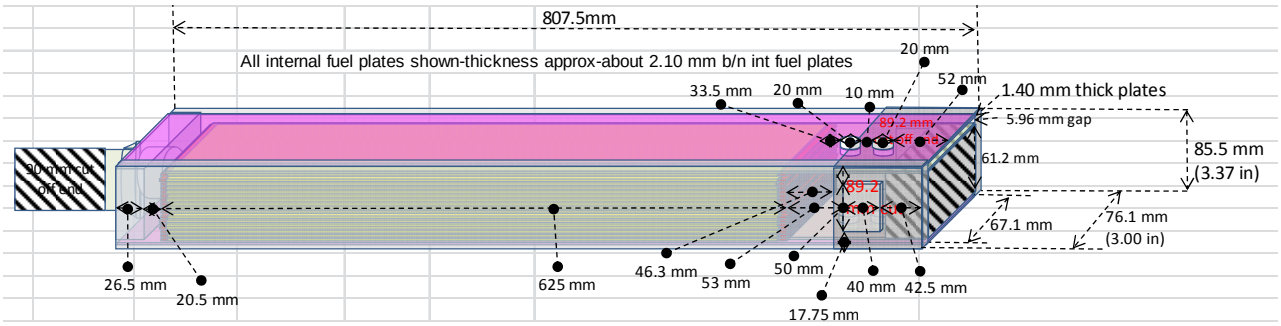

Figure A-7. Sketch of Control HMI Assembly with Cropped Sections Cross Hatched

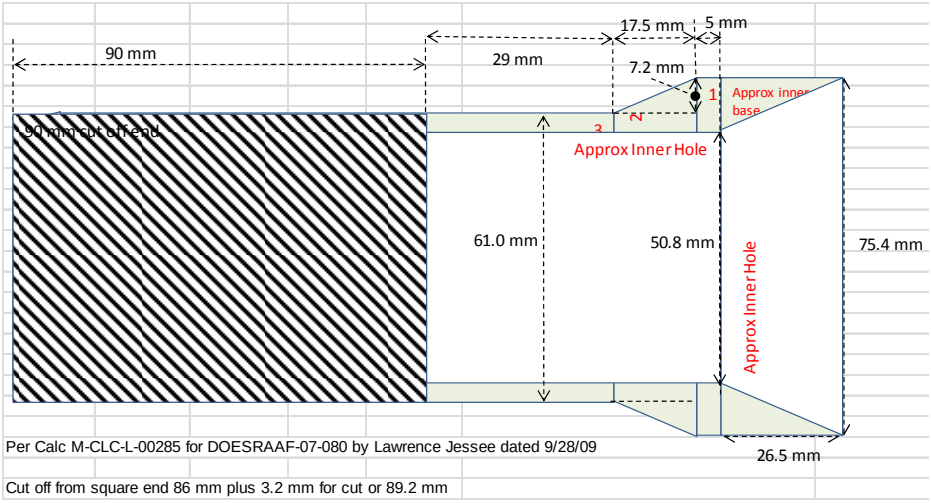

Figure A-8. Sketch of End of Control HMI Assembly with Cropped Sections Cross Hatched

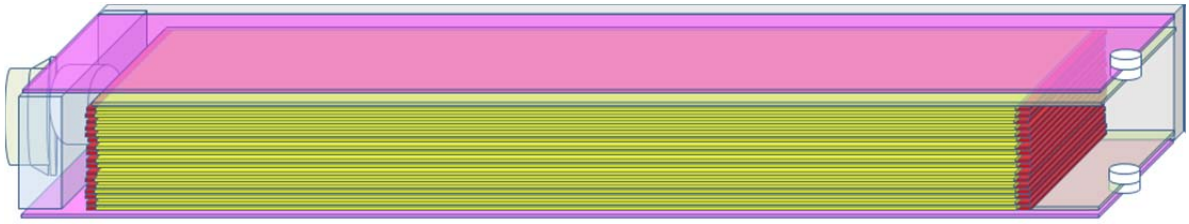

Figure A-9. Sketch of Control HMI Assembly with Front Side Plate Removed

Table A-11. Surface Area Calculation for Control HMI Assembly

Scaling Factor for Height h [in^2/in]	Height h [in]	Constant [in^2]	Cumulative Surface Area [in^2]	From [in]	To [in]	Description	Surface Area Sums
22.53	0.11	1.78	4.26	0.00	0.11	from start of cropped end up to middle of hole	[bottom edges of outer and inner top & bottom Abs plates] + [bottom edges of front & back side plates] +[outside faces of front & back side plates] + [outside faces of top & bottom outer Abs plates] + [outer faces of top & bottom inner Abs plates] + [inner faces of side plates] - [face area of holes in outer top/bot Abs plates] + [inside circumference area of holes in out/in top/bot Abs plates] = [0.0551*2.642*2*2] + [0.177*3.366*2] + [3.366*h*2] + [2.996*h*2] + [2.642*h*2] + [2.409*h*2] - [4*{0.394^2*$\cos^{-1}$(1-h/0.394)-0.394*(0.394-h)*sin($\cos^{-1}$(1-h/0.394))}] + [4*2*0.394*0.0551*$\cos^{-1}$(1-h/0.394))]
21.05	0.39	4.26	12.54	0.11	0.50	from middle of second hole in out/in top/bot Abs plate up to top of second hole	[outside faces of front & back side plates] + [outside faces of top & bottom outer Abs plates] + [outer faces of top & bottom inner Abs plates] + [inner faces of side plates] - [face area of holes in outer top/bot Abs plates] + [inside circumference area of holes in out/in top/bot Abs plates] = [3.366*h*2] + [2.996*h*2] + [2.642*h*2] + [2.409*h*2] - [4*{h*$\sqrt{0.394^2 - h^2}$ + 0.394^2*$\sin^{-1}$(h/0.394)}] + [4*2*0.394*0.0551*$\sin^{-1}$(h/0.394)]
22.83	1.32	12.54	42.65	0.50	1.82	from top of second hole in out/in top/bot Abs plate up to start of internal fuel plates	[outside faces of front & back side plates] + [outside faces of top & bottom outer Abs plates] +[outer faces of top & bottom inner Abs plates] + [inner faces of side plates] = [3.366*h*2] + [2.996*h*2] + [2.642*h*2] + [2.409*h*2]
12.72	24.61	44.88	357.98	1.82	26.43	from start of internal fuel plates up to top of int fuel plates (note don't count inner faces due to closeness of plates)	[outside faces of front & back side plates] + [outside faces of top & bottom outer Abs plates] + [bottom edges of internal fuel plates] = [3.366*h*2] + [2.996*h*2] + [17*0.050*2.62]
12.72	0.81	357.98	368.25	26.43	27.24	from top of int fuel plates up to bottom of end fitting base (don't include any internal surfaces)	[outside faces of front & back side plates] + [outside faces of top & bottom outer Abs plates] = [3.366*h*2] + [2.996*h*2]

Table A-11. Surface Area Calculation for Control HMI Assembly

Scaling Factor for Height h [in^2/in]	Height h [in]	Constant [in^2]	Cumulative Surface Area [in^2]	From [in]	To [in]	Description	Surface Area Sums
12.72	1.04	368.25	381.52	27.24	28.28	from bottom of end fitting base up to top of side/outer Abs plates (don't include any internal surfaces)	[outside faces of front & back side plates] + [outside faces of top & bottom outer Abs plates] = [3.366*h*2] + [2.996*h*2]
9.33	0.20	383.01	384.84	28.28	28.48	from top of side/outer Abs plates up to top of part 1 of end fitting cylinder	[top area if no cylinder or corner holes] - [cross sectional area of cylinder base] - [area of corner holes] + [circumference outside area of end fitting cylinder] = [2.969*2.929] – [π*(2.969/2)^2] – [0.5*0.382*0.382*4] + [π*2.969*h]
9.09	0.69	384.84	391.10	28.48	29.17	from top of part 1 of end fitting cylinder to top of part 2 of end fitting (for derivation see calc for Std HMI)	[circumference area of conical section of part 2] = [total conical area] - [top conical area] = [(π*1.484*4.34) - (π*0.342/(1-0.342^2)*(4.078 - h)^2)]
7.54	1.14	391.10	399.72	29.17	30.31	from top of part 2 of end fitting cylinder up to top of part 3 of end fitting (note calc ends here since cut off top 50 mm)	[circumference area of cylindrical section of part 3] = [π*2.402*h]

A.4. DR-3 (Denmark Reactor) Surface Area Calculations

The surface area per unit height of the DR-3 (Denmark Reactor) assemblies as described in the SRNS drawings VPF 22923-001,002,003,004,005,006,007,008,009,010,011-A-RISO was derived. The original DR-3 assemblies were altered as shown in VPF 22923-001,002,003,004-A-RISO where only the concentric fuel tubes remained in a cup holder assembly. The fuel tubes were of two lengths where the first set is designated as DR-3-1 which was 24.606 inches long and a second set designated as DR-3-2 which was 26.0 inches long. Therefore, the surface area calculations have been broken down into two sections.

A.4.1. DR-3-1 (Denmark Reactor) Surface Area Calculations

A sketch of the side view of the DR-3-1 assembly is shown in Figure A-10. A top cross sectional view of the DR-3-1 assembly is shown in Figure A-11 showing the spacing of the concentric fuel tubes. Figure A-12 shows a cross-section side view of the DR-3-1 assembly with the top and bottom cup plates holding the fuel tubes with a hairpin. Figure A-13 shows a top view of the top and bottom cup plates. Since the cup plates are only 1 mm thick the inside area of holes are not counted in the surface area calculations. The elevation change in the top and bottom cup plates due to a 40.5 mm circular countersunk area around the center point is also ignored in the surface area calculations. The various parts of the DR-3-1 assembly have been color coded and the dimensions of these parts are shown in Table A-12.

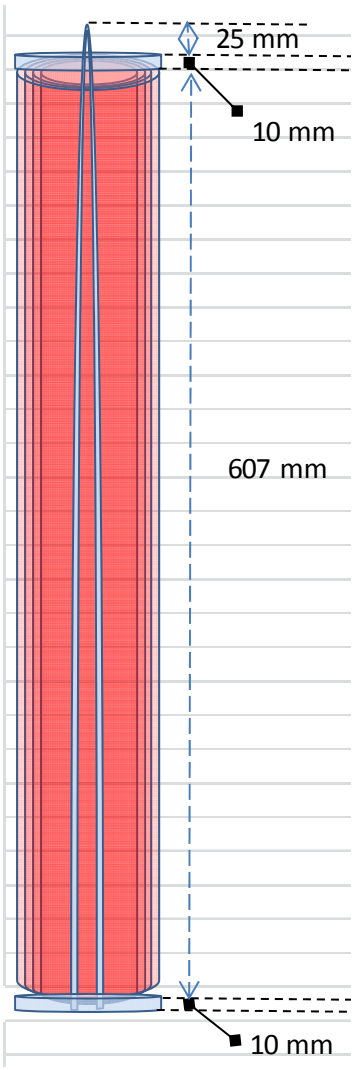

Figure A-10. Sketch of Side View of DR-3-1 Assembly

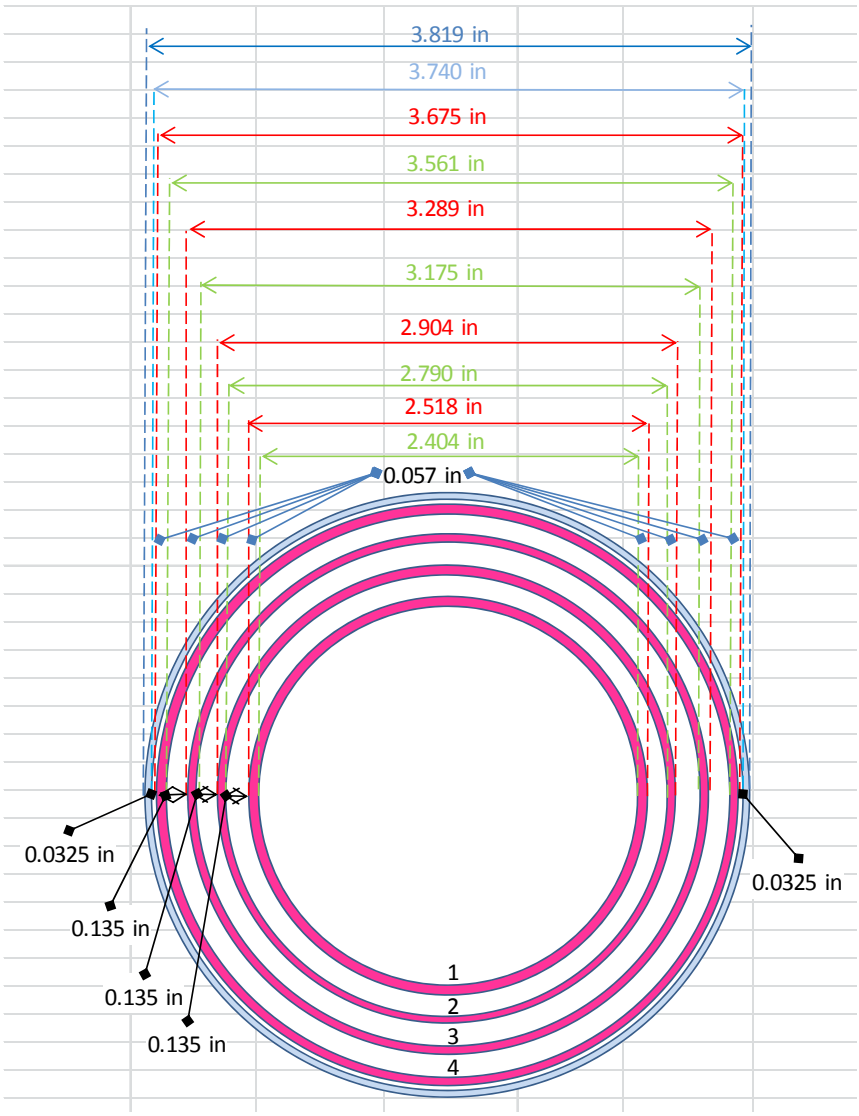

Figure A-11. Sketch of Top Cross-section of DR-3-1 Assembly

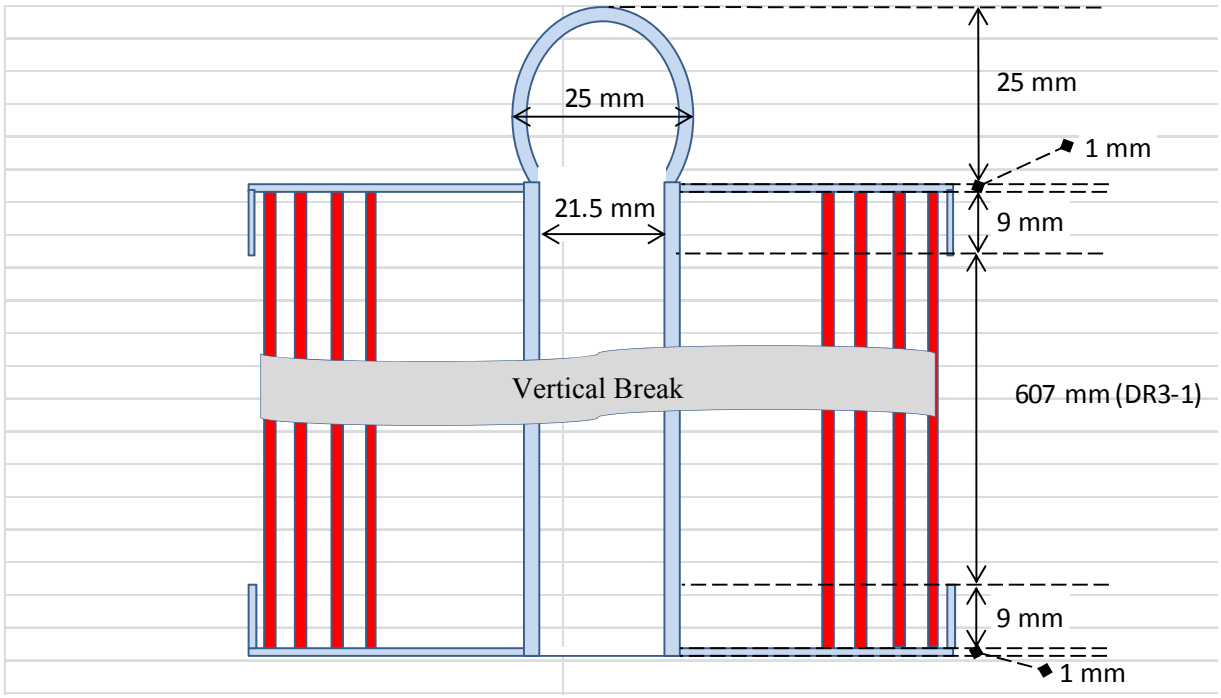

Figure A-12. Sketch of Side Cross-section of DR-3-1 Assembly

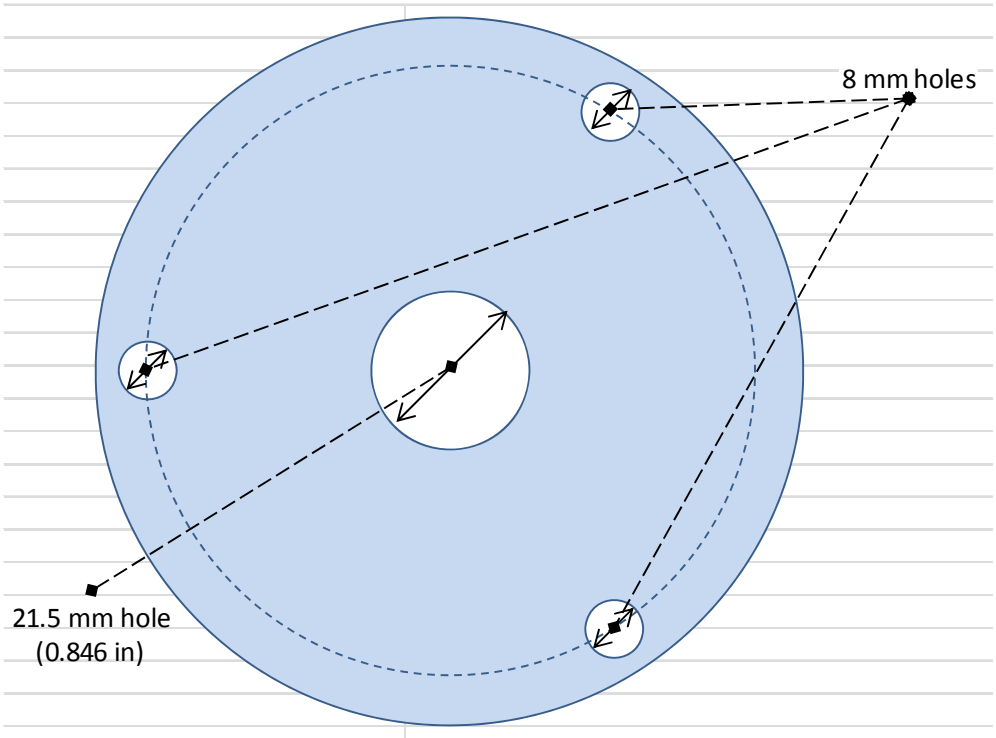

Figure A-13. Sketch of Top and Bottom Cup Plates of DR-3-1 Assembly

Table A-12. Denmark Reactor DR-3-1 Assembly Parts and Dimensions

DR-3-1 Part	Outer Diameter (OD) [in]	Wall [in]	Length (vertical height) [in]	Comments
Fuel Tube 1	2.518	0.057	24.606	Innermost fuel tube
Fuel Tube 2	2.904	0.057	24.606	Outside fuel tube 1
Fuel Tube 3	3.289	0.057	24.606	Outside fuel tube 2
Fuel Tube 4	3.675	0.057	24.606	Outermost fuel tube
Cup Plate Assembly	3.819	NA	25.669	Overall dimensions of cup plate assembly with fuel tubes.
Hairpin	0.98	0.0787	52.56	OD for circular bent hairpin at top. Length is if hairpin straightens out.
Top and Bottom Cup Plates	3.819	0.0394	0.39	Length is height of cup wall.

NA=Not Applicable

Starting from the bottom of the Denmark Reactor DR-3-1 Assembly and going up vertically the exposed inner and outer surface area is calculated as shown in Table A-13. This table details the surface area calculations for specific sections of the DR-3-1 Assembly in terms of height from its bottom. The same terms and structure as defined for the L-Bundle, SRE, and HMI above are used in this table. Using the logic outlined here, the total inner and outer surface area for the DR-3-1 Assembly for the full 25.7 inch height was 513.43 in^2 giving an overall scaling factor for the DR-3-1 Assembly of 20.00 in^2/in or 1.67 ft^2/ft.

Table A-13. Inner and Outer Surface Area Calculation for DR-3-1 Assembly

Scaling Factor for Height h [in^2/in]	Height h [in]	Constant [in^2]	Cumulative Surface Area [in^2]	From [in]	To [in]	Description	Surface Area Sums
12.49	0.04	10.66	11.15	0	0.04	from bottom of bottom cup plate up to start of fuel tubes (ignore inside circumference area of holes since only 1 mm thick and elevation change for 40.5 mm circular countersunk area)	[bottom area of cup plate] + [outer circumference area of bottom cup plate] + [circumference area of 2 legs of hairpin] = $[\pi/4*(3.819^2-3*0.315^2-0.846^2)] + [\pi*3.819*h] + [\pi*0.0787*2*h]$
20.04	0.35	15.13	22.23	0.04	0.39	from start of fuel tubes up to top of bottom cup plate	[inside face area of bottom cup plate] + [outside circumference area of bottom cup plate] + [circumference area of 2 legs of hairpin] + [inner circumference area of fuel tube 1] = $[(\pi/4*(2.404^2-0.846^2))] + [\pi*3.819*h] + [\pi*0.0787*2*h]+ [\pi*2.404*h]$
19.59	23.90	22.23	490.44	0.39	24.29	from top of bottom cup plate up to bottom of top cup plate	[circumference area of 2 legs of hairpin] + [inner circumference area of fuel tube 1] + [outer circumference area of fuel tube 4] = $[\pi*0.0787*2*h] + [\pi*2.404*h] + [\pi*3.675*h]$
20.04	0.35	490.44	497.54	24.29	24.65	from bottom of top cup plate up to top of fuel tubes	[circumference area of 2 legs of hairpin] + [inner circumference area of fuel tube 1] + [outer circumference area of top cup plate] = $[\pi*0.0787*2*h] + [\pi*2.404*h] + [\pi*3.819*h]$
12.49	0.04	501.52	502.01	24.65	24.69	from top of fuel tubes up to top of top cup plate (ignore inside circumference area of holes since only 1 mm thick and elevation change for 40.5 mm circular countersunk area)	[inside face area of top cup plate] + [circumference area of 2 legs of hairpin] + [outer circumference area of top cup plate] = $[\pi/4*(2.404^2--0.846^2)] + [\pi*3.819*h] + [\pi*0.0787*2*h]$
0.78	0.98	512.67	513.43	24.69	25.67	from top of top cup plate up to top of hairpin (assume bent hair pin ~25 mm Outer Diameter)	[top area of top cup plate] + [circumference area of 2 legs of hairpin curved] = $[\pi/4*(3.819^2 - 3*0.315^2 - 0.846^2)] + [\pi*\pi*2/25.4*h]$

A.4.2. DR-3-2 (Denmark Reactor) Surface Area Calculations

A sketch of the side view of the DR-3-2 assembly is shown in Figure A-15.Figure A-14. The top cross sectional view of the DR-3-2 assembly is the same as the DR-3-1 assembly as shown in Figure A-11 showing the spacing of the concentric fuel tubes. Figure A-15 shows a cross-section side view of the DR-3-2 assembly with the top and bottom cup plates holding the fuel tubes with a hairpin. The top and bottom cup plates are the same as in the DR-3-1 assembly as shown in Figure A-13. Since the cup plates are only 1 mm thick the inside area of holes are not counted in the surface area calculations. The elevation change in the top and bottom cup plates due to a 40.5 mm circular countersunk area around the center point is also ignored in the surface area calculations. The various parts of the DR-3-2 assembly have been color coded and the dimensions of these parts are shown in Table A-14.

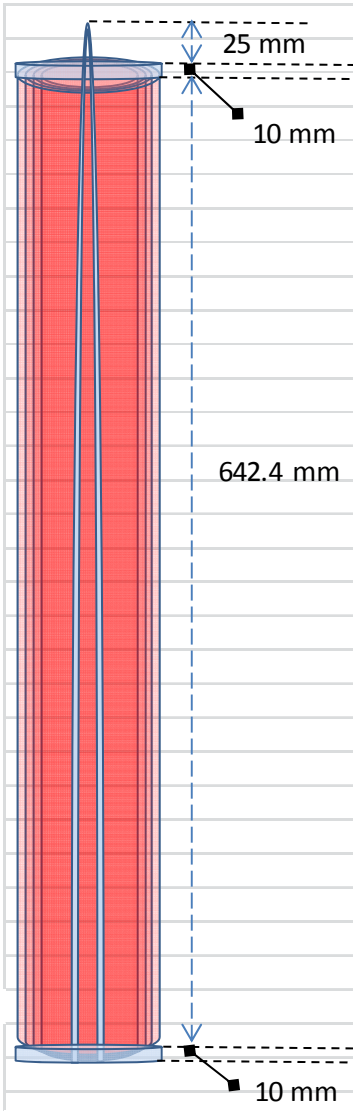

Figure A-14. Sketch of Side View of DR-3-2 Assembly

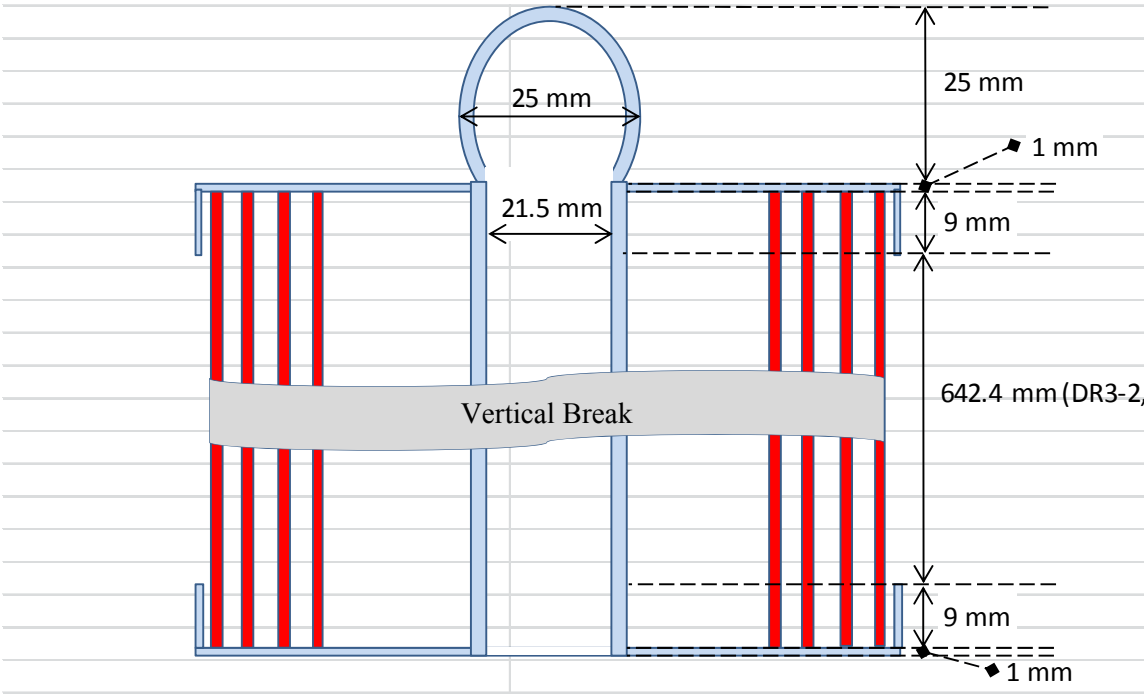

Figure A-15. Sketch of Side Cross-section of DR-3-2 Assembly

Starting from the bottom of the Denmark Reactor DR-3-2 Assembly and going up vertically the exposed inner and outer surface area is calculated as shown in Table A-14. This table details the surface area calculations for specific sections of the DR-3-2 Assembly in terms of height from its bottom. The same terms and structure as defined for the L-Bundle, SRE, and HMI above are used in this table. Using the logic outlined here, the total inner and outer surface area for the DR-3-1 Assembly for the full 27.06 inch height was 540.74 in^2 giving an overall scaling factor for the DR-3-1 Assembly of 19.98 in^2/in or 1.67 ft^2/ft.

Table A-14. Inner and Outer Surface Area Calculation for DR-3-2 Assembly

Scaling Factor for Height h [in^2/in]	Height h [in]	Constant [in^2]	Cumulative Surface Area [in^2]	From [in]	To [in]	Description	Surface Area Sums
12.49	0.04	10.66	11.15	0.00	0.04	from bottom of bottom cup plate up to start of fuel tubes (ignore inside circumference area of holes since only 1 mm thick and elevation change for 40.5 mm circular countersunk area)	[bottom area of cup plate] + [outer circumference area of bottom cup plate] + [circumference area of 2 legs of hairpin] = [$\pi/4*(3.819^2-3*0.315^2-0.846^2)$] + [$\pi*3.819*h$] + [$\pi*0.0787*2*h$]
20.04	0.35	15.13	22.23	0.04	0.39	from start of fuel tubes up to top of bottom cup plate	[inside face area of bottom cup plate] + [outside circumference area of bottom cup plate] + [circumference area of 2 legs of hairpin] + [inner circumference area of fuel tube 1] = [$(\pi/4*(2.404^2-0.846^2))$] + [$\pi*3.819*h$] + [$\pi*0.0787*2*h$]+ [$\pi*2.404*h$]
19.59	25.29	22.23	517.74	0.39	25.69	from top of bottom cup plate up to bottom of top cup plate	[circumference area of 2 legs of hairpin] + [inner circumference area of fuel tube 1] + [outer circumference area of fuel tube 4] = [$\pi*0.0787*2*h$] + [$\pi*2.404*h$] + [$\pi*3.675*h$]
20.04	0.35	517.74	524.85	25.69	26.04	from bottom of top cup plate up to top of fuel tubes	[circumference area of 2 legs of hairpin] + [inner circumference area of fuel tube 1] + [outer circumference area of top cup plate] = [$\pi*0.0787*2*h$] + [$\pi*2.404*h$] + [$\pi*3.819*h$]
12.49	0.04	528.82	529.31	26.04	26.08	from top of fuel tubes up to top of top cup plate (ignore inside circumference area of holes since only 1 mm thick and elevation change for 40.5 mm circular countersunk area)	[inside face area of top cup plate] + [circumference area of 2 legs of hairpin] + [outer circumference area of top cup plate] = [$\pi/4*(2.404^2--0.846^2)$] + [$\pi*3.819*h$] + [$\pi*0.0787*2*h$]

Table A-14. Inner and Outer Surface Area Calculation for DR-3-2 Assembly

Scaling Factor for Height h [in^2/in]	Height h [in]	Constant [in^2]	Cumulative Surface Area [in^2]	From [in]	To [in]	Description	Surface Area Sums
0.78	0.98	539.97	540.74	26.08	27.06	from top of top cup plate up to top of hairpin (assume bent hair pin ~25 mm Outer Diameter)	[top area of top cup plate] + [circumference area of 2 legs of hairpin curved] = $[\pi/4*(3.819^2 - 3*0.315^2 - 0.846^2)] + [\pi*\pi*2/25.4*h]$

Distribution:

S. L. Marra, 773-A
T. B. Brown, 773-A
D. H. McGuire, 999-W
S. D. Fink, 773-A
C. C. Herman, 773-A
E. N. Hoffman, 999-W
F. M. Pennebaker, 773-42A
W. R. Wilmarth, 773-A
Records Administration (EDWS)

E. A. Kyser, 773-A
T. C. Shehee, 773-A
M. C. Thompson, 773-A
W. E. Daniel, 999-W
E. K. Hansen, 999-W

J. L. Bodkin, 221-H
R. T. Burns, 221-H
D. M. Grimm, 704-2H
J. R. Lint, 704-2H
P. M. Palmer, 704-2H
J. B. Schaade, 704-2H
K. J. Usher, 704-2H
T. E. Worth, 704-2H
D. E. Welliver, 704-2H
W. H. Clifton, 704-2H
T. L. Tice, 221-H
S. L. Garrison, 704-2H
R. A. Eubanks, 221-H

P. R. Jackson, DOE-SR, 703-46A